# Continuous Tensor Networks, Conformal Field Theory and Holography

by

Qi Hu

A thesis
presented to the University of Waterloo
in fulfillment of the
thesis requirement for the degree of
Doctor of Philosophy
in
Physics

Waterloo, Ontario, Canada, 2020

**Examining Committee Membership**

The following served on the Examining Committee for this thesis. The decision of the Examining Committee is by majority vote.

| | |
|---|---|
| External Examiner: | Dr. Jutho Haegeman<br>Assistant Professor<br>Dept. of Physics and Astronomy, Ghent University |
| Supervisor(s): | Dr. Guifre Vidal<br>Adjunct Professor<br>Dept. of Physics and Astronomy, University of Waterloo |
| | Dr. Sung-Sik Lee<br>Professor<br>Dept. of Physics and Astronomy, McMaster University |
| Internal Members: | Roger Melko<br>Professor<br>Dept. of Physics and Astronomy, University of Waterloo |
| | Yin-Chen He<br>Adjunct Faculty<br>Dept. of Physics and Astronomy, University of Waterloo |
| Internal-External Member: | Eduardo Martin-Martinez<br>Assistant Professor<br>Dept. of Applied Mathematics, University of Waterloo |

## Author's declaration

This thesis consists of material all of which I authored or co-authored: see Statement of Contributions included in the thesis. This is a true copy of the thesis, including any required final revisions, as accepted by my examiners.

I understand that my thesis may be made electronically available to the public.

## Statement of Contributions

Qi Hu was the sole author for Chapter 1 which was written under the supervision of Dr. Guifre Vidal and was not written for publication.

This thesis consists in part of four manuscripts written for publication. Qi Hu was the first author for the four manuscripts.

Chapter 2 and Appendix A of this thesis consist mostly of material published in Reference [1]. This work was done under the supervision of Guifre Vidal. The copyright of this paper is held by the American Physical Society. Here is the link: Phys. Rev. Lett. 119, 010603. The reuse and permissions license is included in Appendix A.

Chapter 3 and Appendix B of this thesis consist mostly of material published in Reference [2]. This work was done in collaboration with Adrian Franco-Rubio, under the supervision of Guifré Vidal. Qi Hu contributed to the basic idea and wrote the manuscript together with Adrian.

Chapter 4 and Appendix C of this thesis consist mostly of material in a manuscript to be published. This work was done in collaboration with Adrian Franco-Rubio, under the supervision of Guifré Vidal. Qi Hu and Adrian shared the work of numerical analysis and preparing the manuscript draft.

Chapter 5 and Appendix D of this thesis consist mostly of material published in Reference [3]. This work was done under the supervision of Sung-Sik Lee.

**Abstract**

Tensor network methods are playing a central role in multiple disciplines of modern quantum physics, such as condensed matter physics, quantum information and quantum gravity. Based on renormalization group (RG) ideas, they provide a large class of variational ansatz for quantum many-body systems. There are various tensor network structures which are suited for different systems based on their entanglement structures, such as matrix product states (MPS), projected entangled pair states (PEPS), multi-scale entanglement renormalization ansatz (MERA). Numerous techniques involving coarse-graining tensor networks have been developed, such as tensor renormalization group (TRG), tensor network renormalization (TNR) and its variants.

First, we study the generalization of MERA to continuous systems, or cMERA, which is expected to become a powerful variational ansatz for the ground state of strongly interacting quantum field theories. We investigate, in the simpler context of Gaussian cMERA for free theories, the extent to which the cMERA state $|\Psi^\Lambda\rangle$ with finite UV cut-off $\Lambda$ can capture the spacetime symmetries of the ground state $|\Psi\rangle$. For a free boson conformal field theory (CFT) in 1+1 dimensions as a concrete example, we build a quasi-local unitary transformation $V$ that maps $|\Psi\rangle$ into $|\Psi^\Lambda\rangle$ and show two main results. (i) Any spacetime symmetry of the ground state $|\Psi\rangle$ is also mapped by $V$ into a spacetime symmetry of the cMERA $|\Psi^\Lambda\rangle$. However, while in the CFT the stress-energy tensor $T_{\mu\nu}(x)$ (in terms of which all the spacetime symmetry generators are expressed) is local, the corresponding cMERA stress-energy tensor $T^\Lambda_{\mu\nu}(x) = VT_{\mu\nu}(x)V^\dagger$ is quasi-local. (ii) From the cMERA, we can extract quasi-local scaling operators $O^\Lambda_\alpha(x)$ characterized by the exact same scaling dimensions $\Delta_\alpha$, conformal spins $s_\alpha$, operator product expansion coefficients $C_{\alpha\beta\gamma}$, and central charge $c$ as the original CFT. We argue that these results should also apply to interacting theories.

Second we extend TNR to field theories in the continuum. A short-distance length scale $1/\Lambda$ is introduced in the continuum partition function by smearing the fields. The resulting object is still defined in the continuum but has no fluctuations at distances shorter than $1/\Lambda$. An infinitesimal coarse-graining step is then generated by the combined action of a *rescaling* operator $\mathfrak{L}$ and a *disentangling* operator $\mathfrak{K}$ that implements a quasilocal field redefinition. As demonstrated for a free boson in two dimensions, continuous TNR exactly preserves translation and rotation symmetries and can generate a proper RG flow. Moreover, from a critical fixed point of this RG flow one can then extract the conformal data of the underlying conformal field theory.

Leaving behind tensor network methods, we explore the universal structure that emerges from the eigenvectors of the reduced density matrix (RDM) for 1+1 dimensional critical

lattice systems. Using the Ising model as an example, we demonstrate that the large-weight eigenvectors are related to the low-lying states of the underlying CFT with suitable boundary conditions by a conformal map, and they transform accordingly under the Virasoro generators.

Finally, using the quantum renormalization group (QRG), we derive the bulk geometry that emerges in the holographic dual of the fermionic U($N$) vector model at a nonzero charge density. The obstruction that prohibits the metallic state from being smoothly deformable to the direct product state under the renormalization group flow gives rise to a horizon at a finite radial coordinate in the bulk. The region outside the horizon is described by the Lifshitz geometry with a higher-spin hair determined by microscopic details of the boundary theory. On the other hand, the interior of the horizon is not described by any Riemannian manifold, as it exhibits an algebraic non-locality. The non-local structure inside the horizon carries the information on the shape of the filled Fermi sea.

**Acknowledgements**

This work would be impossible without the long-standing support of many people around me. I would like to take this opportunity to express my gratitude towards them.

Most importantly, I want to thank my supervisor Guifre Vidal and cosupervisor Sung-Sik Lee. They have guided me to the very frontier of modern physics. Their persistence in original ideas encourages me to think critically and independently. Their kind support gave me a lot of strength when I was in trouble.

I thank Adrian Franco-Rubio, who has been a very cooperative coauthor with me for two projects. I thank Markus Hauru, Adrian and Yijian Zou, for all the helpful academic discussions along the way.

I thank all the staff at Perimeter Institute for creating a clean and cozy environment for academic research and communication. I thank Debbie Guenther for helping me with numerous adminstrative issues. I thank all my friends at Perimeter Institute, who have given me plenty of help and joy.

Finally, I specially thank my parents. They have been selflessly supporting me all the time. They left behind their jobs to take care of me when I was in a bad physical condition. Without them, I would not be where I am today.

# Table of Contents

# List of Figures

# Chapter 1

# Introduction

As P.W. Anderson pointed out in the celebrated article "*More Is Different*"[4], entirely new properties appear at each level of complexity from large and complex aggregations of elementary particles. Various phases of matter such as superfluid and superconductivity arises from local interactions, exhibiting collective patterns of atoms and electrons. Understanding novel emergent properties from interacting many-body systems is of central importance in condensed matter physics. Originally developed in the context of condensed matter physics, the idea of emergence has become a key concept in a variety of areas, from particle physics to quantum gravity. However, the study of interacting many-body systems is an extremely challenging task. The fundamental difficulty is that the dimension of the Hilbert space for a many-body system increases exponentially as the system size increases. The computational complexity of a straightforward numerical simulation grows so rapidly that even the most powerful supercomputer cannot handle it.

Tensor networks are a family of variational methods for studying many-body systems. Using tensors as building blocks, they provide approximate and efficient representations of many-body states with a lot fewer parameters. For example, an exact representation of the wavefunction for a one-dimensional spin chain of $N$ spins-1/2 requires $2^N$ parameters. However, an MPS representation of a spin chain only has $\mathcal{O}(N)$ parameters[22]. If translational invariance is further imposed, we only need $\mathcal{O}(1)$ parameters to represent the such a wavefunction. Moreover, tensor networks typically allow efficient evaluation of quantities of our interest, such as correlation functions. A well-designed tensor network method should also involve some optimization scheme that can systematically improve the numerical accuracy of the tensor network.

Tensor network methods are closely related to the idea of RG and the concept of quan-

tum entanglement. Historically, White's Density Matrix Renormalization Group (DMRG) method achieved massive success in dealing with lattice systems[10, 11]. It has become the standard tool for one-dimensional quantum lattice systems. The key idea of DMRG is to keep the relevant degrees of freedom in the renormalization procedures. It was later understood that DMRG can be viewed as a variational optimization algorithm over MPS[7]. A significant advantage of tensor network method is that it intuitively encodes the entanglement structure of the quantum state. Each internal index of bond dimension $\chi$ can carry at most $\log \chi$ bits of entanglement across it. From this point of view, it is clear that MPS method is particularly suited for one-dimensional gapped systems[6], since the entanglement entropy for any bipartition is upper-bounded by $\log \chi$. Subsequent generalization was proposed to tackle critical lattice systems, which is the so-called Multi-scale Entanglement Renormalization Ansatz (MERA)[9, 5]. The entanglement structure of MERA implies that the upper bound of the entanglement entropy of a block of length $L$ scales as $\log \chi \cdot \mathcal{O}(\log L)$. This property makes it possible for MERA to represent the ground state of one-dimensional critical lattice systems. Using unitaries and isometries as building blocks, MERA not only provides an ansatz for a quantum state, but also defines a scale transformation that can be applied to the Hilbert space. Investigating how local operators are mapped by the scale transformation, we can extract the universal data of the critical lattice systems[8]. Moreover, MERA has an inherent geometric structure with an emergent dimension, which corresponds to the length scale. Swingle first made the proposal that MERA could be a discrete realization of AdS/CFT correspondence[19]. The possible connection between MERA and gauge/gravity duality has later on been investigated by a lot of authors[16, 15, 17, 14, 13, 12].

Tensor network methods not only involve variational ansatz representing many-body states, but also techniques of coarse-graining tensor networks (two-dimensional tensor networks for most cases) such as TRG[26] and TNR[21]. These tensor networks could represent partition functions of classical statistical models or physical quantities related to a PEPS[27]. The idea is to replace a local patch of tensors by a renormalized tensor while preserving the main features of the tensor network at long distances, much in the spirit of Kadanoff's original spin-blocking proposal[55]. By splitting tensors using singular value decomposition (SVD) and regrouping them, TRG iteratively produces a zoomed-out version of the tensor network. While sharing some features with traditional RG methods, TRG arguably fails to perform a proper RG transformation. On the other hand, by removing local entanglement at each step of coarse-graining, TNR produces a proper RG flow for the tensor network[21]. Indeed, iterative applications of TNR to the partition function of a critical lattice model leads to a fixed point of tensor network, from which the universal data can be extracted. Moreover, TNR is closely related to MERA: iterative applications

of TNR to a tensor network representation of an Eucliean path integral with a boundary produce a MERA[21].

Tensor network methods are naturally suited for lattice systems. Although quantum field theories can be discretized into lattice theories, translational symmetries or other spacetime symmetries will be broken. Therefore it is an important challenge to generalize tensor network methods to the continuum. Plenty of progress has been made over the years, such as continuous MPS (cMPS)[28, 23, 24, 25], continuous MERA (cMERA)[81] and continuous PEPS (cPEPS)[20].

cMERA, proposed by Haegeman *et al.*, describes an entangling evolution of the quantum field degrees of freedom that flows from some large length scale all the way down to an UV length scale $1/\Lambda$. The entangling evolution in scale is generated by a Hermitian operator $L + K$ that explicitly preserves spatial translation and rotation invariance. In Chapter 2, we explore to what extent, and in which sense, cMERA can preserve the spacetime symmetries of the original QFT, beyond translation and rotation symmetry. In Chapter 3, we explain how to extend TNR to field theories in the continuum. Using the free boson theory in two dimensions as an example, we demonstrate that continuous TNR (cTNR) exactly preserves translation and rotation symmetries and can generate a proper RG flow. The conformal data can be extracted from the fixed point of the RG flow.

For 1+1 dimensional critical systems, understanding the entanglement structure is essential for the development of tensor network methods. Entanglement entropy and entanglement spectra, the most commonly used measures of quantum entanglement, have been shown to exhibit universal structures[95, 97, 98, 99, 100, 101, 102, 103]. In Chapter 4, we take a step further by exploring the universal structure that emerges from the eigenvectors of the RDM for 1+1 dimensional critical lattice systems. We show that the eigenvectors can be used as a natural basis to construct a lattice representation of the Virasoro algebra of the underlying CFT with proper boundary conditions.

In Chapter 5, we shift our focus and construct the holographic dual of the fermionic U($N$) vector model using QRG[123]. QRG is very different from the conventional RG schemes, including those defined by MERA, TNR or their generalizations to the continuum. In QRG, only a subset of operators are kept in the renormalization procedure. The price one has to pay is that the coupling constants of these operators are promoted to dynamical variables, whose fluctuations encode the information about the other operators which are not kept in the renormalization procedure. This feature allows QRG to provide a microscopic construction of the holographic dual for a given theory.

# Chapter 2

# Spacetime symmetries and conformal data in cMERA

## 2.1 Introduction

As mentioned earlier, MERA is one of the most useful tensor network methods for lattice models. It can be visualized as the result of a unitary evolution, running from large distances to short distances, that maps an initial unentangled state into a complex many-body wavefunction by gradually introducing entanglement into the system, scale by scale. The success of the MERA in a large class of lattice systems, including systems with topological order [30] or at a quantum critical point [29, 31, 32, 33], teaches us that this *entangling evolution in scale* picture is a valid –and computationally powerful!– way of thinking about ground states and their intricate structure of correlations. With a built-in notion of the renormalization group [34], MERA is also actively investigated in several other contexts, from holography [35, 36, 37] (as a discrete realization of the AdS/CFT correspondence [38]) to statistical mechanics [64], error correction [40], and machine learning [41].

The MERA formalism can also be applied to a quantum field theory (QFT), after introducing a lattice as a UV regulator. For instance, when applied to a conformal field theory (CFT) [96, 43, 44], corresponding to a critical QFT, lattice MERA accurately reproduces the universal properties of the corresponding quantum phase transition (as given by the conformal data) [32, 33]. However, introducing a lattice has a devastating effect on the spacetime symmetries of the original QFT, with e.g. translation and rotation invariance being reduced to invariance under a discrete subset of translations and rotations [45].

To overcome this difficulty, Haegeman, Osborne, Verschelde, and Verstraete [81] proposed the continuous MERA (cMERA). It describes an entangling evolution of the quantum field degrees of freedom that flows from some large length scale all the way down to a UV length scale $1/\Lambda$, directly in the continuum, without introducing a lattice. In this case, the entangling evolution in scale is generated by a Hermitian operator $L + K$ that explicitly preserves translation and rotation invariance. While a fully general cMERA algorithm for interacting QFTs (the truly interesting but much more challenging scenario) is still missing (see however [47]), the simplified Gaussian version of cMERA, also proposed in Ref. [81], provides a valuable proof of principle that lattice MERA can be successfully extended to the continuum –one that has already attracted considerable attention in the context of holography [48, 49] and can extract non-perturbative information of interacting QFTs [47].

In this chapter we explore to what extent, and in which sense, cMERA can preserve the spacetime symmetries of the original QFT, beyond translation and rotation symmetry. Our starting point is the simple observation that, by construction, a successful cMERA approximation $|\Psi^\Lambda\rangle$ should reproduce the targeted QFT ground state $|\Psi\rangle$ at all length scale all the way down to $1/\Lambda$ (the scale at which the entangling evolution ends). Accordingly, there should exist a quasi-local unitary transformation $V$, acting non-trivially only at short distances $\lesssim 1/\Lambda$, that maps $|\Psi\rangle$ into $|\Psi^\Lambda\rangle$, i.e. $|\Psi^\Lambda\rangle = V|\Psi\rangle$. If this was indeed the case, then $V$ would map any local generator $G$ of a symmetry of the ground state, satisfying $G|\Psi\rangle = 0$, into a quasi-local generator $G^\Lambda \equiv VGV^\dagger$ satisfying $G^\Lambda|\Psi^\Lambda\rangle = 0$. That is, all symmetries of $|\Psi\rangle$, including its spacetime sysmmetries, would automatically turn into symmetries of $|\Psi^\Lambda\rangle$, which would however be realized quasi-locally.

In this chapter we will formalise the above intuition and explore its implications for a specific QFT, namely the 1+1 free boson CFT, whose spacetime symmetries are given by the conformal group. However, the above result can be seen to hold more generally for any optimized Gaussian cMERA discussed in Ref. [81], and we expect it to be correct also in the interacting case. We will first show that the optimized cMERA $|\Psi^\Lambda\rangle$ for the 1+1 free boson CFT is invariant under (a quasi-locally generated version of) the global conformal group, which includes scale transformations. We will then see that the quasi-local generator $D^\Lambda \equiv VDV^\dagger$ (where $D$ is the generator of scale transformations or dilations in the CFT) is equal to the generator $L+K$ of the *entangling evolution in scale* that defined the cMERA in the first place. Finally, we will see that the (exact!) conformal data of the target CFT can be extracted from $|\Psi^\Lambda\rangle$ by studying the set of smeared scaling operators $O^\Lambda_\alpha(x)$ associated to $D^\Lambda = L + K$. This result implies that the optimized cMERA exactly captures the universality class of a quantum phase transition.

## 2.2 Continuous MERA for a massless free boson

Consider the 1+1 dimensional massless Klein Gordon QFT,

$$H = \frac{1}{2}\int_{-\infty}^{\infty} dx \ :\big[\pi(x)^2 + (\partial\phi(x))^2\big]: \tag{2.1}$$

for bosonic conjugate field operators $\phi(x)$ and $\pi(x)$, with $[\phi(x),\pi(y)] = i\delta(x-y)$. $H$ can be diagonalized [50],

$$\begin{aligned} H &= \frac{1}{2}\int dk \ :\big[\pi(-k)\pi(k) + k^2\phi(-k)\phi(k)\big]: &(2.2)\\ &= \int dk\ |k|\ a(k)^\dagger a(k). &(2.3)\end{aligned}$$

by first introducing Fourier space mode operators $\phi(k) \equiv \frac{1}{\sqrt{2\pi}}\int dx\ e^{-ikx}\phi(x)$ and $\pi(k) \equiv \frac{1}{\sqrt{2\pi}}\int dx\ e^{-ikx}\pi(x)$ and then annihilation operators $a(k)$,

$$a(k) \ \equiv \ \sqrt{\frac{|k|}{2}}\phi(k) + i\sqrt{\frac{1}{2|k|}}\pi(k), \tag{2.4}$$

with $[a(k),a(q)^\dagger] = \delta(k-q)$. Above, the normal ordering $:\!A\!:$ of an operator $A$ is defined as usual by placing the $a$'s to the right of the $a^\dagger$'s [e.g., if $A = a(k)a(q)^\dagger$, then $:\!A\!: \ = a(q)^\dagger a(k)$] and ensures a vanishing energy for the ground state $|\Psi\rangle$ of $H$, which is characterized by the infinite set of linear constraints

$$a(k)|\Psi\rangle = 0, \quad \forall k. \tag{2.5}$$

On the other hand, the Gaussian cMERA $|\Psi^\Lambda\rangle$ for this CFT, as proposed and optimized in Ref. [81], reads

$$|\Psi^\Lambda\rangle \equiv U(0,-\infty)|\Lambda\rangle, \tag{2.6}$$

namely it is the result of applying a unitary evolution $U$ to a product (unentangled) state $|\Lambda\rangle$, characterized by

$$\left(\sqrt{\frac{\Lambda}{2}}\phi(k) + \frac{i}{\sqrt{2\Lambda}}\pi(k)\right)|\Lambda\rangle = 0, \quad \forall k. \tag{2.7}$$

In the context of a scale invariant QFT, $U$ reads

$$U(s_{UV}, s_{IR}) \equiv e^{-i(L+K)(s_{UV}-s_{IR})}, \tag{2.8}$$

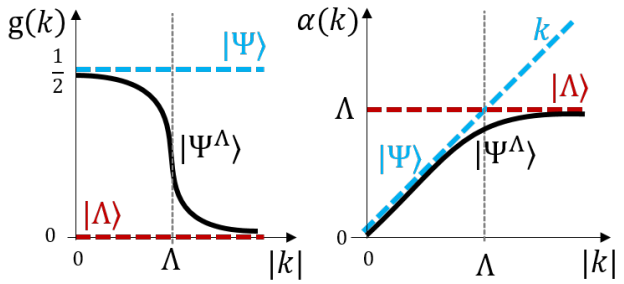


Figure 2.1: Left: function $g(k) = \exp\left(-e^{-\gamma}(k/\Lambda)^2\right)/2$ for the optimized Gaussian cMERA of Ref. [81], where $\gamma \approx 0.57722$ is Euler's constant (see Appendix A). For comparison, the CFT dilation operator $D$ such that $D|\Psi\rangle = 0$ corresponds to choosing $g(k) = 1/2$ and the non-relativistic dilation operator $L$ such that $L|\Lambda\rangle = 0$ corresponds to $g(k) = 0$). Right: function $\alpha(k)$ for $g(k)$, interpolating between the linear dependence $k$ for the CFT ground state $|\Psi\rangle$ at small $k$ and the constant value $\Lambda$ for the product state $|\Lambda\rangle$ at large $k$.

where the generator of non-relativistic dilations $L$ and the so-called entangler $K$ are given by

$$L \equiv \frac{1}{2}\int dk \Big[\pi(-k)(k\partial_k + \frac{1}{2})\phi(k) + h.c.\Big], \tag{2.9}$$

$$K \equiv \frac{1}{2}\int dk\; g(k)\big[\pi(-k)\phi(k) + h.c.\big], \tag{2.10}$$

and the optimized function $g(k)$ in Fig. 2.1 smoothly approaches $1/2$ and $0$ for small and large $k$, respectively,

$$g(k) \sim \begin{cases} 1/2, & |k| \ll \Lambda, \\ 0, & |k| \gg \Lambda. \end{cases} \tag{2.11}$$

By introducing new annihilation operators $a^\Lambda(k)$,

$$a^\Lambda(k) \equiv \sqrt{\frac{\alpha(k)}{2}}\phi(k) + i\sqrt{\frac{1}{2\alpha(k)}}\pi(k), \tag{2.12}$$

with $[a^\Lambda(k), a^\Lambda(q)^\dagger] = \delta(k-q)$, here we start by pointing out that the cMERA state in Eq. 2.6 can be equivalently specified by the modified set of linear constraints

$$a^\Lambda(k)|\Psi^\Lambda\rangle = 0, \quad \forall k, \tag{2.13}$$

provided $\alpha(k)$ and $g(k)$ are related by $d\alpha(k)/dk = 2g(k)\alpha(k)/k$ (see Appendix A). For the $g(k)$ in Fig. 2.1, this implies

$$\alpha(k) \sim \begin{cases} |k|, & |k| \ll \Lambda \quad \text{(CFT limit)}, \\ \Lambda, & |k| \gg \Lambda \quad \text{(product state limit)}. \end{cases} \tag{2.14}$$

To gain insight into the structure of $|\Psi^\Lambda\rangle$, we notice that the constraints it satisfies (Eqs. 2.12-2.14) interpolate between the constraints of the CFT ground state $|\Psi\rangle$ (Eqs. 2.4-2.5) at small $k$ and those of the product state $|\Lambda\rangle$ (Eq. 2.7) at large $k$. In other words, the optimized cMERA should somehow behave as the CFT ground state $|\Psi\rangle$ at large distances $x \gg 1/\Lambda$ and as the product state $|\Lambda\rangle$ at short distances $x \ll 1/\Lambda$ [81]. A direct calculation [51] confirms that, in sharp contrast to the target CFT, in cMERA correlation functions and entanglement entropy remain finite/regulated at short distances, implying that $|\Psi^\Lambda\rangle$ has a built-in UV cut-off.

## 2.3 Smearing symplectic transformation

In order to investigate the spacetime symmetries of $|\Psi^\Lambda\rangle$, let us introduce the unitary map $V$, defined by

$$V\phi(k)V^\dagger = \sqrt{\frac{\alpha(k)}{|k|}}\phi(k) \equiv \phi^\Lambda(k), \tag{2.15}$$

$$V\pi(k)V^\dagger = \sqrt{\frac{|k|}{\alpha(k)}}\pi(k) \equiv \pi^\Lambda(k). \tag{2.16}$$

This map implements a symplectic transformation (preserving canonical commutation relations) that transforms $a(k)$ into $Va(k)V^\dagger = a^\Lambda(k)$ and therefore the CFT ground state into the cMERA, V $|\Psi\rangle = |\Psi^\Lambda\rangle$. The transformation is quasi-local: $V$ maps the sharp field operators $\phi(x)$ and $\pi(x)$ into operators $\phi^\Lambda(x)$ and $\pi^\Lambda(x)$ that are smeared over a length $1/\Lambda$. Indeed, through a Fourier transform of $\phi^\Lambda(k)$ and $\pi^\Lambda(k)$ we obtain

$$\phi^\Lambda(x) = V\phi(x)V^\dagger = \int dy\ \mu_\phi(x-y)\phi(y), \tag{2.17}$$

$$\pi^\Lambda(x) = V\pi(x)V^\dagger = \int dy\ \mu_\pi(x-y)\pi(y), \tag{2.18}$$

where $\mu_\phi$ and $\mu_\pi$ are distributional Fourier transforms [54] of $\sqrt{\frac{\alpha(k)}{|k|}}$ and $\sqrt{\frac{|k|}{\alpha(k)}}$ that are upper bounded by an exponentially decaying function for $\Lambda|x| \gg 1$ (see Appendix A).

We also note that since $V$ acts diagonally in momentum space, its action by conjugation commutes with the spatial derivative $\partial_x$. For instance,

$$(\partial_x\phi)^\Lambda(x) \equiv V\partial_x\phi(x)V^\dagger = \partial_x\left(V\phi(x)V^\dagger\right) = \partial_x(\phi^\Lambda(x)),$$

with the smearing function $\mu_{\phi'}(y)$ for $(\partial_x\phi)^\Lambda(x)$ being the derivative of the smearing function for $\phi^\Lambda(x)$, that is $\mu_{\phi'}(y) = d\mu_\phi(y)/dy = 1/\sqrt{2\pi}\int dk\ e^{iky}\,(ik)\sqrt{\frac{\alpha(k)}{|k|}}$. In particular, the right moving and left moving fields $\partial\phi(x) \equiv (\partial_x\phi(x) - \pi(x))/2$ and $\bar\partial\phi(x) \equiv (\partial_x\phi(x) + \pi(x))/2$ of the CFT [52] are mapped into smeared right and left moving fields, e.g.

$$(\partial\phi)^\Lambda(x) \equiv V\partial\phi(x)V^\dagger = \frac{1}{2}\left(\partial_x\phi^\Lambda(x) - \pi^\Lambda(x)\right). \tag{2.19}$$

## 2.4 Quasi-local stress-energy tensor

The spacetime symmetry generators of the CFT are given by the symmetric, traceless stress-energy tensor $T_{\mu\nu}(x)$ [44], with components $T_{00}(x) = :[\pi(x)^2 + (\partial_x\phi(x))^2]: /2 \equiv h(x)$ and $T_{01}(x) = -:\pi(x)\partial_x\phi(x): \equiv p(x)$, where $h(x)$ and $p(x)$ are the energy and momentum densities. In close analogy, the quasi-local stress-energy tensor $T^\Lambda_{\mu\nu}(x) \equiv VT_{\mu\nu}(x)V^\dagger$ defines quasi-local energy and momentum densities,

$$h^\Lambda(x) \equiv T^\Lambda_{00}(x) = \frac{1}{2}:\left[\pi^\Lambda(x)^2 + (\partial_x\phi^\Lambda(x))^2\right]:, \tag{2.20}$$

$$p^\Lambda(x) \equiv T^\Lambda_{01}(x) = -:\pi^\Lambda(x)\partial_x\phi^\Lambda(x):, \tag{2.21}$$

where we have used that for any two operators $A(x)$ and $B(x)$, $(A(x)B(y))^\Lambda \equiv V\,(A(x)B(y))\,V^\dagger = \left(VA(x)V^\dagger\right)\left(VB(y)V^\dagger\right) = A^\Lambda(x)B^\Lambda(y)$ and the normal order is now with respect to the annihilation operators $a^\Lambda(k)$ in Eq. 2.12. As argued earlier, any generator of a symmetry of the CFT ground state $|\Psi\rangle$ is mapped into a quasi-local generator of a symmetry of $|\Psi^\Lambda\rangle$. Let us now elaborate this point with a few explicit examples.

## 2.5 Translations in time and space

Hamiltonian $H = \int dx\ h(x)$ in Eq. 2.1 and the momentum operator $P \equiv \int dx\ p(x)$, generators of translations in time $(t,x) \to (t+t_0,x)$ and in space $(t,x) \to (t,x+x_0)$, are

mapped into

$$H^\Lambda = \int dx\ h^\Lambda(x) = \int dk\ |k|\ a^\Lambda(k)^\dagger a^\Lambda(k), \tag{2.22}$$

$$P^\Lambda = \int dx\ p^\Lambda(x) = \int dk\ k\ a^\Lambda(k)^\dagger a^\Lambda(k), \tag{2.23}$$

whose expressions in terms of the annihilation operators $a^\Lambda(k)$ make manifest that $H^\Lambda|\Psi^\Lambda\rangle = 0$, $P^\Lambda|\Psi^\Lambda\rangle = 0$, and that $|\Psi^\Lambda\rangle$ is the ground state of the quasi-local Hamiltonian $H^\Lambda$, since $H^\Lambda \geq 0$. Direct inspection shows that $P^\Lambda = P$. We have thus recovered the known invariance of $|\Psi^\Lambda\rangle$ under space translations generated by $P$ [81] (equivalently, $P^\Lambda$), and have in addition shown its invariance under time translations generated by $H^\Lambda$. Notice, moreover, that a complete set of simultaneous eigenstates of $H^\Lambda$ and $P^\Lambda$, can now be built by applying the creation operators $a^\Lambda(k)^\dagger$'s on $|\Psi^\Lambda\rangle$.

## 2.6 Lorentz boosts and scale transformations

We can similarly define cMERA analogues of the generators $B \equiv \int dx\ x\ h(x)$ and $D \equiv \int dx\ x\ p(x)$ of boosts $(x,t) \to \gamma(x - vt, t - vx)$ [where $\gamma \equiv 1/\sqrt{1-v^2}$ is the Lorentz factor and $v$ is the relative velocity] and dilations $(t,x) \to (\lambda t, \lambda x)$ [where $\lambda$ is the re-scaling factor], namely

$$B^\Lambda = \int dx\ x\ h^\Lambda(x) \tag{2.24}$$

$$= i\int_{-\infty}^{\infty} dk\ a^\Lambda(k)^\dagger sgn(k) \left(k\partial_k + \frac{1}{2}\right) a^\Lambda(k), \tag{2.25}$$

$$D^\Lambda = \int dx\ x\ p^\Lambda(x) \tag{2.26}$$

$$= i\int_{-\infty}^{\infty} dk\ a^\Lambda(k)^\dagger \left(k\partial_k + \frac{1}{2}\right) a^\Lambda(k), \tag{2.27}$$

which again manifestly annihilate $|\Psi^\Lambda\rangle$. Operator $B^\Lambda$ generates a continuous symmetry of $|\Psi^\Lambda\rangle$ related to relativistic invariance and with no counter-part on the lattice. Importantly, a direct computation (see Appendix A) shows that $D^\Lambda = L + K$, so that the generator of scale transformations $D^\Lambda$ coincides with the generator $L + K$ of the unitary evolution in scale that defines the cMERA $|\Psi^\Lambda\rangle$. Accordingly, the cMERA state $|\Psi^\Lambda\rangle$ is scale invariant, in spite of containing no entanglement at distances smaller than $1/\Lambda$, if we agree to regard

$D^\Lambda = L + K$ as the generator of dilations. The dilations generated by $D^\Lambda$ not only re-scale spacetime in the usual sense, but also introduce or remove entanglement as needed in order to reset the UV cut-off back to $1/\Lambda$.

We emphasize that, by construction, the operators $H^\Lambda$, $P^\Lambda$, $B^\Lambda$ and $D^\Lambda$ inherit the commutation relations of the CFT generators ($[H^\Lambda, P^\Lambda] = [B^\Lambda, D^\Lambda] = 0$, $-i[D^\Lambda, H^\Lambda] = H^\Lambda$, etc) and therefore close the same algebra, which can be extended to the global conformal group and ev(see Appendix A). Thus, the cMERA realizes a quasi-local, smeared version of conformal symmetry.

In Ref. [81], Haegeman et al. pointed out that the state $|\Psi^\Lambda\rangle$ recovers scale invariance in the limit $\Lambda \to \infty$, where it coincides with the target CFT ground state $|\Psi\rangle$. Here we have just argued, in sharp contrast, that $|\Psi^\Lambda\rangle$ is already scale invariant at *finite* $\Lambda$, provided that we adopt $D^\Lambda = L + K$ as the generator of scale transformations. Admittedly, the scale invariance of $|\Psi^\Lambda\rangle$ is a tautology (because $|\Psi^\Lambda\rangle$ had been introduced in Eqs. 2.6-2.8 as a fixed-point of $L + K$!). To see why these unorthodox notions of scale transformation and scale invariance are nevertheless very useful, next we show that they lead to smeared versions of the scaling operators of the theory from which the conformal data of the target CFT can be extracted.

## 2.7 Quasi-local scaling operators and conformal data

Let us thus search for the quasi-local scaling operators $O^\Lambda_\alpha(x)$ that transform covariantly under $D^\Lambda$ and $B^\Lambda$, that is, such that (choosing $x = 0$ for simplicity)

$$-i[D^\Lambda, O^\Lambda_\alpha(0)] = \Delta_\alpha O^\Lambda_\alpha(0), \tag{2.28}$$

$$-i[B^\Lambda, O^\Lambda_\alpha(0)] = s_\alpha O^\Lambda_\alpha(0), \tag{2.29}$$

where $\Delta_\alpha$ and $s_\alpha$ are the scaling dimension and conformal spin of $O^\Lambda_\alpha(x)$, respectively [53]. One could determine $O^\Lambda_\alpha$ by solving Eqs. 2.28-2.29, but there is no need. Indeed, we can instead use $V$ to translate the sharp scaling operators of the CFT (which are already known [44]) into smeared cMERA scaling operators. A first example is a linear scaling operator of the CFT, namely the right moving field $\partial\phi(x)$ discussed before, which satisfies $-i[D, \partial\phi(0)] = \partial\phi(0)$ and $-i[B, \partial\phi(0)] = \partial\phi(0)$, implying a scaling dimension $\Delta_{\partial\phi} = 1$ and conformal spin $s_{\partial\phi} = 1$. Using the symplectic map $V$ we readily obtain corresponding expressions for $\partial\phi^\Lambda(x)$ in Eq. 2.19, namely

$$-i[D^\Lambda, \partial\phi^\Lambda(0)] = \partial\phi^\Lambda(0), \tag{2.30}$$

$$-i[B^\Lambda, \partial\phi^\Lambda(0)] = \partial\phi^\Lambda(0), \tag{2.31}$$

and thus $\partial\phi^\Lambda(x)$ has the same scaling dimension $\Delta_{\partial\phi^\Lambda} = 1$ and conformal spin $s_{\partial\phi^\Lambda} = 1$ by $D^\Lambda$ and $B^\Lambda$ as $\partial\phi(x)$ has by $D$ and $B$. This results extends to *all* scaling operators of the CFT, including e.g. quadratic scaling operators such as the right moving part of the stress-energy tensor, $T(x) = -2\pi : \partial\phi(x)\partial\phi(x) :$, with $\Delta_T = s_T = 2$, or vertex operators $V_\nu(x) \equiv \ : e^{i\nu\phi(x)} :$. Moreover, operators $O^\Lambda_\alpha(x)$ also inherit from the CFT its operator product expansion (OPE) coefficients $C_{\alpha\beta\gamma}$. For instance, the OPE $T(x)\partial\phi(y) \sim \partial\phi(y)/(x-y)^2 + \partial^2\phi(y)/(x-y)$, translates into

$$T^\Lambda(x)\partial\phi^\Lambda(y) \sim \frac{\partial\phi^\Lambda(y)}{(x-y)^2} + \frac{\partial^2\phi^\Lambda(y)}{(x-y)}. \tag{2.32}$$

Finally, the central charge $c$ can be obtained from (a translation of) the standard OPE of $T(x)$ with itself, namely

$$T^\Lambda(x)T^\Lambda(y) \sim \frac{c/2}{(x-y)^4} + \frac{2T^\Lambda(y)}{(x-y)^2} + \frac{\partial T^\Lambda(y)}{(x-y)}, \tag{2.33}$$

which results in $c = 1$.

## 2.8 Discussion

We have seen that the Gaussian cMERA for a 1+1 free boson CFT, as proposed and optimized in Ref. [81], inherits (a quasi-locally realized version of) the spacetime symmetries of the conformal theory. This result was based on identifying the quasi-local unitary transformation $V$ that maps the CFT ground state $|\Psi\rangle$ into the cMERA $|\Psi^\Lambda\rangle$, and then using it to also map the symmetry generators of the original theory. As an application, we have shown that from the generators $D^\Lambda = L + K$ and $B^\Lambda = \int dx\ x\ h^\Lambda(x)$ we can reconstruct all the conformal data of the original CFT, namely the central charge $c$, and the scaling dimensions $\Delta_\alpha$ and conformal spins $s_\alpha$ of the primary fields, together with their OPE coefficients $C_{\alpha\beta\gamma}$. A similar transformation $V$ can also be built for the optimized Gaussian cMERA of any free QFT analysed in Ref. [81], including higher dimensional CFTs (invariant under the global conformal group) and massive relativistic QFTs (invariant only under the Poincare group, with a scale dependent entangler $K(s)$).

We conclude by briefly commenting on the (non-Gaussian) cMERA for interacting QFTs, for which no optimization algorithm is yet known. Based on the success of MERA [29, 32, 33] for interacting theories on the lattice over the last 10 years, it is reasonable to speculate that a putative interacting cMERA algorithm will produce an optimized state

$|\Psi^\Lambda\rangle$ that will again only differ significantly from its target ground state $|\Psi\rangle$ at short distances. Accordingly, a quasi-local unitary $V$ should also exist relating $|\Psi\rangle$ and $|\Psi^\Lambda\rangle$ that maps the generators of symmetries into quasi-local generators. In this way, for instance, we once again expect to be able to extract an accurate estimate of the conformal data of interacting CFTs from an optimized non-Gaussian cMERA approximation $|\Psi^\Lambda\rangle$.

# Chapter 3

# Continuous tensor network renormalization for quantum fields

## 3.1 Introduction

The study of many-body systems is a major challenge of modern physics. Following the seminal work of Kadanoff [55] and Wilson [56], the renormalization group (RG) allows us to investigate how the physics of a many-body system changes with scale while providing a conceptual framework for understanding universality in second order phase transitions. More recently, ideas from quantum information have led to a new generation of powerful numerical RG algorithms for lattice systems [57, 58, 59, 60, 61, 62, 63, 64, 65, 66, 67, 68, 69, 70, 71], starting with the breakthrough work of Levin and Nave [57], who wrote the partition function of a two-dimensional statistical model as a tensor network and proposed coarse-graining the latter by applying linear algebra compression methods (see [58, 59, 60, 61, 62, 63] for related algorithms). Building on that proposal, Evenbly and Vidal subsequently introduced the tensor network renormalization (TNR) algorithm [64, 65, 66, 67], which was shown to generate a proper RG flow $\{A_1, A_2, \cdots\}$ in the space of tensors $A$ (see [68, 70, 69, 71] for similar proposals). In particular, when applied to a critical lattice model, TNR naturally flows to an RG fixed point, thus explicitly realizing scale invariance on the lattice. From the fixed-point tensor $A_\star$ one can then extract the critical universality class of a second order phase transition, namely the conformal data that characterizes the underlying conformal field theory (CFT) [72, 73, 74]. TNR, which recently inspired research in the context of the holographic principle of quantum gravity [75, 76, 77, 78], can be readily applied also to field theories by bringing them to the lattice. However,

the discretization procedure destroys the field theory spacetime symmetries (continuous translation and rotation symmetries), which are only retained in an approximate, emergent sense. This makes it of interest, both conceptually and computationally, to extend TNR to field theories directly in the continuum, in such a way that the original spacetime symmetries are explicitly preserved.

In this chapter we propose an extension of TNR to the continuum. As a preliminary step, fluctuations at distances shorter than a cutoff $1/\Lambda$ are removed from the Euclidean partition function by smearing the quantum field degrees of freedom. Then an infinitesimal transformation of continuous TNR (cTNR) is generated by the combined action of two operators –a *rescaling* operator $\mathfrak{L}$ that rescales space and a *disentangling* operator $\mathfrak{K}$ that implements a quasilocal field redefinition. When applied to the simple case of a free boson field theory, cTNR is seen to generate the correct RG flow, including a critical fixed point for the massless theory. As in lattice TNR, from this fixed point we can extract the conformal data of the underlying CFT. Our construction resembles, but is not equivalent to, the proposal of the continuous version of the multiscale entanglement renormalization ansatz (MERA) [79, 80], known as continuous MERA (cMERA) [81], for ground states of field theories, which is so far only well-understood for free theories but has nevertheless attracted much attention in the context of holography as a potential toy model realization of the AdS/CFT correspondence [83, 84, 85, 86, 87, 88, 89, 90, 91].

## 3.2 Lattice TNR

Let us briefly review the essential ingredients of the TNR algorithm on the lattice [64, 65, 66, 67]. The object to be coarse-grained is a two-dimensional statistical partition function (equivalently, a discrete Euclidean path integral in two spacetime dimensions) that has been expressed as a two-dimensional tensor network, where each tensor $A$ in the network encodes local Boltzmann weights. The lattice spacing $a$ of the model serves as a short-distance cutoff. Through an intricate sequence of local manipulations of the network, which aims at removing shortly-correlated degrees of freedom, TNR effectively maps a block of four tensors $A_s$ at scale $s$ into a single tensor $A_{s+1}$ at scale $s+1$. Then space is rescaled by a factor $1/2$, so as to reset the lattice spacing $2a$ of the coarse-grained network back to the original lattice spacing $a$, see Fig. 3.1(a). These general features of the method are shared with most previous tensor network coarse-graining schemes [57, 58, 59, 60, 61, 62, 63]. What makes TNR stand out is that, thanks to the use of so-called *disentanglers* $u$ and *isometries* $w$ (a technology borrowed from MERA [79, 80], see Fig. 3.1(b)), it first decouples, and then eliminates, most shortly-correlated degrees of freedom from the partition function, in

such a way as to generate a proper RG flow with the correct structure of fixed points.

## 3.3 Continuous partition function

Let us now move to a quantum field theory (QFT) in the continuum. For concreteness we consider a bosonic field $\phi(\boldsymbol{x})$ in flat $D$-dimensional Euclidean spacetime. Our object of interest is now the partition function

$$Z = \int [d\phi]\ e^{-S[\phi]}, \qquad S[\phi] = \int d\boldsymbol{x}\ \mathcal{L}\Big(\phi(\boldsymbol{x}), \Delta\phi(\boldsymbol{x})\Big), \tag{3.1}$$

where the Euclidean action $S[\phi]$ is the integral of a (generally interacting) local Lagrangian density $\mathcal{L}$, which we assume to be invariant under translations and rotations. As a preliminary step, we introduce a smeared field

$$\phi^\Lambda(\boldsymbol{x}) \equiv \int d\boldsymbol{y}\ \mu(|\boldsymbol{x}-\boldsymbol{y}|)\phi(\boldsymbol{y}), \qquad \int d\boldsymbol{x}\ \mu(|\boldsymbol{x}|) = 1, \tag{3.2}$$

where $\mu(x) \in \mathbb{R}$, with $x \equiv |\boldsymbol{x}|$, is a smearing profile invariant under $\mathrm{O}(D)$ rotations that decays fast to zero (*e.g.* exponentially) for distances $x$ larger than a characteristic smearing length scale $1/\Lambda$, see Fig. 3.2(a) for an example. We then define the smeared action $S^\Lambda[\phi] \equiv S[\phi^\Lambda]$, with corresponding quasilocal Lagrangian

$$\mathcal{L}^\Lambda\Big(\phi(\boldsymbol{x}), \Delta\phi(\boldsymbol{x})\Big) \equiv \mathcal{L}\Big(\phi^\Lambda(\boldsymbol{x}), \Delta\phi^\Lambda(\boldsymbol{x})\Big), \tag{3.3}$$

as well as the new partition function

$$Z^\Lambda \equiv \int [d\phi]\ e^{-S^\Lambda[\phi]} = \int [d\phi]\ e^{-S[\phi^\Lambda]} \tag{3.4}$$

in which fluctuations of $\phi(\boldsymbol{x})$ at distances smaller than $1/\Lambda$ have been suppressed thanks to the smearing. For instance, we expect the correlator for the sharp field $\phi(\boldsymbol{x})$,

$$\langle\phi(\boldsymbol{x})\phi(\boldsymbol{0})\rangle_\Lambda \equiv \frac{1}{Z^\Lambda}\int [d\phi]\ e^{-S^\Lambda[\phi]}\ \phi(\boldsymbol{x})\phi(\boldsymbol{0}) \tag{3.5}$$

not to diverge for $x \to 0$, but to tend to a constant when $\Lambda x \ll 1$, see *i.e.* Fig. 3.2(c). The length $1/\Lambda$ plays here a role analogous to the lattice spacing $a$ in the lattice.

## 3.4 Continuous TNR

The proposed cTNR transformation proceeds through an infinitesimal change of the field

$$\phi(\boldsymbol{x}) \to \phi(\boldsymbol{x}) + \delta\phi(\boldsymbol{x}), \quad \delta\phi(\boldsymbol{x}) \equiv \delta s \, (\mathfrak{L} + \mathfrak{K}_s) \, \phi(\boldsymbol{x}), \tag{3.6}$$

where $\delta s$ is an infinitesimal change of the scale parameter $s$, $\mathfrak{L}$ is the usual *rescaling* operator,

$$\mathfrak{L} \; \phi(\boldsymbol{x}) = (-\boldsymbol{x} \cdot \nabla_{\boldsymbol{x}} - \Delta_\phi)\phi(\boldsymbol{x}), \tag{3.7}$$

with $\Delta_\phi \equiv (D-2)/2$ the classical scaling dimension of the field $\phi(\boldsymbol{x})$, and the *disentangling* operator $\mathfrak{K}_s$ implements a quasilocal field redefinition,

$$\mathfrak{K}_s \phi(\boldsymbol{x}) = F\Big(s, \phi^\Lambda(\boldsymbol{x}), \Delta\phi^\Lambda(\boldsymbol{x}), \Delta^2\phi^\Lambda(\boldsymbol{x}), \dots\Big). \tag{3.8}$$

Here $F$ is some function, not necessarily linear, of the smeared field $\phi^\Lambda(\boldsymbol{x})$ and its derivatives, which is invariant under translations and rotations and may also depend on the scale parameter $s$. While applying $\mathfrak{L}$ to the smeared field $\phi^\Lambda(\boldsymbol{x})$ shrinks its smearing length, applying the quasilocal disentangler $\mathfrak{K}_s$ is expected to restore it back to $1/\Lambda$. Transformation 3.6-3.8 applied to $Z^\Lambda$ generates an RG flow. We write symbolically (see Appendix B)

$$Z^\Lambda_s \;\equiv\; \mathcal{P}e^{\int_0^s du \; (\mathfrak{L}+\mathfrak{K}_u)} \; Z^\Lambda = \int [d\phi] e^{-S^\Lambda_s[\phi]}, \tag{3.9}$$

where $\mathcal{P}e$ denotes a path ordered exponential. In general we should take into account the change of the integration measure when computing the evolution of the action $S^\Lambda_s[\phi]$. Since both $\mathfrak{L}$ and $\mathfrak{K}_s$ act (quasi)locally, it should be possible to write the new action as an integral of a quasilocal Lagrangian density:

$$S^\Lambda_s[\phi] = \int d\boldsymbol{x} \; \mathcal{L}^\Lambda_s\Big(\phi(\boldsymbol{x}), \Delta\phi(\boldsymbol{x}), \Delta^2\phi(\boldsymbol{x}), \dots\Big). \tag{3.10}$$

Off criticality, we expect a flow of $\mathcal{L}^\Lambda_s$ with $s$ towards some massive fixed point Lagrangian. At a critical point, instead, we expect a flow towards an unstable fixed point Lagrangian $\mathcal{L}^\Lambda_\star$ corresponding to a (smeared version of) a CFT. This will be characterized by a spectrum of quasilocal scaling operators $\mathcal{O}^\Lambda_\alpha(\boldsymbol{x})$. For instance, in $D = 2$ dimensions the latter are solutions to

$$(\mathfrak{L} + \mathfrak{K}_\star) \; O^\Lambda_\alpha(\boldsymbol{0}) \;=\; -\Delta_\alpha \; O^\Lambda_\alpha(\boldsymbol{0}), \tag{3.11}$$

$$\mathfrak{R} \; O^\Lambda_\alpha(\boldsymbol{0}) \;=\; s_\alpha \; O^\Lambda_\alpha(\boldsymbol{0}), \tag{3.12}$$

where $\Delta_\alpha$ and $s_\alpha$ are the scaling dimension and conformal spin of $O^\Lambda_\alpha(x)$, $\mathfrak{K}_\star$ is the fixed-point disentangling operator, and $\mathfrak{R}$ is the generator of rotations in the Euclidean plane, $\mathfrak{R} \; \phi(\boldsymbol{x}) = (x_1\partial_{x_2} - x_2\partial_{x_1}) \; \phi(\boldsymbol{x})$.

## 3.5 Continuum versus lattice

As illustrated in Fig. 3.1(c), we can think of $e^{-d\boldsymbol{x}\mathcal{L}_s^\Lambda}$ as the continuum counterpart of a tensor $A_s$ in the network representing a partition function on the lattice. Then $\mathfrak{L} + \mathfrak{K}_s$ implement in the continuum the equivalent of a TNR coarse-graining transformation on the lattice, with the disentangler $\mathfrak{K}_s$ being the continuum version of the disentanglers $u_s$ and isometries $w_s$ on the lattice. Indeed, both the continuum $\mathfrak{K}_s$ and the lattice $u_s$ and $w_s$ implement a (quasi)local reorganization of the degrees of freedom that aims to decouple from the partition function those that are shortly correlated, that is, correlated at lengths on the order $a \sim 1/\Lambda$. However, while on the lattice each step of TNR implements a *discrete* change of scale $s \to s+1$ and the disentanglers $u_s$ and isometries $w_s$ are used to *completely* decouple half of the lattice degrees of freedom, in the continuum TNR implements instead a *continuous* change of scale $s$, during which the disentangler $\mathfrak{K}_s$ *gradually* decouples field degrees of freedom.

## 3.6 Example: free boson in two dimensions

Some features of the above general proposal for interacting field theories can be well illustrated using the simplified scenario of free fields. For concreteness, here we consider a free boson in $D = 2$ spacetime dimensions. The Euclidean action is given by

$$S[\phi] = \frac{1}{2}\int d\boldsymbol{x}\left(-\phi(\boldsymbol{x})\Delta\phi(\boldsymbol{x}) + m^2\phi(\boldsymbol{x})^2\right) \tag{3.13}$$

$$= \frac{1}{2}\int \frac{d\boldsymbol{k}}{(2\pi)^2}\,(k^2+m^2)\phi(\boldsymbol{k})\phi(-\boldsymbol{k}), \tag{3.14}$$

where $\phi(\boldsymbol{k}) \equiv \int d\boldsymbol{x}\;\phi(\boldsymbol{x})e^{-i\boldsymbol{k}\cdot\boldsymbol{x}}$ is a Fourier mode. Although cTNR is a real-space renormalization scheme, for free fields it is insightful to work in momentum space. The following derivations require performing standard Gaussian integrations and Fourier transforms, as detailed in (see Appendix B). The momentum-space two-point correlator reads

$$\langle\phi(\boldsymbol{k})\phi(-\boldsymbol{k})\rangle = \frac{1}{k^2+m^2}, \tag{3.15}$$

leading to a real-space correlator $\langle\phi(\boldsymbol{x})\phi(\boldsymbol{0})\rangle$ that diverges at short distances, $x \to 0$. For instance, for $m = 0$,

$$\langle\phi(\boldsymbol{x})\phi(\boldsymbol{0})\rangle = -\frac{1}{2\pi}\log(x) + \text{const.} \qquad (m=0). \tag{3.16}$$

Instead the smeared action $S^\Lambda[\phi] \equiv S[\phi^\Lambda]$ reads

$$S^\Lambda[\phi] = \frac{1}{2}\int d\boldsymbol{x}\Big( -\phi^\Lambda(\boldsymbol{x})\Delta\phi^\Lambda(\boldsymbol{x}) + m^2\phi^\Lambda(\boldsymbol{x})^2\Big) \tag{3.17}$$

$$= \frac{1}{2}\int \frac{d\boldsymbol{k}}{(2\pi)^2}\,(k^2+m^2)\mu(k)^2\phi(\boldsymbol{k})\phi(-\boldsymbol{k}), \tag{3.18}$$

and leads to the sharp field correlator

$$\langle\phi(\boldsymbol{k})\phi(-\boldsymbol{k})\rangle_\Lambda = \frac{1}{(k^2+m^2)}\frac{1}{\mu(k)^2}. \tag{3.19}$$

Above we have used the Fourier transform of Eq. 3.2, $\phi^\Lambda(\boldsymbol{k}) = \mu(k)\phi(\boldsymbol{k})$. Since the smearing profile $\mu(x)$ is real and rotation invariant, so is $\mu(k)$. We further constrain $\mu(k)$ with two requirements. First, we would like $\langle\phi(\boldsymbol{k})\phi(-\boldsymbol{k})\rangle_\Lambda$ to coincide with $\langle\phi(\boldsymbol{k})\phi(-\boldsymbol{k})\rangle$ for $k \ll \Lambda$, so that the smeared field theory reproduces the large distance physics of the original field theory. Second, we would like to remove the short-distance divergence in $\langle\phi(\boldsymbol{x})\phi(\boldsymbol{0})\rangle$ (see e.g. Eq. 3.16), which demands that $\langle\phi(\boldsymbol{k})\phi(-\boldsymbol{k})\rangle_\Lambda$ tend to a constant (say, $1/\Lambda^2$) sufficiently fast for $k \gg \Lambda$. Accordingly we will require (see Appendix B):

$$\mu(k) = \begin{cases} 1 & \text{for } k/\Lambda \to 0, \\ \Lambda/k & \text{for } k/\Lambda \to \infty, \end{cases}$$
$$\left|\int_\Lambda^\infty \left(\frac{1}{(k^2+m^2)}\frac{1}{\mu(k)^2} - \frac{1}{\Lambda^2}\right)\right| < \infty. \tag{3.20}$$

## 3.7 Free boson cTNR

For a free theory, we can use a disentangling operator $\mathfrak{K}_s$ linear in $\phi(\boldsymbol{x})$,

$$\mathfrak{K}_s\ \phi(\boldsymbol{x}) = \int d\boldsymbol{y}\ g(s,|\boldsymbol{x}-\boldsymbol{y}|)\ \phi(\boldsymbol{y}), \tag{3.21}$$

or $\mathfrak{K}_s\phi(\boldsymbol{k}) = g(s,k)\phi(\boldsymbol{k})$ in momentum space. Notice that $\mathfrak{K}_s$ is built to be invariant under both translations and rotations, since for any $s$, $g(s,|\boldsymbol{x}-\boldsymbol{y}|)$ is only a function of $|\boldsymbol{x}-\boldsymbol{y}|$. In analogy with lattice TNR, where disentanglers $u_s$ and isometries $w_s$ act locally on a region of linear size $a$, we further require $g(s,x)$ to be a quasilocal function of $x$ with characteristic

length scale $1/\Lambda$, see *i.e.* Fig. 3.2(b). For $s=0$, $\mathfrak{L}+\mathfrak{K}_s$ acts on $S^\Lambda[\phi]$ as (see Appendix B)

$$(\mathfrak{L}+\mathfrak{K}_s)\ S^\Lambda[\phi] \tag{3.22}$$

$$= \int \frac{d\boldsymbol{k}}{(2\pi)^2}\Big\{k^2\mu(k)\Big[\big(-k\partial_k+g(k)\big)\mu(k)\Big] \tag{3.23}$$

$$+\ m^2\mu(k)\Big[\big(-k\partial_k+1+g(k)\big)\,\mu(k)\Big]\Big\}\,\phi(\boldsymbol{k})\phi(-\boldsymbol{k}), \tag{3.24}$$

with $g(k)\equiv g(0,k)$. It follows that, in the massless case $m=0$, the action $S^\Lambda[\phi]$ is invariant if and only if

$$g(k)=\frac{k\partial_k\mu(k)}{\mu(k)}. \tag{3.25}$$

Let $\mathfrak{K}_\star$ denote the fixed-point entangler (that is, with $g(k)$ obeying 3.25 ) and let $S^\Lambda_\star[\phi]$ denote the massless action, *i.e.* $(\mathfrak{L}+\mathfrak{K}_\star)\ S^\Lambda_\star[\phi]=0$. It also follows (see Appendix B) that

$$(\mathfrak{L}+\mathfrak{K}_\star)\ \phi^\Lambda(\mathbf{0})=0, \tag{3.26}$$

which implies that the effect of the rescaling operator $\mathfrak{L}$ on the smeared field $\phi^\Lambda(\mathbf{0})$ (namely the shrinking of its smearing profile $\mu(x)$) is exactly compensated by that of the fixed-point disentangler $\mathfrak{K}_\star$ (which re-expands the smearing through a quasilocal field redefinition). Finally, as a concrete example, the pair of functions

$$\mu(k) = \frac{\Lambda}{k}\exp\left(\frac{1}{2}\mathrm{Expi}\left(-\frac{k^2}{\sigma\Lambda^2}\right)\right), \tag{3.27}$$

$$g(k) = -1+\exp\left(-\frac{k^2}{\sigma\Lambda^2}\right), \tag{3.28}$$

where $\mathrm{Expi}(x)$ is the exponential integral function and $\sigma=e^\gamma\approx 1.78$ (with $\gamma$ Euler's constant), fulfill the constraints 3.20 and 3.25 while their Fourier transforms $\mu(x)$ and $g(x)$, depicted in Fig. 3.2(a,b), are quasilocal with characteristic length $1/\Lambda$ (see Appendix B). Fig. 3.2(c) shows the resulting correlator $\langle\phi(\boldsymbol{x})\phi(\mathbf{0})\rangle_\Lambda$, which is UV-finite.

## 3.8 RG flow and critical fixed point

Applying now the above fixed-point disentangler $\mathfrak{K}_\star$ to the action $S^\Lambda[\phi]$ for $m\neq 0$ [92] results in a scale-dependent action

$$S^\Lambda_s[\phi]=\frac{1}{2}\int d\boldsymbol{x}\Big(-\phi^\Lambda(\boldsymbol{x})\Delta\phi^\Lambda(\boldsymbol{x})+m(s)^2\phi^\Lambda(\boldsymbol{x})^2\Big) \tag{3.29}$$

where the mass $m(s) \equiv me^s$ grows exponentially with the RG scale $s$. Thus we have recovered the well-known RG flow of a massive free boson towards its infinite mass fixed point.

Returning to the critical point, with fixed-point Lagrangian $\mathcal{L}^\Lambda_\star \equiv -\frac{1}{2}\phi^\Lambda(\boldsymbol{x})\Delta\phi^\Lambda(\boldsymbol{x})$, it can be shown that the quasilocal scaling operators $\mathcal{O}^\Lambda_\alpha(\boldsymbol{x})$, *cf.* Eqs. 3.11-3.12, are in one to one correspondence with the local scaling operators $\mathcal{O}_\alpha(\boldsymbol{x})$ of the free boson CFT and can obtained by smearing them (see Appendix B). This observation is analogous to that in Ref. [**?**]. For example, the right moving field $\partial\phi(\boldsymbol{x}) \equiv (\partial_{x_1} - i\partial_{x_2})\phi(\boldsymbol{x})$ is a CFT scaling operator with scaling dimension $\Delta_{\partial\phi} = 1$ and conformal spin $s_{\partial\phi} = 1$, satisfying $\mathfrak{L}\ \partial\phi(\mathbf{0}) = -\partial\phi(\mathbf{0})$ and $\mathfrak{R}\ \partial\phi(\mathbf{0}) = \partial\phi(\mathbf{0})$. By smearing those expressions we readily find the corresponding scaling operator $\partial\phi^\Lambda(\boldsymbol{x})$:

$$(\mathfrak{L} + \mathfrak{K}_\star)\ \partial\phi^\Lambda(\mathbf{0}) = -\partial\phi^\Lambda(\mathbf{0}), \tag{3.30}$$

$$\mathfrak{R}\ \partial\phi^\Lambda(\mathbf{0}) = \partial\phi^\Lambda(\mathbf{0}), \tag{3.31}$$

with the exact same scaling dimension and conformal spin. We can similarly recover the operator product expansion and central charge of the original CFT [72, 73, 74], and therefore extract all of its conformal data (see Appendix B).

## 3.9 Discussion

In this chapter we have proposed an extension of the TNR formalism [64, 65, 66, 67] to quantum fields in the continuum and demonstrated with a free boson that, as on the lattice, continuous TNR generates a proper RG flow, including a critical fixed point from which one can extract the universal critical properties (conformal data) of the phase transition. The exact preservation of translation and rotation symmetry, accomplished through the use of explicitly symmetric smearing function $\mu$ and disentangling operator $\mathfrak{K}_s$, demonstrates the possibility of preserving such symmetries in a real space RG approach. It is also expected to lead to increased numerical robustness and reduced computational costs with respect to lattice TNR.

Importantly, an actual cTNR algorithm for interacting QFTs is currently still missing. However, based on the success of TNR and related algorithms for interacting models on the lattice [64, 65, 66, 67, 68, 70, 69, 71], it is reasonable to expect that one such algorithm will be eventually developed. We envisage that cTNR will then represent a powerful alternative to Wilsonian RG methods [56]. Recall that the latter operate in *momentum space* and are based on sequentially *integrating out* thin shells of modes with large momentum. We

emphasize that cTNR, a *real space* method, operates in a fundamentally different way by *decoupling out* shortly-correlated degrees of freedom through the use of a quasilocal field redefinition.

Our proposal parallels the development of the cMERA, put forward by Haegeman, Osborne, Verschelde, and Verstraete in Ref. [81]. As cMERA [81, **?**, 82], the cTNR formalism is based on smeared fields and is only well understood for free particle QFTs. Moreover, at criticality both cMERA [**?**] and cTNR (see Appendix B) can be seen to realize conformal symmetry quasilocally. However, even though TNR and MERA are tightly related on the lattice [65], in the continuum there exist a clear divide between the two formalism. Indeed, in cMERA the fields are only smeared in the space direction, whereas in cTNR the smearing is isotropic in Euclidean spacetime. As a result, in cTNR it is unclear how to even define the Hilbert space attached to a constant time slice in which cMERA would represent a many-body wavefunctional [93]. Finally, while awaiting the development of a cTNR algorithm for interacting QFTs, we hope that cTNR will become a useful framework for holographic studies, thus following the path of both lattice TNR [75, 76, 77, 78] and cMERA [83, 84, 85, 86, 87, 88, 89, 90, 91].

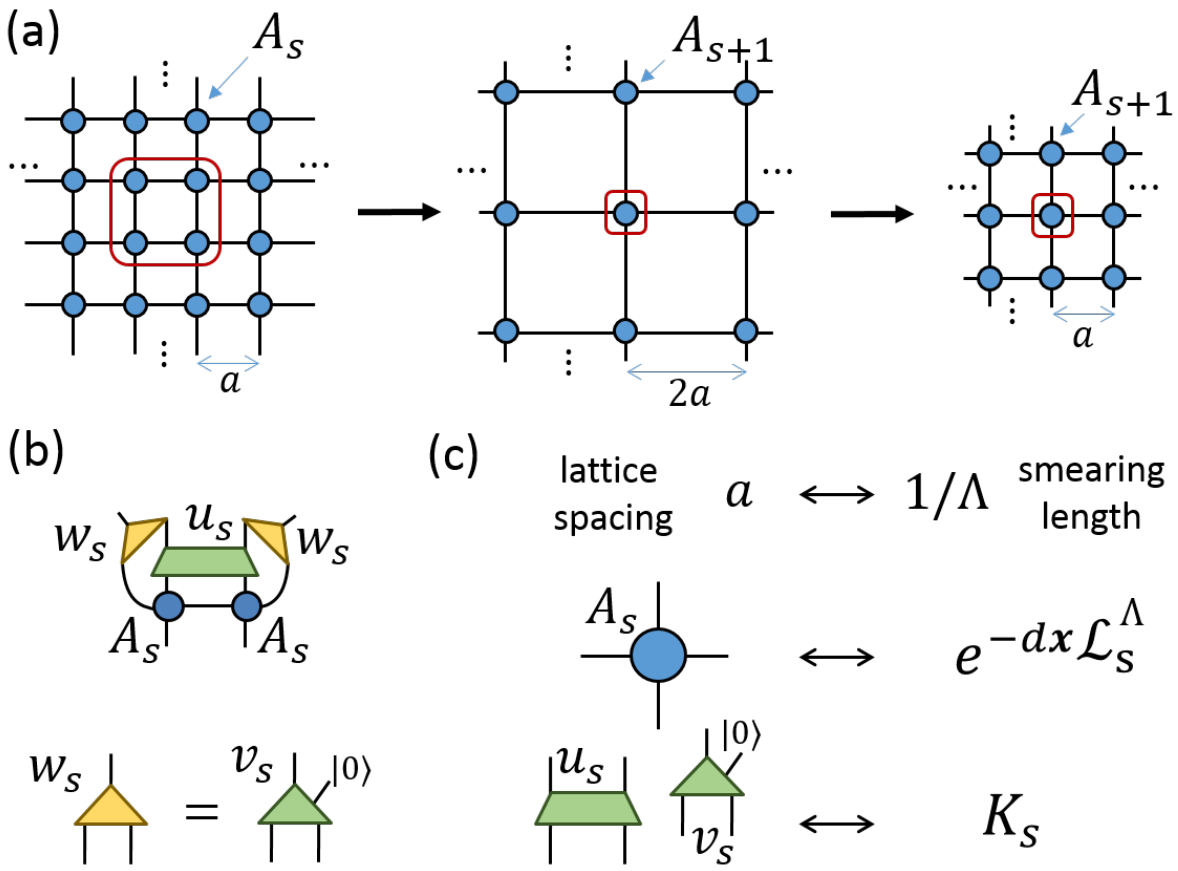


Figure 3.1: (a) TNR acts of a network of tensors $A_s$ representing a partition function on a lattice with spacing $a$, by replacing a block of four tensors $A_s$ with a single tensor $A_{s+1}$, then rescaling the lattice spacing of resulting network from $2a$ back to $a$. (b) As part of the intricate local manipulations that coarse-grain the network, TNR applies disentanglers $u_s$ and isometries $w_s$ to tensors $A_s$. Each isometry $w_s$ can be replaced with a unitary $u_s$ with a fixed input $|0\rangle$ representing a decoupled degree of freedom. (c) Correspondence between objects in lattice and continuum TNR.

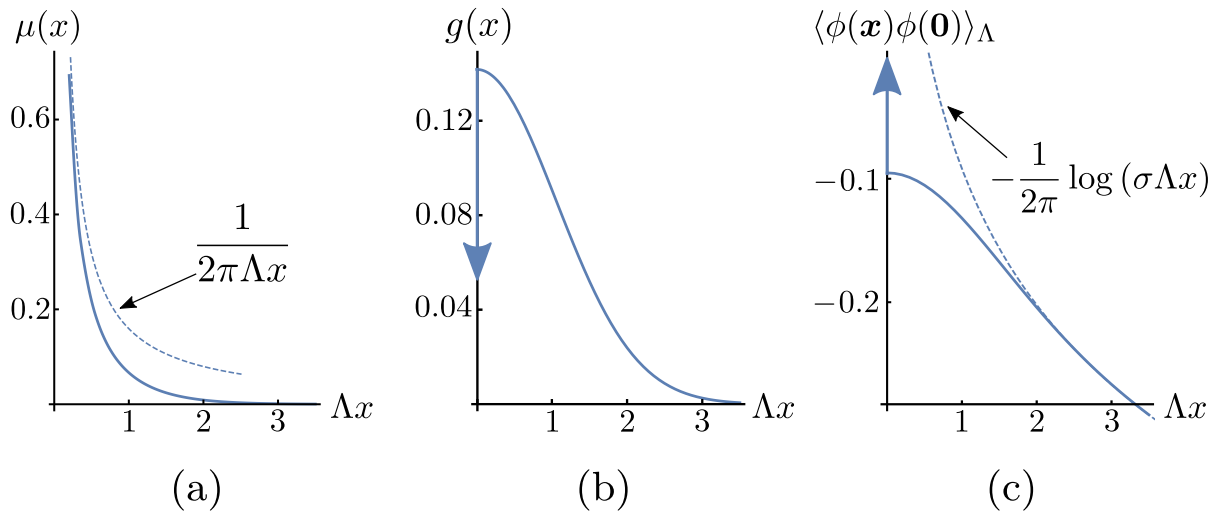


Figure 3.2: (a) $\mu(x)$, 2D Fourier transform of $\mu(k)$ in Eq. 3.27, diverges as $1/x$ (dashed line) at short distances and is upper bounded by an exponentially decaying function at long distances (see Appendix B). (b) $g(x) = -\delta(x) + \sigma\Lambda^2/(4\pi)e^{-\sigma\Lambda^2 x^2/4}$, 2D Fourier transform of $g(k)$ in Eq. 3.28, has a contact term at $x = 0$ and decays as a Gaussian function at long distances. (c) The correlation function $\langle\phi(\boldsymbol{x})\phi(\mathbf{0})\rangle_\Lambda$, Fourier transform of $1/(k^2\mu(k)^2)$, has a delta contact term at $x = 0$, and scales logarithmically (dashed line) at long distances (see Appendix B).

# Chapter 4

# Emergent Universal Entanglement Algebra in Critical Lattice Systems

## 4.1 Introduction

The study of the entanglement structures in quantum many-body states has been the source of considerable insight about their physical properties. In the particular case of systems at a quantum critical point, it has been shown that their entanglement displays *universal* behaviour, i.e., structure that comes dictated by the universality class of the phase transition, irrespective of the microscopic Hamiltonian realization thereof. In the case of 1+1-dimensional systems, universality classes are labeled by 2-dimensional conformal field theories (CFTs), whose structure has been thoroughly elucidated starting with the seminal work of Belavin, Polyakov and Zamolodchikov [96]. Thus, universal entanglement properties of a 1+1 dimensional system will be expressed in terms of conformal data of the CFT describing the universality class where the corresponding system lies.

An important first example of universal behaviour in entanglement-related magnitudes is given by the *entanglement entropy*. For a quantum system in a pure state $|\Psi\rangle$ partitioned into two parts $I$ and $\bar{I}$, subsystem $I$ is described by its reduced density matrix

$$\rho_I = \mathrm{tr}_{\bar{I}} |\Psi\rangle\langle\Psi|, \tag{4.1}$$

and its entanglement entropy is then defined as the von Neumann entropy of $\rho_I$,

$$S = -\mathrm{tr}\, \rho_I \log \rho_I. \tag{4.2}$$

In the case of a 1+1 dimensional critical system, the entanglement entropy has a universal scaling [95, 97, 98]:

$$S \sim \frac{c}{3} \log l_I, \tag{4.3}$$

where $l_I$ is the size of subsystem $I$, and $c$ is the central charge of the underlying CFT. Going further, entanglement entropy is only part of the information contained in the *entanglement spectrum*, defined as the eigenvalues of the entanglement Hamiltonian

$$K_I \equiv -\frac{1}{2\pi} \log \rho_I. \tag{4.4}$$

Entanglement spectra have been extensively studied, and also exhibit an emergent universal structure at criticality, where they reproduce the spectrum of scaling dimensions of a boundary conformal field theory (BCFT) obtained from the CFT that describes the quantum critical point [99, 100, 101, 102, 103].

In this chapter, we take a step further by demonstrating that the eigenvectors of the entanglement Hamiltonian $K_I$ (or equivalently those of the reduced density matrix $\rho_I$) also display emergent universal behaviour for a critical lattice theory, in the form of a nontrivial relation between them and the microscopic Hamiltonian and momentum densities. Specifically, the eigenvectors of $K_I$ can be used as a natural basis to construct an approximate lattice representation of the Virasoro algebra of the corresponding BCFT, where high-weight eigenvectors correspond to low-lying states.

Emergent signatures of universality in critical lattice systems can be used to gather information, such as conformal data, about the universality class of the phase transition they realize. The construction we present allows indeed for the extraction of conformal data, which, however, come out affected by significant finite size effects, so its viability for this particular purpose seems to be limited.

This chapter is organized as follows. In Section 4.2 we review the CFT derivation that motivates our lattice construction: we illustrate the conformal transformation which maps the entanglement Hamiltonian of a finite interval of a CFT to the dilation operator of a BCFT, and compute the transformation of the Virasoro generators. Section 4.3 then introduces our proposed lattice construction in the context of the critical Ising model and presents numerical results as to the accuracy of the approximate Virasoro representation we obtain, computed via the free fermion formalism. We conclude in Section 4.4 with a discussion, and include a brief review of background concepts in the Appendices.

## 4.2 CFT derivation

The long-distance physics of a quantum system at criticality is described by a CFT. Fortunately, CFT is a powerful mathematical tool, which, among others, allows us to perform conformal transformations on the manifold where the theory is defined by path integration, thus relating different objects built from the same theory. In this section we exploit this to relate the reduced density matrix on an interval of the CFT to a semiannulus on the canonical upper half-plane formulation of BCFT (as was done in [100]). This will enable us to compute the form of the Virasoro generators acting on the eigenvectors of the entanglement Hamiltonian as integrals of the stress-energy tensor, which we will then discretize in the following section. Appendices C.1 and C.2 provide brief reviews of CFT and BCFT for the unfamiliar reader.

### 4.2.1 Path integral representation of a reduced density matrix

Consider a general quantum theory of a field $\phi(\tau, x)$ in 2-dimensional Euclidean spacetime $(\tau, x)$, with action functional $S[\phi]$. Its ground state $|0\rangle$ can be prepared, up to normalization, by Euclidean time evolution from $\tau = -\infty$ to $\tau = 0$, and therefore be represented by an Euclidean path integral over the lower half plane

$$\langle \Phi(x)|0\rangle = \int_{\phi(0,x)=\Phi(x)} [D\phi(\tau < 0, x)] e^{-S[\phi]}, \tag{4.5}$$

where $|\Phi(x)\rangle$ is a field eigenstate with spatial field configuration $\Phi(x)$. This is illustrated in Fig. 4.1(a). Similarly, a Euclidean path integral over the upper half plane prepares the Hermitian conjugate of the ground state:

$$\langle 0|\Phi(x)\rangle = \int_{\phi(0,x)=\Phi(x)} [D\phi(\tau > 0, x)] e^{-S[\phi]}. \tag{4.6}$$

To compute the reduced density matrix on a finite interval $I \subset \mathbb{R}$, we trace out the fields on $\bar{I}$, the complement of $I$ (as represented pictorially by Fig. 4.1(b)):

$$\begin{aligned} \langle \Phi_I^-(x^-)|\rho_I|\Phi_I^+(x^+)\rangle &= \int [D\Phi_{\bar{I}}] \langle \Phi_{\bar{I}} \Phi_I^-|0\rangle\langle 0|\Phi_I^+ \Phi_{\bar{I}}\rangle \\ &= \int_{\phi(0^-, x^- \in I) = \Phi_I^-(x^-)}^{\phi(0^+, x^+ \in I) = \Phi_I^+(x^+)} [D\phi(\tau, x)] e^{-S[\phi]}. \end{aligned} \tag{4.7}$$

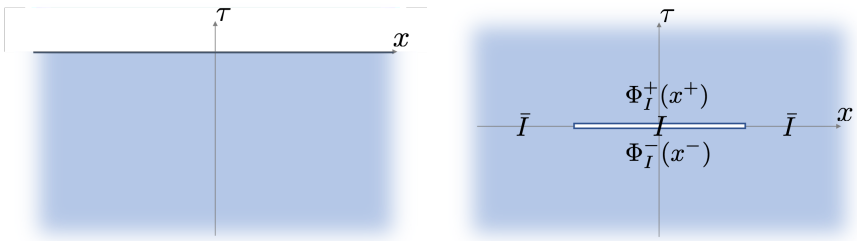


(a) (b)

Figure 4.1: (a) Path integral representation of the ground state $|0\rangle$ of a 1+1-dimensional QFT. (b) The reduced density matrix $\rho_I$ on a finite interval $I$. The field $\phi(\tau, x)$ takes values $\Phi_I^-(x^-)$ and $\Phi_I^+(x^+)$ on the lower and upper edges of the open cut.

The entanglement entropy of $I$ will typically be UV divergent, due to the presence of quantum entanglement at arbitrarily small distances at the boundaries between $I$ and $\bar{I}$. In order to regularize it, we follow [100] and remove small disks of radius $\epsilon$ around the boundaries from the path integral, as displayed in Fig. 4.2. Here $\epsilon$ plays the role of the UV regulator, analogously to, e.g., the lattice constant in a lattice regularization. We assume $\epsilon$ is much smaller than the size of the interval. Note that the boundary conditions on the boundaries of the removed disks are yet to be specified for a complete regularization prescription.

### 4.2.2 Entanglement Hamiltonian of a finite interval in a CFT

In this section, we restrict our attention to a 1+1-dimensional CFT. We show that we can define a Virasoro algebra on the interval $I$, and the generator $L_0$ is affinely related to the entanglement Hamiltonian $K_I$.

Consider the interval $I = (-R, R)$. As we have argued in Sect. 4.2.1, we remove two disks of radius $\epsilon$ ($\epsilon \ll R$) around the two boundary points $-R$ and $R$ to eliminate the UV divergence of the entanglement entropy, and impose some conformal boundary conditions, as shown in Fig. 4.2. For a CFT, the natural boundary conditions are conformal boundary conditions, which are believed to be stable fixed points of the flows of the boundary renormalization group[100]. These boundary conditions determine a universal correction to the entanglement entropy, which is the celebrated Affleck-Ludwig boundary entropy [104].

To exploit the power of the conformal symmetry in 2 dimensions, we use complex

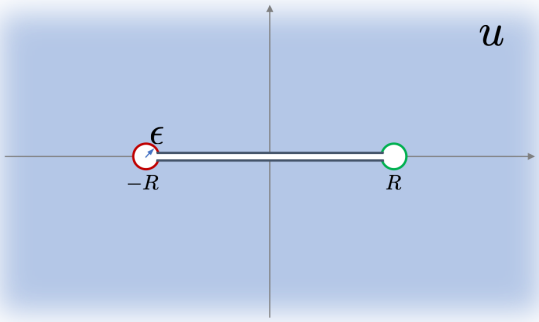


Figure 4.2: The regularized path integral representation of the reduced density matrix $\rho_I$ on a finite interval $I = (-R, R)$ for a 1+1-dimensional CFT. Some conformal boundary conditions are imposed on the red and blue circles.

coordinates $u, \bar{u} = x \pm i\tau$. Applying the conformal transformation

$$w = \log\left(\frac{R+u}{R-u}\right), \tag{4.8}$$

we map the region of the path integral in Fig. 4.2 to a rectangle, with height $2\pi$ and width $2l$, where $l = \log\left(\frac{2R}{\epsilon}\right)$, as shown in Fig. 4.3(a). We can extend the rectangle and define a BCFT on the strip $-l < \mathrm{Re}\, w < l$, so that time flows in the vertical direction. Thus the reduced density matrix $\rho_I$ can be viewed as a thermal state of a Hamiltonian $H_{\alpha\beta}$ on the region $(-l, l)$, where $\alpha$ and $\beta$ represent the corresponding boundary conditions.

We can further apply an exponential map

$$z = i \exp\left(-\frac{i\pi w}{2l}\right), \tag{4.9}$$

so that the BCFT is defined on the upper half-plane of $z$. The boundary conditions $\alpha$ and $\beta$ are imposed on the negative and positive real axis respectively. The region corresponding originally to the reduced density matrix is now a semiannulus comprised between the semicircumferences $|z| = 1$ and $|z| = e^{\pi^2/l}$ (see Fig. 4.3(b)).

The BCFT on the upper half-plane has conformal invariance only if the conformal transformations keep the boundary (the real axis) invariant. The holomorphic and anti-holomorphic transformations are no longer independent, so that only one Virasoro algebra

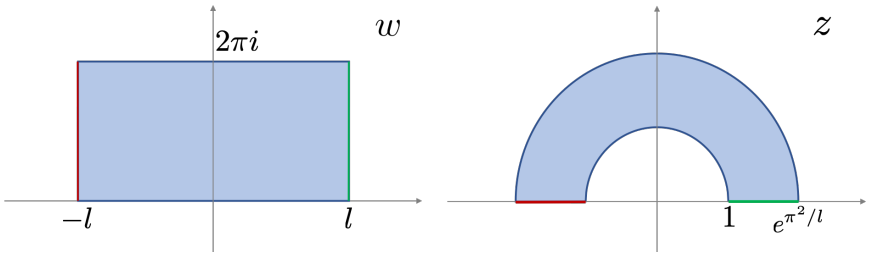


(a) (b)

Figure 4.3: (a) The representation of the reduced density matrix after a conformal transformation $w = \log\left(\frac{R+u}{R-u}\right)$. (b) The representation of the reduced density matrix after a further conformal transformation $z = i\exp(-\frac{i\pi w}{2l})$.

exists. The Virasoro generators $L_n$ in the $z$ coordinates are given by the following (see Appendix C.2):

$$L_n = \frac{1}{2\pi i}\int_{\mathcal{C}} \left[dz\ z^{n+1}T(z) - d\bar{z}\ \bar{z}^{n+1}\bar{T}(\bar{z})\right], \tag{4.10}$$

where the integration contour $\mathcal{C}$ is a semicircle going counterclockwise around the origin.

Applying the aforementioned conformal transformation (4.9), we can transform $L_n$ to the $w$ coordinates (see Appendix C.2 for the full derivation):

$$\begin{aligned} L_n = -\frac{\ell}{\pi^2}\int_{-\ell}^{\ell} dw \Big[ & e^{-\frac{in\pi}{2\ell}(w-\ell)}T(w) \\ & + e^{\frac{in\pi}{2\ell}(w-\ell)}\bar{T}(w)\Big] + \frac{c}{24}\delta_{n,0}. \end{aligned} \tag{4.11}$$

We then apply (4.8) to transform it to the $u$ coordinates (see once again Appendix C.2 for the full derivation):

$$\begin{aligned} L_n = & \frac{c}{24}\left(1+\frac{4\ell^2}{\pi^2}\right)\delta_{n,0} \\ & -\frac{\ell}{\pi^2}\int_{-R+\epsilon}^{R-\epsilon} du \frac{R^2-u^2}{2R}\left\{e^{in\theta(u)}T(u) + e^{-in\theta(u)}\bar{T}(u)\right\}. \end{aligned} \tag{4.12}$$

Here the integration contour is along the real axis, from $-R+\epsilon$ to $R-\epsilon$, and the function $\theta(u)$ is given by

$$\theta(u) = \frac{\pi}{2} - \frac{\pi}{2l}\log\left(\frac{R+u}{R-u}\right), \tag{4.13}$$

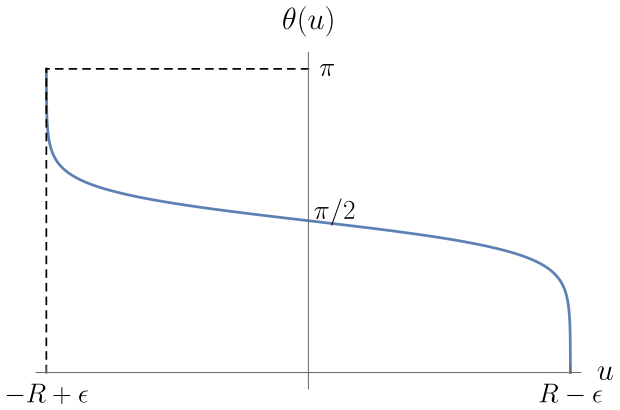


Figure 4.4: Profile $\theta(u)$ for real $u$ and $\epsilon = 10^{-4}R$.

whose profile for real $u$ is shown in Fig. 4.4. The expressions for the Virasoro generators can be rewritten in terms of the Hamiltonian and momentum densities:

$$\begin{aligned} h(x) &= -\frac{1}{2\pi}\left(T(x)+\bar{T}(x)\right) \\ p(x) &= \frac{1}{2\pi}\left(\bar{T}(x)-T(x)\right) \end{aligned} \tag{4.14}$$

resulting in

$$L_0 = \frac{\ell}{\pi R}\int_{-R+\epsilon}^{R-\epsilon} dx\,(R^2-x^2)h(x) + \frac{c}{24} + \frac{c\ell^2}{6\pi^2}, \tag{4.15}$$

and

$$\begin{aligned} L_n = \frac{\ell}{\pi R}\int_{-R+\epsilon}^{R-\epsilon} dx\,\left(R^2-x^2\right)\left[\cos(n\theta(x))h(x)\right. \\ \left. +i\sin(n\theta(x))p(x)\right] \end{aligned} \tag{4.16}$$

for $n \neq 0$.

The entanglement Hamiltonian $K_I$ of the interval $I$ is given by [105, 106]

$$K_I = \int_{-R+\epsilon}^{R-\epsilon} dx \frac{(R^2-x^2)}{2R} h(x). \tag{4.17}$$

Comparing it with the expressions of the Virasoro generators, we find $K_I$ is affinely related to $L_0$:

$$L_0 = \frac{2l}{\pi}K_I + \frac{c}{24} + \frac{c\ell^2}{6\pi^2}. \tag{4.18}$$

As a result, $L_0$ shares eigenvectors with $K_I$ and the reduced density matrix $\rho_I$. The large-weight eigenvectors of $\rho_I$ correspond to the low-lying states of the BCFT. Therefore, the eigenvectors of $\rho_I$ constitute a natural representation basis for the Virasoro algebra, whose generators are represented by Eqs. (4.15)-(4.16).

## 4.3 Emergent Virasoro representation in the critical Ising model

In the previous section we have derived the expression for the Virasoro generators represented on an interval $I$ of a CFT, with the eigenvectors of the reduced density matrix $\rho_I$ providing the natural basis for this representation, i.e., the eigenbasis of the representation of $L_0$. To a certain degree of precision, given by finite size error, this situation should be reproduced in critical lattice models, provided that we find an adequate discrete version of the Virasoro representation. This is because, in the low energy regime, we expect a correspondence between the lattice and continuum frameworks. In this section we show, following a particular example, that this is the case: we build lattice representations of Virasoro generators from the continuous expressions, and compare their action on the eigenvectors of the density matrix (found numerically) with the expected result if the representation were exact.

We will work with the critical quantum Ising model in an infinite one-dimensional lattice with lattice constant 1. Each site of the lattice is occupied by a spin $\frac{1}{2}$ degree of freedom, and the Hamiltonian is given by

$$H = -\frac{1}{2}\sum_{j\in\mathbb{Z}} (X_j X_{j+1} + Z_j) \tag{4.19}$$

where $X_j, Z_j$ are the Pauli operators on site $j$. Note that there is a factor of $\frac{1}{2}$ so that the low-energy excitations have velocity 1. We consider an interval containing $N$ sites, whose boundaries are located at the midpoints between sites, as shown in Fig. 4.5. For the continuum effective formulation, it is then clear that we can set $R = N/2$. The UV regulator $\epsilon$ is not determined a priori. We will determine $\epsilon$ by finite size scaling, as explained later in this section.

The Ising model admits a solution in terms of free fermions, which greatly increases the system sizes we can address for a given computational power. Appendix C.3 gives the details of the computation within this framework. By performing a Jordan-Wigner

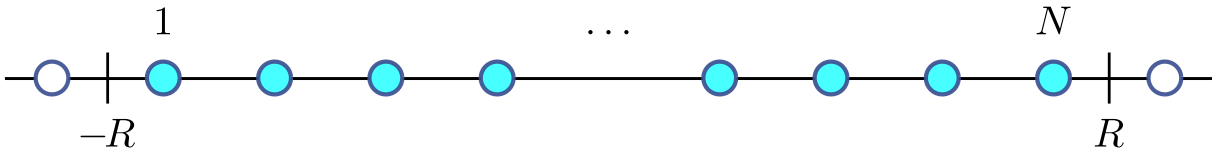


Figure 4.5: The interval whose complement we trace out.

transformation, we map the spin operators $X_j, Y_j, Z_j$ to complex fermion operators $c_j, c_j^\dagger$, which satisfy anticommutation relations

$$\{c_j, c_k\} = \{c_j^\dagger, c_k^\dagger\} = 0, \quad \{c_j, c_k^\dagger\} = \delta_{jk}. \tag{4.20}$$

The RDM of the interval $\rho_I$ can be expressed as a Gaussian thermal state:

$$\rho_I \propto e^{-2\pi \sum_{j=1}^N e_j c_j^\dagger c_j}, \qquad 0 < e_1 < e_2 < \cdots, \tag{4.21}$$

where $\{e_j\}$ is the single particle spectrum of the entanglement Hamiltonian $K_I$. Thus the $2^N$ eigenstates of $\rho_I$ are of the form

$$\left(\prod_{j\in J} c_j^\dagger\right)|0\rangle \qquad J \subseteq \{1, \ldots, N\}, \tag{4.22}$$

where $|0\rangle$ is the vacuum

$$c_j|0\rangle = 0 \qquad j = 1, \ldots, N. \tag{4.23}$$

From Eq. 4.18, we can see that the spectrum of $K_I$ scales with the factor $1/l$. Considering the energy of the first excited state, we have

$$1/e_1 \propto l = \log N - \log \epsilon. \tag{4.24}$$

Therefore, we can compute $e_1$ for various $N$, and find an approximate value for $\epsilon$ by extrapolation, which gives $\epsilon \approx 0.0369$, as shown in Fig. 4.6.

To build the Virasoro generators on the lattice, we use the correspondence between Ising lattice operators and CFT operators established in [107]:

$$\begin{aligned} X_i X_{i+1} &\sim \frac{2}{\pi}\mathbb{1} - h - 0.31831\varepsilon, \\ Z_i &\sim \frac{2}{\pi}\mathbb{1} - h + 0.31831\varepsilon, \\ X_i Y_{i+1} &\sim -2p + 0.1592 i\partial_\tau \varepsilon, \\ Y_i X_{i+1} &\sim 2p + 0.1592 i\partial_\tau \varepsilon, \end{aligned} \tag{4.25}$$

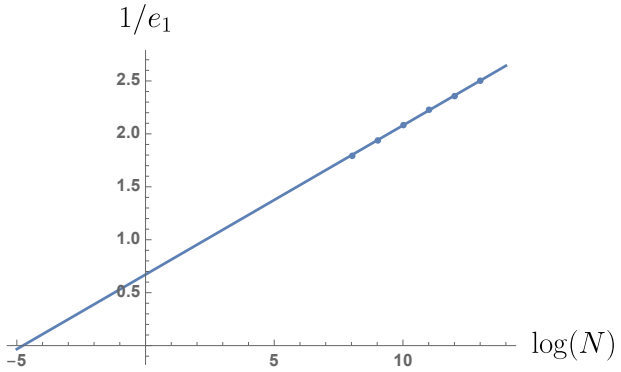


Figure 4.6: We compute $1/e_1$ for $N$=256, 512, 1024, 2048, 4196, 8192. The extrapolation gives an estimate $\epsilon \approx 0.0369$.

where $\varepsilon$ is the energy density operator in Ising CFT. We assign locations $i+\frac{1}{2}$, $i$, $i+\frac{3}{4}$ and $i+\frac{1}{4}$ to the above four operators respectively. Replacing the integrals in Eqs.(4.15)-(4.16) by finite Riemann sums, we obtain the lattice approximations of Virasoro generators $L_n^{\text{lat}}$:

$$\begin{aligned} L_n^{\text{lat}} = \frac{l}{N\pi} \Bigg\{ & -\sum_{j=1}^{N} \left[ \left(N^2/4 - x_j^2\right) \cos\left(n\theta(x_j)\right) Z_j \right] \\ & + \sum_{j=1}^{N-1} \Bigg[ -\left(N^2/4 - x_{j+\frac{1}{2}}^2\right) \cos\left(n\theta(x_{j+\frac{1}{2}})\right) X_j X_{j+1} \\ & - \frac{i}{2} \left(N^2/4 - x_{j+\frac{3}{4}}^2\right) \sin\left(n\theta(x_{j+\frac{3}{4}})\right) X_j Y_{j+1} \\ & + \frac{i}{2} \left(N^2/4 - x_{j+\frac{1}{4}}^2\right) \sin\left(n\theta(x_{j+\frac{1}{4}})\right) Y_j X_{j+1} \Bigg] \Bigg\}, \end{aligned} \tag{4.26}$$

where $x_j = -(N+1)/2 + j$. Note that in the above expression we have ignored constant terms and contribution from $\varepsilon$ terms, which is negligible in the large $N$ limit. These operators can be expressed in a quadratic form in terms of the fermionic operators (see Appendix C.3):

$$L_n^{\text{lat}} = \sum_{jk} \beta_{jk} \mathcal{O}_j^\dagger \mathcal{O}_k \tag{4.27}$$

where $\mathcal{O} = (c_1, \ldots, c_N, c_1^\dagger, \ldots, c_N^\dagger)$ is just a vector with all fermion operators in it. This makes it easy to compute expectation values for these operators.

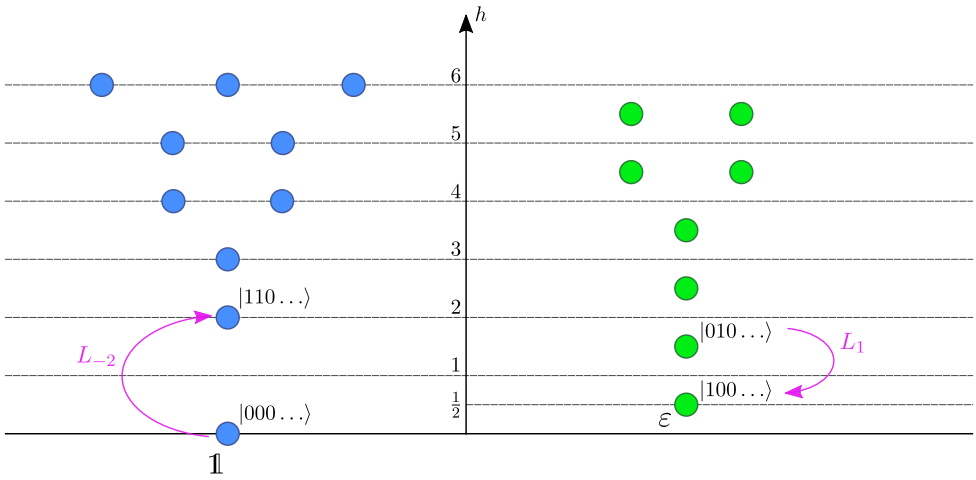


Figure 4.7: Operator content of the Ising CFT with free boundary conditions. The Hilbert space decomposes into the direct sum of two modules, or conformal towers, each of them closed under the action of the Virasoro generators $L_n$. We use the horizontal axis only to resolve degeneracies. Note that in the free fermion language the two towers correspond to the two sectors of different fermion parity.

It has been shown in [103] that the natural entanglement cut of the Ising chain corresponds to free boundary conditions, or the Cardy state $|\sigma\rangle$ in the CFT language. The fusion rule $\sigma \times \sigma = \mathbb{1} + \varepsilon$ indicates that the corresponding operator content contains two primaries: the identity operator $\mathbb{1}$ and the energy operator $\epsilon$, as shown in Fig. 4.7. Now we compute the matrix elements of the lattice operators $L_n^{\text{lat}}$ in the basis of low energy eigenstates of $K_I$, and compare them with the predictions from CFT.

$\underline{L_0^{\text{lat}}}$: We begin with the operator $L_0^{\text{lat}}$, whose low-lying eigenspaces should coincide with those of $\rho_I$. The one-particle spectrum of the free fermion dictates that it should be of the form:

$$L_0 = \sum_k \left(k - \frac{1}{2}\right) c_k^\dagger c_k. \tag{4.28}$$

Indeed, this results in the scaling dimensions depicted in Fig. 4.7, the first few of them being:

$$\begin{aligned} L_0|000\ldots\rangle &= 0, \\ L_0|100\ldots\rangle &= \frac{1}{2}|100\ldots\rangle, \end{aligned}$$

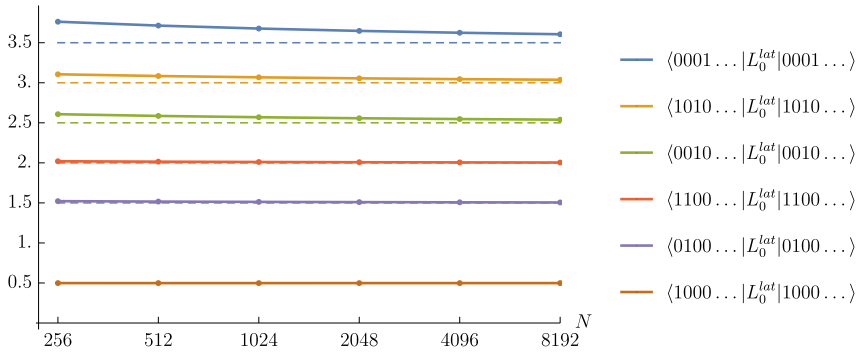


Figure 4.8: The diagonal elements of $L_0^{\text{lat}}$ converge to those of $L_0$(dashed lines) as the system size increases.

$$L_0|010\ldots\rangle = \frac{3}{2}|010\ldots\rangle,$$
$$L_0|110\ldots\rangle = \left(\frac{1}{2}+\frac{3}{2}\right)|110\ldots\rangle,$$

etc. We compute the matrix elements of $L_0^{\text{lat}}$ for different values of $N$, and compare them with those of $L_0$. The resulting matrices are diagonal – just as the matrix form of $L_0$ – up to machine precision. The diagonal elements converge to $L_0$'s as $N$ increases(see Figure 4.8).

$\underline{L_1^{\text{lat}}}$: The expected expression for this generator in terms of the creation-annihilation operators is

$$L_1 = \sum_k k c_k^\dagger c_{k+1} \tag{4.29}$$

When computing the matrix elements of $L_1^{\text{lat}}$ we find that indeed the nonzero matrix elements of $L_1$ are obtained in the large $N$ limit through a very slow convergence (Fig. 4.9). However, we also find some spurious matrix elements that should be zero but are however only order of magnitude smaller than the other ones, at the system sizes we explore. This we interpret as an artifact of the discretization, and indeed those matrix elements decrease as $N$ increases (Fig. 4.10).

$\underline{L_2^{\text{lat}}}$: Again, we can give the expression for the CFT generator in terms of creation - annihilation operators:

$$L_2 = \frac{1}{2}c_1 c_2 + \sum_k \left(k+\frac{1}{2}\right) c_k^\dagger . c_{k+2} \tag{4.30}$$

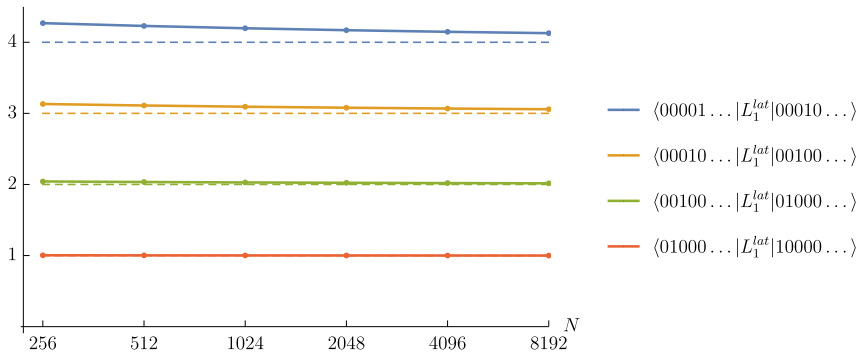


Figure 4.9: The nonzero elements of $L_1^{\text{lat}}$ converge to those of $L_1$(dashed lines) as the system size increases.

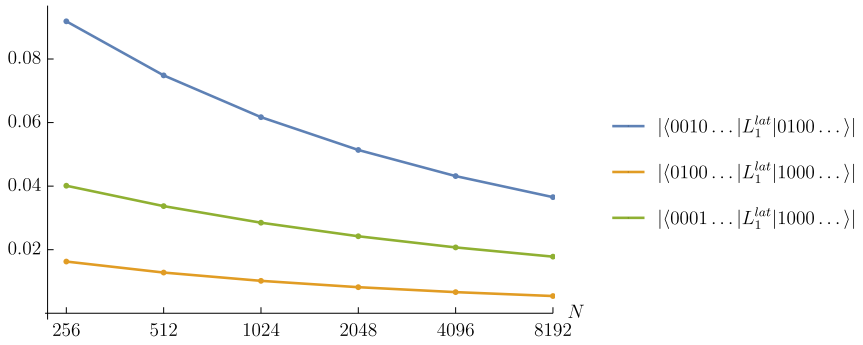


Figure 4.10: Matrix elements of $L_1^{\text{lat}}$ that should be zero.

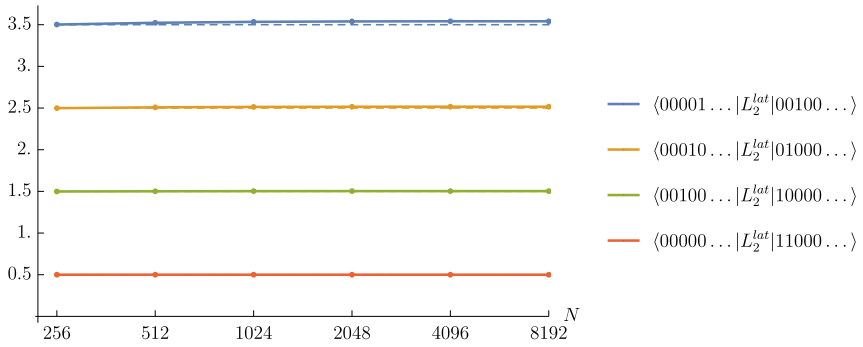


Figure 4.11: The nonzero elements of $L_2^{\text{lat}}$ converge to those of $L_2$(dashed lines) as the system size increases.

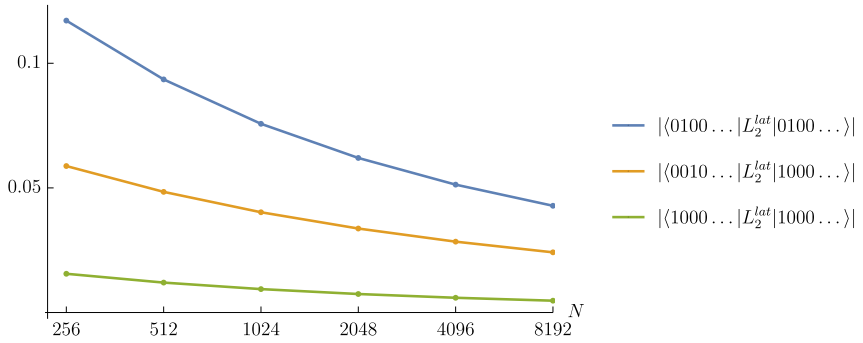


Figure 4.12: Matrix elements of $L_2^{\text{lat}}$ that should be zero.

We compare the matrix elements of this operator to those of our matrix representation. The result is similar to the $n = 1$ case (see Fig. 4.11 and Fig. 4.12). We still observe improvement of the lattice approximation when increasing $N$.

## 4.4 Discussion

Even though the numerical implementation for the Ising model yields approximately correct values for CFT data, it would be hard to turn this into an efficient computational scheme due to the persistence of finite size corrections. Indeed, because of the logarithmic character of the transformation from Fig. 4.3(a), the reduced density matrix of an interval of $N$ sites only constitutes an "effective" number of sites which grows as the logarithm of $N$. Only

systems that admit efficient descriptions of density matrices for high numbers of sites (such as the Ising model, via the free fermion formulation) can be expected to present acceptable finite size errors. For generic models, computationally efficient representations for the ground state, such as those based on Matrix Product States (MPS) are not guaranteed to provide a reliable representation of reduced density matrices, and they require large computational resources to keep correlation lengths longer than few thousand sites with adequate precision.

# Chapter 5

# Non-local Geometry inside Lifshitz Horizon

## 5.1 Introduction

Black hole horizon hosts tensions among basic principles of physics established within the framework of local field theories, and understanding what is behind the horizon may hold the key to the resolution[108, 109, 110, 111, 112]. Given that there is so far no non-perturbative definition of quantum gravity except through the AdS/CFT correspondence[113, 114, 115], it is desired to have an access to the interior of horizon via boundary field theories[116, 117, 118, 119, 120]. However, probing the interior of horizon may require a full microscopic theory of the bulk beyond the local field theory approximation whose validity can not be taken for granted near horizon.

Quantum renormalization group (RG) provides a microscopic prescription to derive holographic duals for general field theories[121, 122, 123]. In quantum RG, renormalization group flow is mapped to a dynamical system, where the action principle replaces classical beta functions. The sources for a subset of operators (called single-trace operators) become dynamical variables whose fluctuations encode the information about all other operators which are not explicitly included in the RG flow. The resulting bulk theory generally includes dynamical gravity[122, 123] and gauge theory[124, 125] because the background metric and gauge field that source the energy-momentum tensor and a conserved current are promoted to dynamical variables. From the bulk perspective, this accounts for the fact that multi-trace operators are generated once bulk fields for single-trace operators are integrated out[126, 127, 128]. Because the complete set of single-trace operators include

operators of all sizes in general, the bulk theory is kinematically non-local[129, 122]. In the presence of non-local dynamical degrees of freedom, locality in the bulk is a feature that is determined dynamically rather than a kinematical structure put in by hand. This provides a natural setting to study horizon within the framework of RG flow.

In quantum RG, horizon corresponds to a Hagedorn-like dynamical phase transition where non-local operators proliferate at a critical RG scale[130]. This is best understood in terms of quantum states defined on spacetime, where RG flow of an action is viewed as a quantum evolution of the corresponding state generated by a coarse graining operator. The coarse graining generator projects the state associated with an action toward a reference state that represents an IR fixed point. Whether the true IR physics of the theory is described by the putative IR fixed point or not is determined by whether the state can be smoothly projected to the reference state or not. Although a local action is mapped to a short-range entangled state, the range of entanglement increases under the RG flow as non-local operators are generated. If the theory is in a gapless phase, the quantum state can not be smoothly projected to a reference state which represents a gapped state. The obstruction manifests itself as a proliferation of non-local operators at a critical RG scale. This marks as a dynamical phase transition whose order parameter is locality (or loss of locality), and the critical point gives rise to a horizon in the bulk.

In an earlier work[130], the correspondence between critical phenomenon and horizon has been demonstrated in a boson model. However, it is not possible to cross the horizon in the boson model because the critical point arises at an infinite RG scale. In this chapter, we study a fermionic model with a nonzero charge density which undergoes a phase transition at a finite RG scale associated with the chemical potential. Since a horizon arises at a finite radial coordinate, one can go through it to reach the interior via RG flow. While the outside of horizon is described by a Lifshitz geometry[131, 132, 133, 134], the interior of the horizon exhibits a non-local geometry which can not be described by a Riemannian manifold. We show that the non-local structure inside the horizon is sensitive not only to the universal long-distance properties of the boundary theory but also to microscopic details.

## 5.2 Holographic dual for the fermionic vector model

We consider a $D$-dimensional fermionic U(N) vector model,

$$\mathcal{S} = \int d\tau d^{D-1}x \left[\bar{\boldsymbol{\psi}}^a \partial_\tau \boldsymbol{\psi}^a + \nabla\bar{\boldsymbol{\psi}}^a \cdot \nabla\boldsymbol{\psi}^a - \mu\, \bar{\boldsymbol{\psi}}^a\boldsymbol{\psi}^a + \frac{\lambda}{N}\,(\bar{\boldsymbol{\psi}}^a \cdot \boldsymbol{\psi}^a)^2\right]. \tag{5.1}$$

Here $\tau$ is the imaginary time, $\bar{\boldsymbol{\psi}}^a$ and $\boldsymbol{\psi}^a$ are Grassmann fields with flavour $a = 1, 2, .., N$. $\mu$ is the chemical potential for the $U(1)$ charge, and $\lambda$ is a quartic coupling. We regularize the field theory on a $D$-dimensional lattice as

$$\mathcal{S} = -\sum_{ij} t_{ij}^{(0)} (\bar{\boldsymbol{\psi}}_i \cdot \boldsymbol{\psi}_j) + m \sum_i (\bar{\boldsymbol{\psi}}_i \cdot \boldsymbol{\psi}_i) + \frac{\lambda}{N} \sum_i (\bar{\boldsymbol{\psi}}_i \cdot \boldsymbol{\psi}_i)^2. \tag{5.2}$$

Here $i, j$ indicate sites on the $D$-dimensional spacetime lattice. $\bar{\boldsymbol{\psi}}_i \cdot \boldsymbol{\psi}_j \equiv \sum_a \bar{\boldsymbol{\psi}}_i^a \boldsymbol{\psi}_j^a$ represents the set of bi-local single-trace operators, and $t_{ij}^{(0)}$'s are hopping amplitudes on the lattice. The local chemical potential can be identified as $\mu_i = \sum_j t_{ij}^{(0)} - m$, where $m > 0$ is assumed. If the hopping is small compared to $m$, the chemical potential is below the bottom of the band, and the system is in the insulating state. On the other hand, a finite charge density is generated and the system becomes a metal when the hopping is large. The system goes through the insulator to metal transition as the magnitude of $t_{ij}^{(0)}$ is increased, as is illustrated in Fig. 5.1. Our goal is to derive the bulk geometry that emerges in each state. For other holographic approaches to related vector models, see Refs. [135, 136, 137, 138, 139, 140, 141, 142, 143, 144, 145, 146, 147, 148, 149].

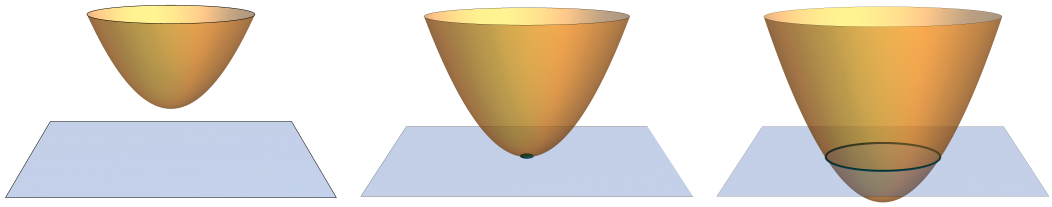

(a) (b) (c)

Figure 5.1: The energy dispersion for (a) insulator, (b) critical point and (c) metal plotted in the two-dimensional momentum space. The dot in (b) represents the bottom of the band which touches the chemical potential at the critical point, and the circle in (c) represents the Fermi surface.

To set up the RG procedure, we divide $\mathcal{S}$ into a reference action and a deformation. The reference action is chosen to be the ultra-local theory which describes the insulating fixed point,

$$\mathcal{S}_0 = m \sum_i (\bar{\boldsymbol{\psi}}_i \cdot \boldsymbol{\psi}_i), \tag{5.3}$$

and the rest is treated as a deformation,

$$\mathcal{S}_1 = -\sum_{ij} t_{ij}^{(0)} (\bar{\boldsymbol{\psi}}_i \cdot \boldsymbol{\psi}_j) + \frac{\lambda}{N} \sum_i (\bar{\boldsymbol{\psi}}_i \cdot \boldsymbol{\psi}_i)^2. \tag{5.4}$$

Following [130], we define quantum states associated with $S_0$ and $S_1$ as

$$\begin{aligned} |S_0\rangle &= \int D\bar{\psi} D\psi \; e^{-S_0[\bar{\psi},\psi]} |\bar{\psi},\psi\rangle, \\ |S_1\rangle &= \int D\bar{\psi} D\psi \; e^{-S_1[\bar{\psi},\psi]} |\bar{\psi},\psi\rangle, \end{aligned} \tag{5.5}$$

where $|\bar{\psi},\psi\rangle$ are the basis states labeled by the Grassmannian fields,

$$|\bar{\psi},\psi\rangle = \prod_{i,a} (1 - \bar{\psi}_i^a c_{1i}^{a\dagger})(1 - \psi_i^a c_{2i}^{a\dagger})|0\rangle. \tag{5.6}$$

The basis states are constructed from a Fock space which can accommodate up to $2N$ auxiliary fermions at each site on the $D$-dimensional spacetime lattice : $c_{1i}^{a\dagger}$ ($c_{2i}^{a\dagger}$) with $a = 1, 2, .., N$ represents the creation operator of the fermions associated with $\bar{\psi}_i^a$ ($\psi_i^a$), and $|0\rangle$ is the vacuum annihilated by $c_{\alpha i}^a$. It is emphasized that the auxiliary fermions occupy sites in the $D$-dimensional *spacetime* lattice, and they are different from the original fermions that live on the $(D-1)$-dimensional space. We define an inner product between quantum states defined in spacetime as

$$\langle \Psi' || \Psi \rangle \equiv \langle \Psi' | O | \Psi \rangle \tag{5.7}$$

with $O \equiv \prod_{i,a} (c_{1i}^{a\dagger} - c_{1i}^a)(c_{2i}^{a\dagger} - c_{2i}^a)$. The inner product is chosen such that the basis states satisfy the orthonormality condition,

$$\langle \psi', \bar{\psi}' || \bar{\psi}, \psi \rangle = \prod_{i,a} \delta(\bar{\psi}_i'^a - \bar{\psi}_i^a) \delta(\psi_i'^a - \psi_i^a), \tag{5.8}$$

where $\langle \psi', \bar{\psi}'|$ is the Hermitian conjugate of $|\psi', \bar{\psi}'\rangle$. Then the partition function is given by the overlap between the two quantum states,

$$Z = \int D\bar{\psi} D\psi \; e^{-S_0[\bar{\psi},\psi] - S_1[\bar{\psi},\psi]} = \langle S_0' || S_1 \rangle, \tag{5.9}$$

where $|S_0'\rangle$ is the complex conjugate of $|S_0\rangle$.

Renormalization group flow can be understood as a quantum evolution of $|S_1\rangle$ generated by an operator $\hat{H}$[130]. Since the partition function is invariant under the coarse-graining transformation,

$$Z = \langle S_0' || S_1 \rangle = \langle S_0' || e^{-dz\hat{H}} | S_1 \rangle, \tag{5.10}$$

where $dz$ is an infinitesimal parameter, the reference state should be annihilated by $\hat{H}$,

$$\hat{H}^\dagger O^\dagger |S_0'\rangle = 0. \tag{5.11}$$

This is equivalent to the statement that $S_0$ represents a fixed point. Because $|S_0'\rangle$ is a direct-product state in spacetime, the coarse graining operator that satisfies Eq. (5.11) is ultra-local,

$$\hat{H} = \sum_{i,a} \left[ -\frac{2}{m} c_{1i}^{a\dagger} c_{2i}^{a\dagger} + c_{1i}^{a} c_{1i}^{a\dagger} + c_{2i}^{a} c_{2i}^{a\dagger} \right]. \tag{5.12}$$

The evolution generated by $\hat{H}$ corresponds to a real space coarse graining in which the mass $m$ is gradually increased such that fluctuations of fields are suppressed at each site[150]. While $\hat{H}$ is not Hermitian, it can be mapped to a Hermitian operator through a similarity transformation as all eigenvalues are real. As the evolution operators are repeatedly inserted between the overlap, $e^{-z\hat{H}}|S_1\rangle$ is gradually projected to the unentangled ground state of $\hat{H}$. Whether the initial state $|S_1\rangle$ can be smoothly projected to the direct product state depends on whether the system belongs to the insulating phase described by the reference action[130].

Now we fix $\lambda$, and label the state associated with the deformation in terms of hopping amplitudes,

$$|t\rangle = \int D\bar{\psi} D\psi \; e^{\sum_{i,j} t_{ij} \bar{\psi}_i \cdot \psi_j - \frac{\lambda}{N} \sum_i (\bar{\psi}_i \cdot \psi_i)^2} |\bar{\psi}, \psi\rangle. \tag{5.13}$$

Apart from the fixed quartic interaction, $|t\rangle$ contains only single-trace hoppings. However, multi-trace operators are generated under the coarse graining evolution. In quantum RG, the multi-trace operators are traded with non-trivial dynamics of the single-trace sources[121, 122, 123]. As a result, the partition function is given by a path integration over the scale dependent single-trace sources $t_{ij}(z)$[150, 130],

$$Z = \lim_{z\to\infty} \langle S_0' || e^{-z\hat{H}} | t^{(0)} \rangle = \int Dt(z) Dt^*(z) \;\; \langle S_0' || t(\infty) \rangle \; e^{-N \int_0^\infty dz \left( t_{ij}^* \partial_z t_{ij} + \mathcal{H}[t^*, t] \right)} \Big|_{t_{ij}(0) = t_{ij}^{(0)}}, \tag{5.14}$$

where $\mathcal{H}[t^*, t]$ is the coherent state representation of the bulk Hamiltonian $\hat{\mathcal{H}}$ given by

$$\begin{aligned}\hat{\mathcal{H}} &= \sum_i \Big[\frac{2}{m}t_{ii} + \frac{4\lambda(-1+\frac{1}{N})}{m}t_{ii}^\dagger - 4\lambda(t_{ii}^\dagger)^2 - \frac{8\lambda^2}{m}(t_{ii}^\dagger)^3\Big] \\ &\quad + \sum_{i,j}\Big[2 + \frac{4\lambda}{m}(t_{ii}^\dagger + t_{jj}^\dagger)\Big]t_{ij}^\dagger t_{ij} - \frac{2}{m}\sum_{i,j,k}\Big[t_{kj}^\dagger t_{ki} t_{ij}\Big]. \end{aligned} \tag{5.15}$$

Here the gauge is fixed so that the speed of coarse graining is uniform in spacetime, and the shift is zero at all $z$[130]. The bi-local fields are the fundamental degrees of freedom in the bulk, which include the metric and higher spin fields. In the Hamiltonian picture, the bi-local fields are promoted to quantum operators : $t_{ij}$ ($t_{ij}^\dagger$) represents the annihilation (creation) operator of quantized link between sites $i$ and $j$. Despite the fact that the original theory is fermionic, the bulk theory is bosonic because there is no U(N) invariant fermionic operator in the theory.

In the large $N$ limit, quantum fluctuations in the RG path are suppressed, and the saddle point approximation becomes reliable. The saddle point equation reads

$$\begin{aligned}\partial_z \bar{t}_{ij} &= -2\Big\{ -\frac{2\lambda\delta_{ij}}{m} - \delta_{ij}[4\lambda + \frac{12\lambda^2}{m}\bar{p}_{ii}]\bar{p}_{ii} + \frac{2\lambda\delta_{ij}}{m}\sum_k(\bar{t}_{ik}\bar{p}_{ik} + \bar{t}_{ki}\bar{p}_{ki}) \\ &\quad + [1 + \frac{2\lambda}{m}(\bar{p}_{ii} + \bar{p}_{jj})]\bar{t}_{ij} - \frac{1}{m}\sum_k \bar{t}_{ik}\bar{t}_{kj}\Big\}, \\ \partial_z \bar{p}_{ij} &= 2\Big\{\frac{\delta_{ij}}{m} + [1 + \frac{2\lambda}{m}(\bar{p}_{ii} + \bar{p}_{jj})]\bar{p}_{ij} - \frac{1}{m}\sum_k(\bar{p}_{ik}\bar{t}_{jk} + \bar{t}_{ki}\bar{p}_{kj})\Big\}. \end{aligned} \tag{5.16}$$

Here $\bar{t}_{ij}(z)$ and $\bar{p}_{ij}(z)$ denote the saddle point configuration of $t_{ij}(z)$ and $t_{ij}^*(z)$, which satisfy the boundary conditions,

$$\bar{t}_{ij}(0) = t_{ij}^{(0)}, \tag{5.17}$$

$$\bar{p}_{ij}(\infty) = \frac{1}{N}\left.\frac{\partial ln\langle S_0'||\bar{t}\rangle}{\partial \bar{t}_{ij}}\right|_{z=\infty}. \tag{5.18}$$

It is noted that $\bar{p}_{ij}$ is not necessarily the complex conjugate of $\bar{t}_{ij}$ at the saddle point. If $t_{ij}^{(0)}$ depends only on $r_i - r_j$, the saddle point solution is also invariant under the translation. In this case, the equations in momentum space are reduced to

$$\partial_z \bar{T}_q = -2\Big\{ -\frac{2\lambda}{m} - \Big[4\lambda + \frac{12\lambda^2}{m}\bar{p}_0\Big]\bar{p}_0 + \frac{4\lambda}{Vm}\sum_{q'}\bar{T}_{q'}\bar{P}_{q'} + \Big[1 + \frac{4\lambda}{m}\bar{p}_0\Big]\bar{T}_q - \frac{1}{m}(\bar{T}_q)^2\Big\}, \tag{5.19}$$

$$\partial_z \bar{P}_q = \frac{2}{m} + 2\Big[1 + \frac{4\lambda}{m}\bar{p}_0\Big]\bar{P}_q - \frac{4}{m}\bar{P}_q\bar{T}_q, \tag{5.20}$$

where $\bar{T}_q = \sum_r \bar{t}_{i+r,i} e^{iqr}$, $\bar{P}_q = \sum_r \bar{p}_{i+r,i} e^{-iqr}$, $\bar{p}_0 \equiv \bar{p}_{ii} = \frac{1}{V}\sum_q \bar{P}_q$. $q = (\omega, k)$ denotes frequency, $\omega$ and $(D-1)$-dimensional momentum, $k = (k_1, k_2, .., k_{D-1})$. The solution to the saddle point equations is given by

$$\bar{P}_q(z) = -\frac{e^{-2z}}{-i\bar{T}_q(0) + m + 2\lambda p_0(0)} - (1 - e^{-2z})\frac{1}{m}, \tag{5.21}$$

$$\bar{T}_q(z) = -\frac{2\lambda}{m} + m + \frac{2\lambda}{m} e^{-2z}(m\bar{p}_0(0) + 1) + \frac{1}{\bar{P}_q(z)}. \tag{5.22}$$

Eqs. (5.21) and (5.22) completely determine the saddle-point configurations of the bulk fields in terms of $\bar{T}_q(0)$, which encodes all the information about the microscopic theory. For example, the $(D-1)$-dimensional hypercubic lattice with a continuous imaginary time gives $\bar{T}_q(0) = -i\omega - 2t\sum_{i=1}^{D-1}\cos(k_i) - \mu$, where $t$ is the nearest neighbor hopping amplitude and $\mu$ is the chemical potential. In general, any local hopping in space can be written in power series of $k$,

$$\bar{T}_q(0) = \bar{T}_0(0) - i\omega - e(k), \tag{5.23}$$

where

$$e(k) = \boldsymbol{k}^2 + \sum_{n=2}^{\infty} \frac{c_{i_1,i_2,..,i_{2n}}}{m^{n-1}} k_{i_1} k_{i_2} .. k_{i_{2n}}. \tag{5.24}$$

Here the chemical potential $\bar{T}_0(0)$ is singled out, and the coefficient of the quadratic term is normalized by rescaling $k$. $c_{i_1,i_2,..,i_{2n}}$ can be independently tuned by further neighbor hoppings on a microscopic lattice. It is assumed that the minimum of the band is $k = 0$, and the lattice respects the parity to allow only even powers of momentum in the dispersion. In terms of $e(k)$, the saddle point solutions are written as

$$\begin{aligned} \bar{P}_q(z) &= -\frac{e^{-2z}}{i\omega + e(k) + \delta} - (1 - e^{-2z})\frac{1}{m}, \\ \bar{T}_q(z) &= -\frac{2\lambda}{m} + m + \frac{2\lambda}{m} e^{-2z}(m\bar{p}_0(0) + 1) - m\frac{i\omega + e(k) + \delta}{(1 - e^{-2z})(i\omega + e(k) + \delta) + me^{-2z}}, \end{aligned} \tag{5.25}$$

where $\delta = -\bar{T}_0(0) + m + 2\lambda\bar{p}_0(0)$ is the gap.

## 5.3 Emergent geometry in the bulk

Because the reference state is ultra-local, there is no background metric in the bulk. The bulk geometry is dynamically determined by the saddle point solution. Since the bulk

theory involves the bi-local fields of all sizes, it is kinematically non-local. A sense of locality emerges only when single-trace sources decay fast enough in spacetime. In this section, we examine the geometry that emerges in the bulk in the insulating phase and in the metallic phase.

### 5.3.1 Insulating phase

To study the behavior of the hopping field in real space, we first transform $\bar{T}_q(z)$ to the time domain,

$$\bar{T}_{\tau,\boldsymbol{k}}(z) = \int \bar{T}_{\omega,k}(z) e^{-i\omega\tau} \frac{d\omega}{2\pi} = \frac{m^2 e^{2z}}{(e^{2z}-1)^2} \Big[ -\theta(\tau)\theta(-E(\boldsymbol{k},z)) + \theta(-\tau)\theta(E(\boldsymbol{k},z)) \Big] e^{E(\boldsymbol{k},z)\tau}, \tag{5.26}$$

where

$$E(\boldsymbol{k},z) = e(k) + \delta + \frac{m}{e^{2z}-1}. \tag{5.27}$$

$\theta(\tau)$ is the theta function, and ultra-local terms are ignored. In the insulating phase with $\delta > 0$, $E(\boldsymbol{k},z)$ is positive for all $k$ and $z$, and the first term on the right hand side of Eq. (5.26) vanishes. Because $E(\boldsymbol{k},z)$ is analytic in $k$, the hopping field decays exponentially in real space at all $z$. For example, for $e(k) = k^2$ the bi-local field in the real space is given by

$$\bar{t}_{i+r,i}(z) = \int \bar{T}_{\tau,\boldsymbol{k}}(z) e^{-i\boldsymbol{k}\cdot\boldsymbol{x}} \frac{d\boldsymbol{k}}{(2\pi)^{d-1}} = \left( \frac{1}{2\sqrt{-\pi\tau}} \right)^{d-1} \frac{m^2 e^{2z}}{(e^{2z}-1)^2} \theta(-\tau) e^{(\delta + \frac{m}{e^{2z}-1})\tau} e^{\frac{\boldsymbol{x}^2}{4\tau}}, \tag{5.28}$$

where $r = (\tau, x)$ with $x = (x_1, x_2, .., x_{D-1})$ representing $(D-1)$-dimensional vector in real space.

Fluctuations of the bi-local fields propagate on the background set by the saddle-point configuration. Therefore, the bulk geometry can be extracted by inspecting the equation of motions obeyed by the fluctuations of the hopping fields around the saddle point,

$$\begin{aligned} \tilde{t}_{ij} &= t_{ij} - \bar{t}_{ij}, \\ \tilde{p}_{ij} &= t^*_{ij} - \bar{p}_{ij}. \end{aligned} \tag{5.29}$$

The quadratic action for the fluctuations is

$$
\begin{aligned}
S_2 = \int dz \Bigg\{ & -4\lambda \sum_i \left(1 + \frac{6\lambda}{m}\bar{p}_0\right) \tilde{p}_{ii}^2 \\
& + \sum_{ij} \left[ \tilde{p}_{ij} \left( \partial_z + 2 + \frac{8\lambda}{m}\bar{p}_0 \right) \tilde{t}_{ij} + \frac{4\lambda}{m} (\tilde{p}_{ii} + \tilde{p}_{jj}) \left( \bar{p}_{ij}\tilde{t}_{ij} + \bar{t}_{ij}\tilde{p}_{ij} \right) \right] \\
& - \frac{2}{m} \sum_{ijk} \left( \bar{p}_{ij}\tilde{t}_{ik}\tilde{t}_{kj} + \bar{t}_{ik}\tilde{p}_{ij}\tilde{t}_{kj} + \bar{t}_{kj}\tilde{p}_{ij}\tilde{t}_{ik} \right) \Bigg\}.
\end{aligned}
\tag{5.30}
$$

To extract the background metric, we focus on the imaginary part of the hopping field $\tilde{t}_{ij}^A = \tilde{t}_{ij} - \tilde{t}_{ij}^*$ which satisfies a simple equation of motion,

$$
\left( \partial_z + 2 + \frac{8\lambda}{m}\bar{p}_0(z) \right) \tilde{t}_{ij}^A - \frac{2}{m} \left( \bar{t}_{ik}\tilde{t}_{kj}^A + \bar{t}_{kj}\tilde{t}_{ik}^A \right) = 0 \tag{5.31}
$$

for $i \neq j$. We take the continuum limit, and define $\tilde{t}_{ij}^A = e^{-2z}\tilde{t}^A(r, r', z)$, where $r$ and $r'$ represent spacetime coordinates $(\tau, \boldsymbol{x})$ and $(\tau', \boldsymbol{x}')$. For large $z$ and $r \neq r'$, the equation of motion becomes

$$
\left[ (m + \delta e^{2z})\partial_z + 4\delta - \frac{2m}{1 - \frac{\partial_\tau + e(\partial_i)}{m e^{-2z} + \delta}} - \frac{2m}{1 - \frac{-\partial'_\tau + e(\partial'_i)}{m e^{-2z} + \delta}} \right] \tilde{t}^A(r, r', z) = 0, \tag{5.32}
$$

where $\partial_i \equiv \frac{\partial}{\partial x_i}$, $\partial'_i \equiv \frac{\partial}{\partial x'_i}$. This can be written in a covariant form,

$$
\begin{aligned}
& \Bigg[ \sqrt{g^{zz}(z)}\partial_z + 4\delta - \frac{2m}{1 - \frac{1}{m}\left( \sqrt{g^{\tau\tau}(z)}\partial_\tau + g^{ij}(z)\partial_i\partial_j + \sum_{n>1} \frac{\tilde{c}_{i_1,..,i_{2n}}(z)}{m^{n-1}} \partial_{i_1}..\partial_{i_{2n}} \right)} \\
& - \frac{2m}{1 - \frac{1}{m}\left( -\sqrt{g^{\tau\tau}(z)}\partial_{\tau'} + g^{ij}(z)\partial'_i\partial'_j + \sum_{n>1} \frac{\tilde{c}_{i_1,..,i_{2n}}(z)}{m^{n-1}} \partial'_{i_1}..\partial'_{i_{2n}} \right)} \Bigg] \tilde{t}^A(r, r', z) = 0,
\end{aligned}
\tag{5.33}
$$

where $\sqrt{g^{zz}}(z) = m + \delta e^{2z}$, $\sqrt{g^{\tau\tau}}(z) = g^{ii}(z) = \frac{m}{m e^{-2z} + \delta}$, $\tilde{c}_{i_1,..,i_{2n}}(z) = \frac{m}{m e^{-2z} + \delta} c_{i_1,..,i_{2n}}$. The bulk metric is identified from the terms up to two derivatives,

$$
ds^2 = \frac{dz^2}{(m + \delta e^{2z})^2} + (e^{-2z} + \delta/m)^2 d\tau^2 + (e^{-2z} + \delta/m) d\boldsymbol{x}^2. \tag{5.34}
$$

$\tilde{c}_{i_1,..,i_{2n}}(z)$ encodes the vacuum expectation values of the higher spin fields in the bulk.

In the insulating phase, the geometry ends at a finite proper distance from the UV boundary,

$$L = \int_0^\infty \frac{dz}{m + \delta e^{2z}} = \frac{log(\frac{m+\delta}{\delta})}{2m}. \tag{5.35}$$

The finite depth in the bulk reflects the fact that the quantum state associated with the action can be smoothly projected to the direct product state through a series of RG transformations with a finite depth. The proper distance in the radial direction measures the "distance" between theories[130].

### 5.3.2 Metallic phase

As the system deviates further from the insulating state with decreasing gap, the depth of the bulk space diverges logarithmically. When the system reaches the critical point at $\delta = 0$, the bulk geometry develops an infinitely long throat with a Lifhistz horizon at $z = \infty$. At the critical point, the metric in Eq. (5.34) becomes the Lifshitz geometry,

$$ds^2 = \frac{dz^2}{m^2} + e^{-4z} d\tau^2 + e^{-2z} d\boldsymbol{x}^2 \tag{5.36}$$

which is invariant under the scaling

$$z \to z + s, \ \tau \to e^{2s}\tau, \ \boldsymbol{x} \to e^s \boldsymbol{x}. \tag{5.37}$$

The dynamical critical exponent $z = 2$ reflects the quadratic dispersion at the bottom of the band in Eq. (5.23). The isometry of the bulk metric is expected from the form of the hopping field in Eq. (5.28) which is invariant under Eq. (5.37) at $\delta = 0$. If one tuned parameters in $t_{ij}$ at UV to make the dispersion to scale as $\bar{T}_q(0) \sim k^{2r}$ at the bottom of the band, the resulting geometry would have the dynamical critical exponent $2r$. It is noted that the higher-derivative terms in Eq. (5.33) are suppressed by the curvature scale in the bulk. For the locality at a shorter length scale in the bulk, there are stringent constraints on field theories[151, 152, 153].

At the critical point, the Lifshitz horizon is located at $z = \infty$. However, the horizon arises at a finite $z$ in the metallic phase. Unlike the bosonic model[130], the chemical potential can be further increased across the bottom of the band. For $\delta < 0$, a Fermi surface forms, and the system becomes a metal. In the metallic phase, the horizon moves to $z_H \equiv \frac{1}{2} log(1 + \frac{m}{-\delta})$ at which $g_{\tau\tau}$ vanishes. Outside the horizon, $E(\boldsymbol{k}, z)$ remains positive for all $k$, and the metric is given by

$$ds^2 = \frac{dz^2}{4m^2(z_H - z)^2} + \frac{4\delta^2}{m^2}(z_H - z)^2 d\tau^2 + \frac{-2\delta}{m}(z_H - z) d\boldsymbol{x}^2 \tag{5.38}$$

for small $z_H - z$ with $z_H >> 1$. The geometry no longer has an isometry associated with a global translation of $z$ because there is a scale represented by $z_H$. However, the space outside the horizon has an isometry associated with rescaling of $z$ toward $z_H$. The isometry becomes manifest in a new coordinate system, $z' = -\frac{1}{2} log(z_H - z)$, $\tau' = -\frac{2\delta}{m}\tau$, $\boldsymbol{x}' = \sqrt{\frac{-2\delta}{m}}\boldsymbol{x}$ in which the metric reduces to the Lifshitz geometry in Eq. (5.36). Although the horizon arises at a finite $z$, the proper distance from the UV boundary to the horizon is still infinite. This is consistent with the fact that the metallic state belongs to a different universality class from the insulating state.

Although the metric near the horizon takes the universal form, the background higher-spin fields, $\tilde{c}_{i_1,..,i_{2n}}(z)$ encodes the information about the microscopic details such as the underlying lattice and further neighbor hoppings in the boundary theory[154, 155, 156]. The effect of the higher-spin hair on the fluctuation fields in Eq. (5.33) depends on the momentum of the fluctuation mode and the radial position. For a mode whose proper momentum is $O(\sqrt{m})$ at radial location $z$, the $2n$ derivative term in Eq. (5.33) scales as $(z_H - z)^{(n-1)}$. The bulk equation of motion for the low-momentum modes becomes insensitive to the higher-spin fields close to the horizon. However, in order to extract the full low-energy data from the UV boundary, one should probe particle-hole excitations whose momenta are comparable to the Fermi momentum $k_F \sim \sqrt{|\delta|}$. If a mode with proper momentum $k_F$ at the UV boundary is sent into the bulk, the momentum is blue shifted to $p \sim \sqrt{\frac{|\delta|}{(z_H - z)}}$ near the horizon. For these modes, the higher-derivative terms in Eq. (5.33) remain important. The sensitivity to the higher-spin fields signifies the need to go beyond the low-energy effective theory near the horizon. This is expected because the shape of Fermi surface is determined not just by the quadratic term but also by all higher-order terms in Eq. (5.24).

The horizon corresponds to a phase transition at which the length scale associated with the size of bi-local operators in $e^{-z\hat{H}}|S_1\rangle$ diverges[130]. At the horizon, the range of hoping diverges, which causes the collapse of the $D$-dimensional spacetime volume. Zero area of the horizon is consistent with the fact that the metal has zero entropy density. Although the Lifshitz horizon has a divergent tidal force, nothing stops one from being able to continue the coarse graining procedure across the horizon. Inside the horizon with $z > z_H$, $E(\boldsymbol{k}, z)$ changes sign as a function of momentum. The discontinuity of $\bar{T}_{\tau,\boldsymbol{k}}(z)$ as a function of momentum results in a slow decay of the hopping field along with a Friedel-like oscillation in real space. The specific form of the oscillation depends on the microscopic details. From now on, we will focus on the dispersion $e(k) = k^2$, which describes the spherical Fermi surface. For different shapes of Fermi surface, the structure inside the horizon will be different. For the spherical Fermi surface, $E(\boldsymbol{k}, z)$ becomes negative for

$|k| < k_s(z) \equiv \sqrt{-\delta - \frac{m}{e^{2z}-1}}$,

$$\bar{T}_{\tau,\boldsymbol{k}}(z) = \frac{m^2 e^{2z}}{(e^{2z}-1)^2}\Big( -\theta(\tau)\theta(k_s(z)-|\boldsymbol{k}|) + \theta(-\tau)\theta(|\boldsymbol{k}|-k_s(z))\Big) e^{(\boldsymbol{k}^2 - k_s(z)^2)\tau}. \tag{5.39}$$

The asymptotic behavior of $\bar{t}_{i+r,i}$ as a function of $r = (\tau, x)$ is given by $t_{i+r,i} = \frac{m^2 e^{2z}}{(e^{2z}-1)^2} K(\tau, x; z)$, where

$$K(\tau, x; z) \sim -\frac{\cos(k_s(z)x)}{2\pi k_s(z)\tau} + O(\frac{1}{\tau^2}), \text{ as } |\tau| \to \infty, \tag{5.40}$$

$$K(\tau, x; z) \sim -\frac{\sin(k_s(z)x)}{\pi x} + O(\frac{1}{x^2}), \text{ as } x \to \infty \tag{5.41}$$

in $D = 1+1$, and

$$K(\tau, x; z) \sim -\frac{1}{8\pi^2\tau} \cdot J_0(k_s(z)|x|) + O(\frac{1}{\tau^2}), \text{ as } |\tau| \to \infty, \tag{5.42}$$

$$K(\tau, x; z) \sim -\sqrt{\frac{k_s(z)}{2\pi^3|\boldsymbol{x}|^3}} \cdot \sin(k_s(z)|\boldsymbol{x}| - \frac{\pi}{4}) + O(|\boldsymbol{x}|^{-\frac{5}{2}}), \text{ as } \boldsymbol{x} \to \infty \tag{5.43}$$

in $D = 2+1$, where $J_0(x)$ is the 0th order Bessel function of the first kind.

Inside the horizon, the saddle point configuration of the hopping field decays in a power-law as a function of $r$. The hopping field sets a non-local background on which fluctuation fields propagate according to Eq. (5.31). In the large $z$ limit, the equation of motion for $\tilde{t}^A(\tau, x, \tau', x', z)$ becomes

$$\begin{aligned}(me^{2z}\ \partial_z + 4m)\tilde{t}^A(\tau, x, \tau', x', z) - 2m^2 \int d\tau_1 dx_1\ K(\tau-\tau_1, x-x_1; z)\ \tilde{t}^A(\tau_1, x_1, \tau', x', z) \\ - 2m^2 \int d\tau_1' dx_1'\ \tilde{t}^A(\tau, x, \tau_1', x_1', z)\ K(\tau_1'-\tau', x_1'-x'; z) = 0,\end{aligned} \tag{5.44}$$

where the asymptotic behavior of $K(\tau, x; z)$ is given in Eqs.(5.40)-(5.43). The non-local saddle point configuration allows the bi-local fields to jump to far sites in the $D$-dimensional spacetime. This implies that the space inside the horizon can not be described by a local geometry.

The wavevector for the Friedel-like oscillation at radial position $z$ is given by $k_s(z)$, which gradually increases from 0 at $z_H$ to the true Fermi momentum $k_F = \sqrt{-\delta}$ in the large $z$ limit. $k_s(z)$ can be regarded as the size of the Fermi surface with a $z$-dependent chemical potential $\mu(z) = -\delta - \frac{m}{e^{2z}-1}$. As $z$ increases from the horizon, the bulk effectively scans

through the occupied states from the bottom of the band to the Fermi level. Therefore, the non-local structure inside the horizon is determined by the full dispersion below the Fermi surface. The region deep inside the horizon keeps the data on the low-energy modes close to the Fermi surface. Different metals have different non-local structures in the large $z$ limit because the Fermi liquids have infinitely many marginal deformations, including the shape of the Fermi surface. On the other hand, the region close to the horizon in the interior is sensitive to the occupied states below the Fermi surface, which is not part of the universal low-energy data of the boundary theory. A change in the shape of the band below the Fermi surface that does not involve a change near the Fermi surface does affect the wavevector of the oscillation near the horizon. This implies that the interior of the horizon keeps not only the universal low-energy data of the theory but also non-universal microscopic information of the boundary field theory.

## 5.4 Summary and Discussion

In this chapter, we apply the quantum renormalization group to construct the holographic dual of the fermionic $U(N)$ vector model with a nonzero charge density. The bulk equations of motion are exactly solved in the large $N$ limit to derive the geometries that emerge in different phases of the model. In the insulating phase, the bulk geometry caps off at a finite proper distance in the radial direction. At the critical point between the metal to insulator phase transition, the proper size in the radial direction diverges, which results in a Lifshitz geometry in the bulk. In the metallic phase, the Lifshitz horizon moves to a finite radial coordinate. The geometry outside of the Lifshitz horizon carries a higher-spin hair determined by microscopic hopping amplitudes of the boundary theory. On the other hand, the interior of the horizon is characterized by an algebraic non-locality, and can not be described by a Riemannian geometry. Certain microscopic data of the boundary field theory is encoded in the interior of the horizon.

The non-local space inside the horizon is different from a globally connected network where every site is connected to every other sites with an equal hopping strength. Since the non-local connectivity decreases as a power-law in coordinate distance, there is still a sense in which certain points are 'closer' than other points to a given point. However, this notion of distance can not be captured within the framework of Riemannian geometry. In order to define a notion of distance in this space, one might rewrite the non-local kernel in Eq. (5.44) as

$$K(\tau, x) = \tilde{K}(\tau, x) e^{-md(\tau-\tau_1, x-x_1)}, \tag{5.45}$$

where $\tilde{K}(\tau, x)$ is a function which captures the modulation in the sign of the hopping function with $|\tilde{K}(\tau, x)| \sim 1$ and $d(\tau, x)$ is a function that measures physical distance. The idea behind this is to define the physical distance by insisting that the kernel in the kinetic term decays exponentially. This agrees with the geodesic distance measured by the metric in Eq. (5.38) outside the horizon, but the definition is general enough to be applicable to the region inside the horizon. Because the hopping amplitude decays in power-law in Eq. (5.41) and Eq. (5.43), the distance between two points increases only logarithmically in coordinate, e.g. $d(x, y) \sim \frac{1}{m} \log |x - y|$. No metric on a Riemannian manifold can reproduce the distance function of this form. One way of obtaining such distance function is by embedding the space in a higher dimensional Riemannian space, and define the distance between two points on the original space in terms of geodesics that can go through the higher dimensional space. For example, the logarithmic distance function can be obtained from the geodesic distance between points on the boundary of a hyperbolic space (see Fig. 5.2). The non-local geometry is 'anomalous' in that distance function can be realized from a local metric only through a higher-dimensional space.

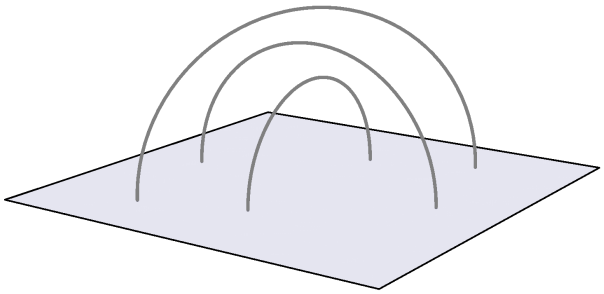

Figure 5.2: Examples of geodesics in the three-dimensional hyperbolic space $\mathbf{H}_3$. The shortest geodesic distances between two points on the plane scales logarithmically in the coordinate distance in the plane.

For $D > 2$, the metallic state becomes unstable against superconductivity at an energy scale which is exponentially small in $N$. As a result, the geometry for the metallic state becomes unstable once quantum fluctuations are included in the bulk. However, this should not be the case for all metals. If one breaks the parity and the time-reversal symmetry, one can have a Fermi liquid state without perturbative superconducting instability. The geometries dual to those stable metals are expected to exhibit similar non-local structures behind the horizon.

Since we use the imaginary time formalism in this study, the bulk theory captures only

the ground state of the theory. It shows how bulk geometry depends on the microscopic information of the ground state determined by Hamiltonian. It will be interesting to extend this to the real time formalism to understand the dependence of bulk geometry on state and Hamiltonian separately.

# References


[1] Q. Hu, G. Vidal, *Spacetime symmetries and conformal data in the continuous multi-scale entanglement renormalization ansatz*, Phys. Rev. Lett. 119, 010603 (2017), arxiv:1703.04798

[2] Q. Hu, A. Franco-Rubio, G. Vidal, *Continuous tensor network renormalization for quantum fields*, arxiv:1809.05176

[3] Q. Hu, S. Lee, *Non-local geometry inside Lifshitz horizon*, J. High Energ. Phys. 2017, 56 (2017), arxiv:1809.05176

[4] P. W. Anderson, *More is different*, Science 177(4047):393–396, 1972.

[5] G. Evenbly, G. Vidal, *Algorithms for entanglement renormalization*, Phys. Rev. B. 79(14):144108, 2009.

[6] M. B. Hastings, *Solving gapped hamiltonians locally*, Phys. Rev. B. 73(8):085115, 2006.

[7] S. Östlund, S. Rommer, *Thermodynamic limit of density matrix renormalization*, Phys. Rev. Lett. 75(19):3537, 1995.

[8] Robert NC Pfeifer, Glen Evenbly, and Guifré Vidal. *Entanglement renormalization, scale invariance, and quantum criticality*, Phys. Rev. A 79(4):040301, 2009.

[9] G. Vidal. *Entanglement renormalization*, Phys. Rev. Lett. 99(22):220405, 2007.

[10] S. R. White. *Density matrix formulation for quantum renormalization groups*, Phys. Rev. Lett. 69(19):2863, 1992.

[11] S. R. White. *Density-matrix algorithms for quantum renormalization groups*, Phys. Rev. B 48(14):10345, 1993.

[12] B. Czech, L. Lamprou, S. McCandlish, and J. Sully, *Integral geometry and holography*, Journal of High Energy Physics, 2015(10):175, 2015.

[13] R. S. Kunkolienkar and K. Banerjee. *Towards a ds/mera correspondence*, International Journal of Modern Physics D, 26(13):1750143, 2017.

[14] Masamichi Miyaji and Tadashi Takayanagi. *Surface/state correspondence as a generalized holography*, Progress of Theoretical and Experimental Physics, 2015(7):073B03, 2015.

[15] Ali Mollabashi, Masahiro Naozaki, Shinsei Ryu, and Tadashi Takayanagi. *Holographic geometry of cmera for quantum quenches and finite temperature*, Journal of High Energy Physics, 2014(3):98, 2014.

[16] Masahiro Nozaki, Shinsei Ryu, and Tadashi Takayanagi. *Holographic geometry of entanglement renormalization in quantum field theories*, Journal of High Energy Physics, 2012(10):193, 2012.

[17] Sukhwinder Singh. *Tensor network state correspondence and holography*, Physical Review D, 97(2):026012, 2018.

[18] Brian Swingle. *Constructing holographic spacetimes using entanglement renormalization*, arXiv preprint arXiv:1209.3304, 2012.

[19] Brian Swingle. *Entanglement renormalization and holography*, Physical Review D, 86(6):065007, 2012.

[20] Christoph Brockt, Jutho Haegeman, David Jennings, Tobias J Osborne, and Frank Verstraete. *The continuum limit of a tensor network: a path integral representation*, arXiv preprint arXiv:1210.5401, 2012.

[21] G. Evenbly, G. Vidal, *Tensor network renormalization*, Phys. Rev. Lett. 115(18):180405, 2015.

[22] Mark Fannes, Bruno Nachtergaele, and Reinhard F Werner. *Finitely correlated states on quantum spin chains*, Communications in mathematical physics, 144(3):443–490, 1992.

[23] Jutho Haegeman, J Ignacio Cirac, Tobias J Osborne, Henri Verschelde, and Frank Verstraete. *Applying the variational principle to (1+ 1)-dimensional quantum field theories*, Physical review letters, 105(25):251601, 2010.

[24] Jutho Haegeman, J Ignacio Cirac, Tobias J Osborne, and Frank Verstraete. *Calculus of continuous matrix product states*, Physical Review B, 88(8):085118, 2013.

[25] David Jennings, Christoph Brockt, Jutho Haegeman, Tobias J Osborne, and Frank Verstraete. *Continuum tensor network field states, path integral representations and the encoding of spatial symmetries*, arXiv preprint arXiv:1212.3833, 2012.

[26] Michael Levin and Cody P Nave. *Tensor renormalization group approach to two-dimensional classical lattice models*, Physical review letters, 99(12):120601, 2007.

[27] Frank Verstraete and J Ignacio Cirac. *Renormalization algorithms for quantum-many body systems in two and higher dimensions*, arXiv preprint cond-mat/0407066, 2004.

[28] Frank Verstraete and J Ignacio Cirac. *Continuous matrix product states for quantum fields*, Physical review letters, 104(19):190405, 2010.

[29] G. Vidal, *Entanglement renormalization*, Phys. Rev. Let. 99, 220405 (2007), arXiv: cond-mat/0512165; *A class of quantum many-body states that can be efficiently simulated*, Phys. Rev. Lett. 101, 110501 (2008), arXiv: quant-ph/0610099.

[30] M. Aguado, G. Vidal, *Entanglement renormalization and topological order*, Phys. Rev. Lett. 100, 070404 (2008), arXiv: 0712.0348. R. Koenig, B.W. Reichardt, G. Vidal, *Exact entanglement renormalization for string-net models*, Phys. Rev. B 79, 195123 (2009), arXiv: 0806.4583.

[31] V. Giovannetti, S. Montangero, R. Fazio, *Quantum multiscale entanglement renormalization channels*, Phys. Rev. Lett. 101, 180503 (2008), arXiv:0804.0520

[32] R.N.C. Pfeifer, G. Evenbly and G. Vidal, *Entanglement renormalization, scale invariance, and quantum criticality*, Phys. Rev. A 79(4), 040301(R) (2009), arXiv: 0810.0580.

[33] G. Evenbly and G. Vidal, *Quantum Criticality with the Multi-scale Entanglement Renormalization Ansatz*, chapter in "Strongly Correlated Systems, Numerical Methods", edited by Adolfo Avella and Ferdinando Mancini (Springer Series in Solid-State Sciences volume 176, Springer 2013); arXiv: 1109.5334.

[34] L.P. Kadanoff, *Scaling Laws for Ising Models Near Tc*, Physics (Long Island City, N.Y.) 2, 263 (1966). K.G. Wilson, *Renormalization group methods*, Adv. Math., Volume 16, Issue 2, Pages 170-186 (1975). K.G. Wilson, *The renormalization group: Critical phenomena and the Kondo problem* Rev. Mod. Phys. 47, 773 (1975)

[35] B. Swingle, *Entanglement Renormalization and Holography*, Phys. Rev. D 86, 065007 (2012), arXiv:0905.1317. B. Swingle, *Constructing holographic spacetimes using entanglement renormalization*, arXiv:1209.3304.

[36] C. Beny, *Causal structure of the entanglement renormalization ansatz*, New J. Phys. 15 (2013) 023020, arXiv:1110.4872. H. Matsueda, M. Ishihara and Y. Hashizume, *Tensor Network and Black Hole*, Phys. Rev. D 87, (2013) 066002, arXiv:1208.0206. T. Hartman and J. Maldacena, *Time Evolution of Entanglement Entropy from Black Hole Interiors*, JHEP 05(2013) 014, arXiv:1303.1080 J. Molina-Vilaplana, J. Prior, *Entanglement, Tensor Networks and Black Hole Horizons*, Gen. Relativ. Gravit (2014)46:1823, arXiv:1403.5395 G. Evenbly, G. Vidal, *Tensor network states and geometry* J. Stat. Phys. (2011) 145:891-918, arXiv:1106.1082. M. Miyaji, T. Takayanagi, Prog. Theor. Exp. Phys. (2015) 073B03, *Surface/State Correspondence as a Generalized Holography* arXiv:1503.03542. X.-L. Qi, *Exact holographic mapping and emergent spacetime geometry*, arXiv:1309.6282. N. Bao, C. Cao, S. M. Carroll, A. Chatwin-Davies, N. Hunter-Jones, J. Pollack and G. N. Remmen, *Consistency Conditions for an AdS/MERA Correspondence* Phys. Rev. D 91, 125036 (2015), arXiv:1504.06632. R.S. Kunkolienkar, K. Banerjee, *Towards a dS/MERA correspondence*, arXiv:1611.08581.

[37] B. Czech, L. Lamprou, S.l McCandlish, and J. Sully, *Tensor Networks from Kinematic Space*, 10.1007/JHEP07 (2016) 100, arXiv:1512.01548. B. Czech, P.H. Nguyen, S. Swaminathan *A defect in holographic interpretations of tensor networks*, arXiv:1612.05698.

[38] J.M. Maldacena, *The Large N Limit of Superconformal Field Theories and Supergravity*, Adv. Theor. Math. Phys.2:231-252 (1998), arXiv:hep-th/9711200.

[39] G. Evenbly, G. Vidal *Tensor network renormalization yields the multi-scale entanglement renormalization ansatz*, Phys. Rev. Lett. 115, 200401 (2015), arXiv:1502.05385

[40] A.J. Ferris, D. Poulin *Tensor Networks and Quantum Error Correction* Phys. Rev. Lett. 113, 030501 (2014), arXiv:1312.4578, A. J. Ferris, D. Poulin, Branching MERA codes: a natural extension of polar codes, arXiv:1312.4575

[41] C. Beny, *Deep learning and the renormalization group* arXiv:1301.3124 E.M. Stoudenmire, D.J. Schwab *Supervised Learning with Quantum-Inspired Tensor Networks*, Advances in Neural Information Processing Systems 29, 4799 (2016), arXiv:1605.05775.

[42] A.A. Belavin, A.M. Polyakov, and A.B. Zamolodchikov, *Infinite conformal symmetry in two-dimensional quantum field theory*, Nucl. Phys. B241 (1984) 333-380.

[43] J. L. Cardy, *Conformal invariance and universality in finite-size scaling*, J. Phys. A 17, L385 (1984).

[44] P. DiFrancesco, P. Mathieu, and D. Senechal, Conformal Field Theory, Springer, New York (1997).

[45] To make things worse, on the lattice MERA does not exactly reproduce discrete translation and rotation symmetry, which is only recovered approximately after optimizing the ansatz.

[46] Jutho Haegeman, Tobias J. Osborne, Henri Verschelde, Frank Verstraete, *Entanglement renormalization for quantum fields*, Phys. Rev. Lett. 110, 100402 (2013), arXiv:1102.5524. The cMERA for a 1+1 free massless boson was described at the end of the supplementary material of arXiv:1102.5524v1, not available in the journal version.

[47] J.S. Cotler, J. Molina-Vilaplana, M.T. Mueller *cMERA for Interacting Fields* arXiv:1612.02427.

[48] Masahiro Nozaki, Shinsei Ryu, Tadashi Takayanagi, *Holographic Geometry of Entanglement Renormalization in Quantum Field Theories*, JHEP10(2012)193, arXiv:1208.3469. A. Mollabashi, M. Nozaki, S. Ryu, T. Takayanagi, *Holographic Geometry of cMERA for Quantum Quenches and Finite Temperature* JHEP03(2014)098, arXiv:1311.6095. M. Miyaji, T. Takayanagi, K. Watanabe *From Path Integrals to Tensor Networks for AdS/CFT* arXiv:1609.04645. M. Miyaji, T. Numasawa, N. Shiba, T. Takayanagi, K. Watanabe *cMERA as Surface/State Correspondence in AdS/CFT* Phys. Rev. Lett. 115, 171602 (2015), arXiv:1506.01353.

[49] X. Wen, G.Y. Cho, P.L.S. Lopes, Y.Gu, X.-L. Qi, S. Ryu *Holographic Entanglement Renormalization of Topological Insulators* Phys. Rev. B 94, 075124 (2016), arXiv:1605.07199.

[50] M. E. Peskin, D. V. Schroeder, An Introduction to Quantum Field Theory, Westview Press, 1995.

[51] A. Franco-Rubio, G. Vidal. *Entanglement and correlations in the continuous multiscale entanglement renormalization ansatz*, J. High Energ. Phys. 2017(12):129, 2017.

[52] Right and left moving fields are the Lorentzian version of holomorphic and antiholomorphic fields in Euclidean CFT [44].

[53] For general $x$ the conditions relating to dilations and boosts read $-i[D^\Lambda, O^\Lambda_\alpha(x)] = (x\partial_x + \Delta_\alpha)\, O^\Lambda_\alpha(x)$ and $-i[B^\Lambda, O^\Lambda_\alpha(x)] = s_\alpha O^\Lambda_\alpha(x) - i\, x[H^\Lambda, O^\Lambda_\alpha(x)]$ for boosts. A version of the first condition was already mentioned in Ref. [81]. We note, however, that the discussion in Ref. [81] referred to the limit $\Lambda \to \infty$, whereas here we are concerned with the finite $\Lambda$ case.

[54] W. Rudin, *Functional Analysis* (2nd ed.), McGraw–Hill, ISBN 0-07-054236-8, 1991. Chan, Youn-Sha, et al, *Finite part integrals and hypersingular kernels* Adv. Dyn. Syst 14.S2 (2007): 264-269.

[55] L.P. Kadanoff *Scaling laws for Ising models near $T_c$*, Physics (Long Island City, N.Y.) 2, 263 (1966).

[56] K.G. Wilson, *Group and Critical Phenomena. I. Renormalization Group and the Kadanoff Scaling Picture*, Phys. Rev. B 4, 3174 (1971). *Renormalization Group and Critical Phenomena. II. Phase-Space Cell Analysis of Critical Behavior*, Phys. Rev. B 4, 3184 (1971). *The renormalization group: critical phenomena and the Kondo problem* Rev. Mod. Phys. 47, 773 (1975).

[57] M. Levin, C. P. Nave *Tensor renormalization group approach to 2D classical lattice models* Phys. Rev. Lett. 99, 120601 (2007), arXiv:cond-mat/0611687.

[58] H.-H. Zhao, Z.-Y. Xie, Q.-N. Chen, Z.-C. Wei, J. W. Cai, T. Xiang, *Renormalization of tensor-network states*, Phys. Rev. B 81, 174411 (2010), arXiv:1002.1405.

[59] Z.-Y. Xie, H.-C. Jiang, Q.-N. Chen, Z.-Y. Weng, T. Xiang, *Second Renormalization of Tensor-Network States* Phys. Rev. Lett. 103:160601 (2009), arXiv:0809.0182.

[60] Z.-C. Gu, X.-G.Wen *Tensor-Entanglement-Filtering Renormalization Approach and Symmetry Protected Topological Order*, Phys. Rev. B 80, 155131 (2009), arXiv:0903.1069.

[61] H. C. Jiang, Z. Y. Weng, T. Xiang *Accurate determination of tensor network state of quantum lattice models in two dimensions*, Phys. Rev. Lett. 101, 090603 (2008), arXiv:0806.3719.

[62] Z.-C. Gu, M. Levin, X.-G. Wen, *Tensor-entanglement renormalization group approach as a unified method for symmetry breaking and topological phase transitions* Phys. Rev. B 78, 205116 (2008), arXiv:0806.3509.

[63] B. Dittrich, F. C. Eckert, M. Martin-Benito, *Coarse graining methods for spin net and spin foam models*, New J. Phys. 14 035008 (2012), arXiv:1109.4927.

[64] G. Evenbly, G. Vidal, *Tensor network renormalization*, Phys. Rev. Lett. 115 (18), 180405 (2015), arXiv:1412.0732.

[65] G. Evenbly, G. Vidal *Tensor network renormalization yields the multi-scale entanglement renormalization ansatz*, Phys. Rev. Lett. 115, 200401 (2015), arXiv:1502.05385

[66] G. Evenbly, *Algorithms for tensor network renormalization* Phys. Rev. B 95, 045117 (2017), arXiv:1509.07484.

[67] G. Evenbly, G. Vidal *Local scale transformations on the lattice with tensor network renormalization*, Phys. Rev. Lett. 116, 040401 (2016), arXiv:1510.00689.

[68] S. Yang, Z.-C. Gu, and X.-G. Wen, *Loop Optimization for Tensor Network Renormalization*, Phys. Rev. Lett. 118, 110504 (2017), arXiv:1512.04938.

[69] L. Ying. *Tensor Network Skeletonization*, Multiscale Model. Sim. 15-4 pp. 1423-1447 (2017), arXiv:1607.00050.

[70] M. Bal, M. Marien, J. Haegeman, and F. Verstraete, *Renormalization group flows of Hamiltonians using tensor networks*, Phys. Rev. Lett. 118, 250602 (2017), arXiv:1703.00365.

[71] M. Hauru, C. Delcamp, S. Mizera, *Renormalization of tensor networks using graph independent local truncations*, Phys. Rev. B 97, 045111 (2018), arXiv:1709.07460.

[72] P. Ginsparg, *Applied Conformal Field Theory*, arXiv:hep-th/9108028 (1988).

[73] P. Di Francesco, P. Mathieu, and D. Senechal, *Conformal Field Theory* (Springer, New York, 2012).

[74] M. Henkel, *Conformal Invariance and Critical Phenomena*, (Springer, New York, 1999).

[75] M. Miyaji, T. Takayanagi, K. Watanabe, *From Path Integrals to Tensor Networks for AdS/CFT*, Phys. Rev. D 95, 066004 (2017), arXiv:1609.04645.

[76] P. Caputa, N. Kundu, M. Miyaji, T. Takayanagi, K. Watanabe, *Anti-de Sitter Space from Optimization of Path Integrals in Conformal Field Theories*, Phys. Rev. Lett. 119, 071602 (2017), arXiv:1703.00456.

[77] P. Caputa, N. Kundu, M. Miyaji, T. Takayanagi, K. Watanabe, *Liouville Action as Path-Integral Complexity: From Continuous Tensor Networks to AdS/CFT*, JHEP 11(2017)097, arXiv:1706.07056.

[78] B. Czech, *Einstein's equations from Varying Complexity*, Phys. Rev. Lett. 120, 031601 (2018), arXiv:1706.00965.

[79] G. Vidal, *Entanglement renormalization*, Phys. Rev. Let. 99, 220405 (2007), arXiv:cond-mat/0512165.

[80] G. Vidal, *A class of quantum many-body states that can be efficiently simulated*, Phys. Rev. Lett. 101, 110501 (2008), arXiv: quant-ph/0610099.

[81] J. Haegeman, T. J. Osborne, H. Verschelde and F. Verstraete, *Entanglement Renormalization for Quantum Fields in Real Space*, Phys. Rev. Lett., 110, 100402 (2013), arxiv:1102.5524

[82] A. Franco-Rubio, G. Vidal, *Entanglement and correlations in the continuous multiscale entanglement renormalization ansatz*, JHEP 2017 (12), 129, arxiv:1706.02841.

[83] A. Mollabashi, M. Naozaki, S. Ryu and T. Takayanagi, *Holographic geometry of cMERA for quantum quenches and finite temperature*, JHEP (2014) 2014: 98, arxiv:1311.6095.

[84] M. Nozaki, S. Ryu and T. Takayanagi, *Holographic geometry of entanglement renormalization in quantum field theories*, JHEP (2012) 2012: 10, arxiv:1208.3469.

[85] J. Molina-Vilaplana, *Information geometry of entanglement renormalization for free quantum fields*, JHEP (2015) 2015:2 (mar, 2015), arxiv:1503.07699.

[86] J. Molina-Vilaplana, *Entanglement renormalization and two dimensional string theory*, Phys. Lett. B 755 (2016) 421-425, arxiv:1510.09020.

[87] M. Miyaji, S. Ryu, T. Takayanagi and X. Wen, *Boundary states as holographic duals of trivial spacetimes*, JHEP (2015) 2015: 152, arxiv:1412.6226.

[88] M. Miyaji, T. Numasawa, N. Shiba, T. Takayanagi, K. Watanabe, *cMERA as Surface/State Correspondence in AdS/CFT*, Phys. Rev. Lett. 115, 171602 (2015), arXiv:1506.01353.

[89] M. Miyaji and T. Takayanagi, *Surface/state correspondence as a generalized holography*, Progress of Theoretical and Experimental Physics 2015 (mar, 2015) , arxiv:1503.03542.

[90] X. Wen, G. Y. Cho, P. L. S. Lopes, Y. Gu, X. L. Qi and S. Ryu, *Holographic entanglement renormalization of topological insulators*, Phys. Rev. B 94, 075124 (2016), arxiv:1605.07199.

[91] J. R. Fliss, R. G. Leigh and O. Parrikar, *Unitary Networks from the Exact Renormalization of Wave Functionals*, Phys. Rev. D 95, 126001 (2017), arxiv:1609.03493.

[92] We expect a scale-dependent $K_s$ to be generically required in order to generate a proper RG flow. However, in the simple example of a massive free boson the scale-independent $K_\star$ suffices.

[93] The proposed extension of TNR to the continuum is based on explicitly preserving rotation invariance (in Euclidean spacetime), which requires introducing isotropic smearing of the fields. Alternative extensions of TNR to the continuum are possible using anisotropic smearing. In the limit of strong anisotropy, namely when the smearing affects only the space direction while keeping the fields local in the time direction, we obtain a version of cTNR where it is still straightforward to define a Hilbert space on time slices. There the cMERA appears naturally when using cTNR to coarse-grain an Euclidean path integral with an open (constant time) boundary, exactly as it occurs in the lattice [65].

[94] A. Tilloy, J.I. Cirac, *Continuous Tensor Network States for Quantum Fields*, arXiv:1808.00976

[95] G. Vidal, J. I. Latorre, E. Rico and A. Kitaev, Entanglement in quantum critical phenomena, Phys. Rev. Lett. **90**, 227902 (2003) doi:10.1103/PhysRevLett.90.227902 [quant-ph/0211074].

[96] A. A. Belavin, A. M. Polyakov and A. B. Zamolodchikov, *Infinite Conformal Symmetry in Two-Dimensional Quantum Field Theory*, Nucl. Phys. B **241**, 333 (1984). doi:10.1016/0550-3213(84)90052-X

[97] C. Holzhey, F. Larsen and F. Wilczek, *Geometric and renormalized entropy in conformal field theory*, Nucl. Phys. B **424**, 443 (1994) doi:10.1016/0550-3213(94)90402-2 [hep-th/9403108].

[98] P. Calabrese and J. L. Cardy, *Entanglement entropy and quantum field theory*, J. Stat. Mech. **0406**, P06002 (2004) doi:10.1088/1742-5468/2004/06/P06002 [hep-th/0405152].

[99] A. M. Läuchli, *Operator content of real-space entanglement spectra at conformal critical points*, arXiv:1303.0741 [cond-mat.stat-mech].

[100] J. Cardy and E. Tonni, *Entanglement hamiltonians in two-dimensional conformal field theory*, J. Stat. Mech. **1612**, no. 12, 123103 (2016) doi:10.1088/1742-5468/2016/12/123103 [arXiv:1608.01283 [cond-mat.stat-mech]].

[101] G. Y. Cho, AWW Ludwig, and S. Ryu. Universal entanglement spectra of gapped one-dimensional field theories. Physical Review B, 95(11):115122, 2017.

[102] H. Li and FDM Haldane. Entanglement spectrum as a generalization of entanglement entropy: Identification of topological order in non-abelian fractional quantum hall effect states. Physical review letters, 101(1):010504, 2008.

[103] K. Ohmori and Y. Tachikawa. Physics at the entangling surface. Journal of Statistical Mechanics: Theory and Experiment, 2015(4):P04010, 2015.

[104] I. Affleck and AWW Ludwig. Universal noninteger "ground-state degeneracy"in critical quantum systems. Physical Review Letters, 67(2):161, 1991.

[105] H. Casini, M. Huerta, and R. C. Myers. Towards a derivation of holographic entanglement entropy. Journal of High Energy Physics, 2011(5):36, 2011.

[106] P. D. Hislop and R. Longo. Modular structure of the local algebras associated with the free massless scalar field theory. Communications in Mathematical Physics, 84(1):71–85, 1982.

[107] Y. Zou, A. Milsted, and G. Vidal. Conformal fields and operator product expansion in critical quantum spin chains. Physical Review Letters, 124(4):040604, 2020.

[108] S. W. Hawking, *Particle creation by black holes*, Communications in Mathematical Physics **43** (1975), no. 3 199–220.

[109] G. 't Hooft, *The black hole interpretation of string theory*, *Nuclear Physics B* **335** (1990), no. 1 138 – 154.

[110] L. Susskind, L. Thorlacius, and J. Uglum, *The stretched horizon and black hole complementarity*, Phys. Rev. D **48** (Oct, 1993) 3743–3761.

[111] S. D. Mathur, *The information paradox: a pedagogical introduction*, *Classical and Quantum Gravity* **26** (2009), no. 22 224001.

[112] A. Almheiri, D. Marolf, J. Polchinski, and J. Sully, *Black holes: complementarity or firewalls?*, Journal of High Energy Physics **2013** (2013), no. 2 1–20.

[113] J. M. Maldacena, *The Large N limit of superconformal field theories and supergravity*, Int.J.Theor.Phys. **38** (1999) 1113–1133, [hep-th/9711200].

[114] E. Witten, *Anti-de Sitter space and holography*, *Adv.Theor.Math.Phys.* **2** (1998) 253–291, [hep-th/9802150].

[115] S. Gubser, I. R. Klebanov, and A. M. Polyakov, *Gauge theory correlators from non-critical string theory*, Phys.Lett. **B428** (1998) 105–114, [hep-th/9802109].

[116] P. Kraus, H. Ooguri, and S. Shenker, *Inside the horizon with ads/cft*, Phys. Rev. D **67** (Jun, 2003) 124022.

[117] A. Hamilton, D. Kabat, G. Lifschytz, and D. A. Lowe, *Local bulk operators in ads/cft correspondence: A holographic description of the black hole interior*, Phys. Rev. D **75** (May, 2007) 106001.

[118] K. Papadodimas and S. Raju, *An infalling observer in ads/cft*, *Journal of High Energy Physics* **2013** (2013), no. 10 212.

[119] D. Kabat and G. Lifschytz, *Finite n and the failure of bulk locality: black holes in ads/cft*, Journal of High Energy Physics **2014** (2014), no. 9 77.

[120] K. Papadodimas and S. Raju, *Black hole interior in the holographic correspondence and the information paradox*, Phys. Rev. Lett. **112** (Feb, 2014) 051301.

[121] S.-S. Lee, *Holographic Matter: Deconfined String at Criticality*, *Nucl.Phys.* **B862** (2012) 781–820, [arXiv:1108.2253].

[122] S.-S. Lee, *Background independent holographic description : From matrix field theory to quantum gravity*, JHEP **1210** (2012) 160, [arXiv:1204.1780].

[123] S.-S. Lee, *Quantum Renormalization Group and Holography*, JHEP **1401** (2014) 076, [arXiv:1305.3908].

[124] Y. Nakayama, *Vector beta function*, International Journal of Modern Physics A **28** (2013), no. 31 1350166, [http://www.worldscientific.com/doi/pdf/10.1142/S0217751X13501662].

[125] G. Bednik, *Construction of holographic duals for quantum field theories with global symmetries from quantum renormalization group*, MSc thesis, McMaster University (May, 2014).

[126] I. Heemskerk and J. Polchinski, *Holographic and Wilsonian Renormalization Groups*, JHEP **1106** (2011) 031, [arXiv:1010.1264].

[127] T. Faulkner, H. Liu, and M. Rangamani, *Integrating out geometry: holographic Wilsonian RG and the membrane paradigm*, Journal of High Energy Physics **8** (Aug., 2011) 51, [arXiv:1010.4036].

[128] E. Kiritsis, *Lorentz violation, gravity, dissipation and holography*, Journal of High Energy Physics **1** (Jan., 2013) 30, [arXiv:1207.2325].

[129] D. Marolf, *Emergent Gravity Requires Kinematic Nonlocality*, *Physical Review Letters* **114** (Jan., 2015) 031104, [arXiv:1409.2509].

[130] S.-S. Lee, *Horizon as critical phenomenon*, Journal of High Energy Physics **2016** (2016), no. 9 44.

[131] S. Kachru, X. Liu, and M. Mulligan, *Gravity duals of lifshitz-like fixed points*, Phys. Rev. D **78** (Nov, 2008) 106005.

[132] K. Balasubramanian and K. Narayan, *Lifshitz spacetimes from ads null and cosmological solutions*, Journal of High Energy Physics **2010** (2010), no. 8 1–27.

[133] A. Donos and J. P. Gauntlett, *Lifshitz solutions of D=10 and D=11 supergravity*, Journal of High Energy Physics **12** (Dec., 2010) 2, [arXiv:1008.2062].

[134] S. Harrison, S. Kachru, and H. Wang, *Resolving Lifshitz Horizons*, ArXiv e-prints (Feb., 2012) [arXiv:1202.6635].

[135] I. R. Klebanov and A. M. Polyakov, *AdS dual of the critical O( N) vector model*, Physics Letters B **550** (Dec., 2002) 213–219, [hep-th/0210114].

[136] S. R. Das and A. Jevicki, *Large N collective fields and holography*, Phys.Rev. **D68** (2003) 044011, [hep-th/0304093].

[137] R. d. M. Koch, A. Jevicki, K. Jin, and J. P. Rodrigues, *$AdS_4/CFT_3$ Construction from Collective Fields*, Phys.Rev. **D83** (2011) 025006, [arXiv:1008.0633].

[138] M. R. Douglas, L. Mazzucato, and S. S. Razamat, *Holographic dual of free field theory*, Phys.Rev. **D83** (2011) 071701, [arXiv:1011.4926].

[139] L. A. Pando Zayas and C. Peng, *Toward a Higher-Spin Dual of Interacting Field Theories*, ArXiv e-prints (Mar., 2013) [arXiv:1303.6641].

[140] R. G. Leigh, O. Parrikar, and A. B. Weiss, *Holographic geometry of the renormalization group and higher spin symmetries*, Phys.Rev. **D89** (2014), no. 10 106012, [arXiv:1402.1430].

[141] R. G. Leigh, O. Parrikar, and A. B. Weiss, *Exact renormalization group and higher-spin holography*, Phys.Rev. **D91** (Jan., 2015) 026002, [arXiv:1407.4574].

[142] E. Mintun and J. Polchinski, *Higher Spin Holography, RG, and the Light Cone*, ArXiv e-prints (Nov., 2014) [arXiv:1411.3151].

[143] M. A. Vasiliev, *Higher spin gauge theories in four-dimensions, three-dimensions, and two-dimensions*, Int.J.Mod.Phys. **D5** (1996) 763–797, [hep-th/9611024].

[144] M. A. Vasiliev, *Higher spin gauge theories: Star product and AdS space*, hep-th/9910096.

[145] S. Giombi and X. Yin, *Higher Spin Gauge Theory and Holography: The Three-Point Functions*, JHEP **1009** (2010) 115, [arXiv:0912.3462].

[146] M. Vasiliev, *Nonlinear equations for symmetric massless higher spin fields in (A)dS(d)*, Phys.Lett. **B567** (2003) 139–151, [hep-th/0304049].

[147] J. Maldacena and A. Zhiboedov, *Constraining Conformal Field Theories with A Higher Spin Symmetry*, J.Phys. **A46** (2013) 214011, [arXiv:1112.1016].

[148] J. Maldacena and A. Zhiboedov, *Constraining conformal field theories with a slightly broken higher spin symmetry*, Class.Quant.Grav. **30** (2013) 104003, [arXiv:1204.3882].

[149] I. Sachs, *Higher spin versus renormalization group equations*, *Phys.Rev.* **D90** (Oct., 2014) 085003, [arXiv:1306.6654].

[150] P. Lunts, S. Bhattacharjee, J. Miller, E. Schnetter, Y. B. Kim, and S.-S. Lee, *Ab initio holography*, Journal of High Energy Physics **2015** (2015), no. 8 1–45.

[151] I. Heemskerk, J. Penedones, J. Polchinski, and J. Sully, *Holography from Conformal Field Theory*, JHEP **0910** (2009) 079, [arXiv:0907.0151].

[152] Y. Nakayama, *Local renormalization group functions from quantum renormalization group and holographic bulk locality*, Journal of High Energy Physics **2015** (2015), no. 6 92.

[153] V. Shyam, *General Covariance from the Quantum Renormalization Group*, ArXiv e-prints (Nov., 2016) [arXiv:1611.05315].

[154] S. Mathur, *The fuzzball proposal for black holes: an elementary review*, Fortschritte der Physik **53** (2005), no. 7-8 793–827.

[155] D. Grumiller, A. Pérez, S. Prohazka, D. Tempo, and R. Troncoso, *Higher spin black holes with soft hair*, Journal of High Energy Physics **2016** (2016), no. 10 119.

[156] S. W. Hawking, M. J. Perry, and A. Strominger, *Soft hair on black holes*, Phys. Rev. Lett. **116** (Jun, 2016) 231301.

# APPENDICES

# Appendix A

# Appendices for Chapter 2

This chapter consists of four sections that provide further details on the cMERA discussed in the main text and review basic background material on conformal field theory.

Section A.1 discusses the *entangling evolution in scale* picture of cMERA for a 1+1 free boson CFT and explains how to obtain an alternative characterization of the cMERA state $|\Psi^\Lambda\rangle$ in terms of fixed point linear constraints. Section A.2 expands on a specific choice of quasi-local entangler $K$ (in terms of a Gaussian function $g(k)$) and analyses the smeared field operators $\phi^\Lambda(x)$ and $\pi^\Lambda(x)$ that results from it. Sections A.3 and A.4 take a step back and review several aspects of conformal field theory in 1+1 dimensions that are relevant to the current discussion but do not involve cMERA. Sect. A.3 discusses different ways in which a 1+1 CFT can be quantized while Sect. A.4 provides more details on the 1+1 free boson CFT.

## A.1 Entangling evolution in scale

The Gaussian cMERA state $|\Psi^\Lambda\rangle$ for the ground state $|\Psi\rangle$ is defined in terms of an entangling evolution in scale, which for the case of a 1+1 free boson CFT is determined by a function $g(k)$. In this section we discuss an alternative characterization of the same Gaussian cMERA $|\Psi^\Lambda\rangle$ in terms of the linear constraints it satisfies. These linear constraints are specified by a function $\alpha(k)$. We derive a (fixed point) differential equation for $\alpha(k)$, which is written in terms of the function $g(k)$, and produce a formal solution for each $g(k)$, which allows us to write constraints on both $\alpha(k)$ and $g(k)$. We also derive and solve a partial differential equation for the function $\alpha_s(k)$ that describes the linear constraints

fulfilled by the Gaussian state $|\Psi^\Lambda(s)\rangle$ resulting from the entangling evolution. In this way we can connect the initial product state $|\Lambda\rangle$ of the entangling evolution with its fixed point state $|\Psi^\Lambda\rangle$. Finally, we show that the cMERA momentum operator $P^\Lambda$ equals the CFT momentum operator $P$, whereas the cMERA dilation operator $D^\Lambda$ equals the generator of the entangling evolution $L+K$.

The authors thank Mr. Yijian Zou, *private communication*, for pointing out how to build a solution $\alpha_s(k)$ for the partial differential equation from each solution $\alpha(k)$ of the fixed point differential equation.

### A.1.1 Scale invariant cMERA as a fixed point of an entangling evolution

Let us start by recalling the original characterization/definition of the cMERA state $|\Psi^\Lambda\rangle$ from Ref. [81] as the result of an entangling evolution. When the target state $|\Psi\rangle$ is the ground state of a CFT, we expect that the generator $L+K$ of the entangling evolution can be chosen to be scale independent, in which case we can write

$$|\Psi^\Lambda\rangle = \lim_{s\to\infty} e^{-is(L+K)}|\Lambda\rangle, \tag{A.1}$$

and thus regards $|\Psi^\Lambda\rangle$ as the fixed point of an infinitely long unitary evolution generated by $L+K$ acting on an initial product state $|\Lambda\rangle$. For a free, relativistic, massless boson in 1+1 dimensions, operators $L$ and $K$ can be chosen to be quadratic and they read

$$L \equiv \frac{1}{2}\int dk \Big[\pi(-k)(k\partial_k + \frac{1}{2})\phi(k) + h.c.\Big], \tag{A.2}$$

$$K \equiv \frac{1}{2}\int dk\; g(k)\big[\pi(-k)\phi(k) + h.c.\big]. \tag{A.3}$$

The non-relativistic scaling operator $L$, which generates scale transformations in a non-relativistic theory, acts on the fields as

$$-i[L,\phi(k)] = -\left(k\partial_k + \frac{1}{2}\right)\phi(k), \tag{A.4}$$

$$-i[L,\pi(k)] = -\left(k\partial_k + \frac{1}{2}\right)\pi(k). \tag{A.5}$$

Thus, under a finite transformation by $e^{-isL}$ we have

$$\phi(k) \to e^{-\frac{s}{2}}\phi(e^{-s}k), \quad \pi(k) \to e^{-\frac{s}{2}}\pi(e^{-s}k). \tag{A.6}$$

On the other hand, following Ref. [81], we parametrize the entangler $K$ by a function $g(k)$ subject to a number of conditions that will be discussed later on. This function $g(k)$ contains the variational parameters of the Gaussian cMERA state $|\Psi^\Lambda\rangle$. Here we will not attempt to optimize the function $g(k)$, but will assume instead that it is given to us and will focus on exploring the resulting fixed point state $|\Psi^\Lambda\rangle$.

### A.1.2 Product state $|\Lambda\rangle$

The product state $|\Lambda\rangle$ from which the entangling evolution starts is a Gaussian state that is completely characterized by the set of linear constraints

$$\left(\sqrt{\frac{\Lambda}{2}}\phi(k) + \frac{i}{\sqrt{2\Lambda}}\pi(k)\right)|\Lambda\rangle = 0, \quad \forall k. \tag{A.7}$$

To see that $|\Lambda\rangle$ is indeed a product state, notice that Eq. A.7 is equivalent, through a Fourier transform, to

$$\left(\sqrt{\frac{\Lambda}{2}}\phi(x) + \frac{i}{\sqrt{2\Lambda}}\pi(x)\right)|\Lambda\rangle = 0, \quad \forall x. \tag{A.8}$$

That is, $|\Lambda\rangle$ is annihilated at each point $x$ in real space by a linear constraint that only involves $\phi(x)$ and $\pi(x)$ on that point, so that the field mode attached to point $x$ is in a pure state and thus unentangled from the rest of field modes.

From Eqs. A.4-A.5 it follows that

$$-i\left[L, \sqrt{\frac{\Lambda}{2}}\phi(k) + \frac{i}{\sqrt{2\Lambda}}\pi(k)\right] \tag{A.9}$$

$$= -\left(k\partial_k + \frac{1}{2}\right)\left(\sqrt{\frac{\Lambda}{2}}\phi(k) + \frac{i}{\sqrt{2\Lambda}}\pi(k)\right), \tag{A.10}$$

and therefore $L|\Lambda\rangle \propto |\Lambda\rangle$. (Indeed, using the above commutator and Eq. A.7 it can be easily checked that the state $L|\Lambda\rangle$ is also annihilated by the same linear constraints as $|\Lambda\rangle$, which implies that it must be proportional to $|\Lambda\rangle$.) We conclude that $|\Lambda\rangle$ is a fixed point of an evolution generated by $L$ alone, that is $e^{-isL}|\Lambda\rangle \propto |\Lambda\rangle$.

### A.1.3 CFT ground state $|\Psi\rangle$

We would like to produce a cMERA state $|\Psi^\Lambda\rangle$ that approximates the target state $|\Psi\rangle$, which in our case is the ground state of a CFT. Specifically, for the massless Klein Gordon Hamiltonian the ground state is completely characterized by a different set of linear constraints, namely

$$\left(\sqrt{\frac{|k|}{2}}\phi(k)+\frac{i}{\sqrt{2|k|}}\pi(k)\right)|\Psi\rangle=0,\quad\forall k. \tag{A.11}$$

An important symmetry of the CFT ground state $|\Psi\rangle$ is its invariance under scale transformations or dilations, as generated by the CFT dilation operator $D$ (named relativistic scaling operator $L'$ in Ref. [81]), that is

$$D\equiv\frac{1}{2}\int dk\Big[\pi(-k)(k\partial_k+1)\phi(k)+h.c.\Big]. \tag{A.12}$$

The dilation generator $D$ acts on the field operators as

$$-i[D,\phi(k)] = -(k\partial_k+1)\,\phi(k), \tag{A.13}$$
$$-i[D,\pi(k)] = -(k\partial_k+0)\,\pi(k). \tag{A.14}$$

Thus, under a finite transformation $e^{-isD}$ we have

$$\phi(k)\to e^{-s}\phi(e^{-s}k),\quad \pi(k)\to\pi(e^{-s}k). \tag{A.15}$$

Eqs. A.13-A.14 can be seen to imply that

$$-i\left[D,\sqrt{\frac{|k|}{2}}\phi(k)+\frac{i}{\sqrt{2|k|}}\pi(k)\right] \tag{A.16}$$
$$=-\left(k\partial_k+\frac{1}{2}\right)\left(\sqrt{\frac{|k|}{2}}\phi(k)+\frac{i}{\sqrt{2|k|}}\pi(k)\right), \tag{A.17}$$

so that, the state $D|\Psi\rangle$ fulfils the same set of linear constraints as $|\Psi\rangle$ and thus $D|\Psi\rangle\propto|\Psi\rangle$. As a matter of fact, if we had used normal ordering in the definition of $D$, as we will do in Sect. A.4, we would then have $D|\Psi\rangle=0$.

### A.1.4 Complete set of linear constraints for the scale invariant Gaussian cMERA $|\Psi^\Lambda\rangle$

As any Gaussian state, such as the product state $|\Lambda\rangle$ or the target CFT ground state $|\Psi\rangle$, the cMERA state $|\Psi^\Lambda\rangle$ can also be completely characterized by a set of linear constraints, which read

$$\left(\sqrt{\frac{\alpha(k)}{2}}\phi(k) + \frac{i}{\sqrt{2\alpha(k)}}\pi(k)\right)|\Psi^\Lambda\rangle = 0, \quad \forall k. \tag{A.18}$$

Our goal in this section is to determine the function $\alpha(k) \geq 0$ that corresponds to a specific $g(k)$ (that is, a specific choice of entangler $K$). For this purpose, we introduce a family of Gaussian states,

$$|\Psi^\Lambda(s)\rangle \equiv e^{-is(L+K)}|\Lambda\rangle, \tag{A.19}$$

labelled by the scale parameter $s$. For each value of $s$, $|\Psi^\Lambda(s)\rangle$ is also a Gaussian state, characterized by the set of linear constraints

$$\left(\sqrt{\frac{\alpha_s(k)}{2}}\phi(k) + \frac{i}{\sqrt{2\alpha_s(k)}}\pi(k)\right)|\Psi^\Lambda(s)\rangle = 0, \tag{A.20}$$

which are given by the function $\alpha_s(k)$.

### A.1.5 Differential equation for $\alpha_s(k)$

Let us obtain a differential equation for the evolution of $\alpha_s(k)$ as a function of $s$. Given that under an evolution by $L + K$ the field operators $\phi(k)$ and $\pi(k)$ change as

$$\frac{\partial}{\partial s}\phi_s(k) = -i\left[L + K, \phi_s(k)\right], \tag{A.21}$$

$$\frac{\partial}{\partial s}\pi_s(k) = -i\left[L + K, \pi_s(k)\right], \tag{A.22}$$

where

$$-i\left[L + K, \phi(k)\right] = -\left(k\partial_k + \frac{1}{2} + g(k)\right)\phi(k), \tag{A.23}$$

$$-i\left[L + K, \pi(k)\right] = -\left(k\partial_k + \frac{1}{2} - g(k)\right)\pi(k), \tag{A.24}$$

we consider a solution for $\phi_s(k)$ and $\pi_s(k)$ of the form

$$\phi_s(k) = \sqrt{\frac{\alpha_s(e^{-s}k)}{\Lambda}} e^{-s/2} \phi(e^{-s}k), \tag{A.25}$$

$$\pi_s(k) = \sqrt{\frac{\Lambda}{\alpha_s(e^{-s}k)}} e^{-s/2} \pi(e^{-s}k), \tag{A.26}$$

in terms of the function $\alpha_s(k)$, where we impose $\alpha_0(k) = \Lambda$ so that at $s = 0$ we recover the constraints for the product state $|\Lambda\rangle$. The differential equation for $\alpha_s(k)$ is then obtained by replacing Eq. A.25 in Eq. A.21, which leads to

$$\frac{\partial}{\partial s}\phi_s(k) = -i\sqrt{\frac{\alpha_s(e^{-s}k)}{\Lambda}} e^{-s/2} \left[L + K, \phi(e^{-s}k)\right] \tag{A.27}$$

$$= -\sqrt{\frac{\alpha_s(e^{-s}k)}{\Lambda}} e^{-s/2} \left(k\partial_k + \frac{1}{2} + g(e^{-s}k)\right) \phi(e^{-s}k) \tag{A.28}$$

$$= -\sqrt{\frac{\alpha_s(e^{-s}k)}{\Lambda}} e^{-s/2} \left(\frac{1}{2} + g(e^{-s}k)\right) \phi(e^{-s}k) \tag{A.29}$$

$$- \sqrt{\frac{\alpha_s(e^{-s}k)}{\Lambda}} e^{-s/2} e^{-s} k \phi'(e^{-s}k), \tag{A.30}$$

where $\phi'(k) \equiv \partial\phi(k)/\partial k$ and, on the other hand, by taking the derivative of Eq. A.25 with respect to $s$,

$$\frac{\partial}{\partial s}\phi_s(k) = \frac{e^{-s/2}}{2\sqrt{\Lambda\alpha_s(e^{-s}k)}} \alpha_s^{(s)}(e^{-s}k)\phi(e^{-s}k) \tag{A.31}$$

$$- \frac{e^{-s/2}}{2\sqrt{\Lambda\alpha_s(e^{-s}k)}} e^{-s} k \alpha_s^{(k)}(e^{-s}k)\phi(e^{-s}k) \tag{A.32}$$

$$- \frac{1}{2}\sqrt{\frac{\alpha_s(e^{-s}k)}{\Lambda}} e^{-s/2} \phi(e^{-s}k) \tag{A.33}$$

$$- \sqrt{\frac{\alpha_s(e^{-s}k)}{\Lambda}} e^{-s/2} e^{-s} k \phi'(e^{-s}k), \tag{A.34}$$

where

$$\alpha_s^{(s)}(k) \equiv \frac{\partial\alpha_s(k)}{\partial s}, \qquad \alpha_s^{(k)}(k) \equiv \frac{\partial\alpha_s(k)}{\partial k}. \tag{A.35}$$

Equating the two expressions for $k' = e^{-s}k$ we obtain

$$\sqrt{\frac{\alpha_s(k')}{\Lambda}} e^{-s/2} \phi(k') \times \tag{A.36}$$

$$\left(\alpha_s^{(s)}(k') - k'\alpha_s^{(k)}(k') + 2\alpha(k')g(k')\right) = 0 \tag{A.37}$$

or simply

$$\frac{\partial \alpha_s(k)}{\partial s} = k\frac{\partial \alpha_s(k)}{\partial k} - 2\alpha_s(k)g(k). \tag{A.38}$$

A similar analysis for the derivative of $\pi_s(k)$ with respect to $s$ leads to the same differential equation.

### A.1.6 Fixed point differential equation for $\alpha(k)$

The cMERA $|\Psi^\Lambda\rangle$ is characterized by a *fixed point* $\alpha(k)$ in the limit of large $s$,

$$\alpha(k) \equiv \lim_{s\to\infty} \alpha_s(k), \tag{A.39}$$

which is thus solution of the *fixed point* differential equation

$$k\frac{\partial \alpha(k)}{\partial k} = 2g(k)\alpha(k), \tag{A.40}$$

obtained from Eq. A.38 by requiring that $\frac{\partial \alpha_s(k)}{\partial s} = 0$ in the limit of large $s$. We will show later on that given a solution $\alpha(k)$ of the fixed point differential equation A.40, we can indeed find a solution $\alpha_s(k)$ of the differential eqaution A.38 such that Eq. A.39 holds.

### A.1.7 Solution of the fixed point differential equation

We can formally integrate Eq. A.40 and write

$$\alpha(k) = c_0 \exp\left(-\int_k^\infty dq\ \frac{2g(q)}{q}\right) \tag{A.41}$$

where $c_0 \equiv \lim_{k\to\infty} \alpha(k)$. To further characterize the functions $g(k)$ and $\alpha(k)$, let us first list the conditions we have on $g(k)$. Recall that the entangler $K$ must be quasi-local in real space, and such that $|\Psi^\Lambda\rangle$ approximates the CFT ground state $|\Psi\rangle$ at distances larger than $1/\Lambda$.

Quasi-locality of the entangler $K$ implies that it must go to a constant at large $k$, which without loss of generality we choose to be zero (any other value corresponds to a delta $\delta(x-y)$ in real space, which could be absorbed into the rescaling operator $L$). In addition, this constant should be reached sufficiently fast. For instance, in the example below we will choose $g(k)$ to vanish as a Gaussian $e^{-(k/\Lambda)^2/\sigma}$, as in Ref. [81].

That $|\Psi^\Lambda\rangle$ approximates the CFT ground state $|\Psi\rangle$ at long distances implies two additional conditions, which we announce next and will justify below. Consider the expansion of the integral in the exponent of Eq. A.41 around $k=0$ (for $k>0$) as

$$-\int_k^\infty dq\ \frac{2g(q)}{q} = \mu\log(k) + \nu + \sum_{n=1}^{\infty}\nu_n k^n, \tag{A.42}$$

which we obtained by assuming that $g(k)$ is sufficiently smooth (as required again for the entangler $K$ to be quasi-local in real space) and by extracting the logarithmic divergence. Here $\mu$, $\nu$, and $\nu_n$ are constants that depend on $g(k)$. Then we will see below that we must demand $\mu=1$ (which can be seen to amount to $\lim_{k\to 0} g(k) = 1/2$) and $\nu = -\log(c_0)$. Therefore $g(k)$ is required to satisfy

$$g(k) \sim \begin{cases} 1/2, & |k| \ll \Lambda, \\ 0, & |k| \gg \Lambda, \end{cases} \tag{A.43}$$

together with $\nu = -\log(c_0)$ in the expansion of Eq. A.42.

Let us now discuss what the above conditions imply for the function $\alpha(k)$ resulting from the fixed point differential equation in Eq. A.40. First, quasi-locality of the entangler $K$ required a vanishing $g(k)$ for large $|k|$, which Eq. A.40 translates into requiring that $\alpha(k)$ tend to a constant $c_0$ for large $|k|$. On the other hand, demanding that $|\Psi^\Lambda\rangle$ approximate the CFT ground state $|\Psi\rangle$ at long distances requires that $\alpha(k)$ tend to $|k|$ for small $|k|\to 0$. This can be seen e.g. by studying the correlator

$$\langle\Psi^\Lambda|\pi(x)\pi(y)|\Psi^\Lambda\rangle = \frac{1}{2\pi}\int dk\ e^{ik(x-y)}\frac{\alpha(k)}{2} \tag{A.44}$$

and demanding that it correspond to the CFT correlator

$$\langle\Psi|\pi(x)\pi(y)|\Psi\rangle = -\frac{1}{2\pi}\frac{1}{|x-y|^{2\Delta_\pi}} \tag{A.45}$$

at large distances $\Lambda|x-y| \gg 1$, both in exponent and amplitude. Specifically, matching the exponent $\Delta_\pi = 1$ requires that $\alpha(k) \sim c_1|k|$ while matching the amplitude $-1/2\pi$ sets

$c_1 = 1$. Therefore $\alpha(k)$ is required to satisfy

$$\alpha(k) \sim \begin{cases} |k|, & |k| \ll \Lambda, \\ c_0, & |k| \gg \Lambda. \end{cases} \tag{A.46}$$

Notice that Eqs. A.41 and A.42 imply that, for small $|k|$, $\alpha(k) = c_0 e^{\nu} |k|^{\mu} + O(k^2)$. We therefore conclude that $\nu = -\log(c_0)$ and $\mu = 1$, as stated above.

### A.1.8 Building $\alpha_s(k)$ from the fixed point $\alpha(k)$

Given a solution $\alpha(k)$ of the fixed point differential equation A.40, we can build a solution $\alpha_s(k)$ of the scale dependent differential equation A.38 simply as

$$\alpha_s(k) \equiv \alpha(k) h(e^s k), \tag{A.47}$$

for any function $h(e^s k)$. In can indeed be easily check by direct substitution that such $\alpha_s(k)$ fulfils A.38.

In our case, we are interested in a solution $\alpha_s(k)$ such that, at the beginning of the scale evolution, $s = 0$, the function $\alpha_0(k)$ represents the constraints of the product state $|\Lambda\rangle$,

$$\alpha_0(k) = \Lambda. \tag{A.48}$$

This can be achieved with the choice $h(e^s k) = \Lambda / \alpha(e^s k)$, that is

$$\alpha_s(k) = \Lambda \frac{\alpha(k)}{\alpha(e^s k)}. \tag{A.49}$$

For small $|k|$ ($|k| \ll \Lambda$) and large $s$ such that $e^s |k| \gg \Lambda$, this expression tends to $\Lambda |k| / c_0$ and thus we must choose $c_0 = \Lambda$ in Eq. A.46, which we update to

$$\alpha(k) \sim \begin{cases} |k|, & |k| \ll \Lambda, \\ \Lambda, & |k| \gg \Lambda. \end{cases} \tag{A.50}$$

### A.1.9 Symplectic transformation $V$

Let us now define the following symplectic transformation $V$

$$V \phi(k) V^{\dagger} = \sqrt{\frac{\alpha(k)}{|k|}} \phi(k) \equiv \phi^{\Lambda}(k), \tag{A.51}$$

$$V \pi(k) V^{\dagger} = \sqrt{\frac{|k|}{\alpha(k)}} \pi(k) \equiv \pi^{\Lambda}(k). \tag{A.52}$$

Clearly, under this transformation we have

$$V\left(\sqrt{\frac{|k|}{2}}\phi(k)+\frac{i}{\sqrt{2|k|}}\pi(k)\right)V^{\dagger} \tag{A.53}$$
$$=\left(\sqrt{\frac{\alpha(k)}{2}}\phi(k)+\frac{i}{\sqrt{2\alpha(k)}}\pi(k)\right),$$

so that the linear constraints fulfilled by the CFT ground state $|\Psi\rangle$ are mapped into the linear constraints fulfilled by the cMERA $|\Psi^{\Lambda}\rangle$, implying that $V|\Psi\rangle \propto |\Psi^{\Lambda}\rangle$.

At this point, it is useful to introduce two sets of annihilation operators, corresponding to the linear constraints for the CFT ground state $|\Psi\rangle$ and the cMERA $|\Psi^{\Lambda}\rangle$, namely

$$a(k) \equiv \sqrt{\frac{|k|}{2}}\phi(k)+\frac{i}{\sqrt{2|k|}}\pi(k), \tag{A.54}$$

$$a^{\Lambda}(k) \equiv \sqrt{\frac{\alpha(k)}{2}}\phi(k)+\frac{i}{\sqrt{2\alpha(k)}}\pi(k), \tag{A.55}$$

so that $a(k)|\Psi\rangle = 0$ for all $k$, $a^{\Lambda}(k)|\Psi^{\Lambda}\rangle = 0$ for all $k$, and Eq. A.53 reads $Va(k)V^{\dagger} = a^{\Lambda}(k)$.

### A.1.10 Momentum operator $P^{\Lambda} = P$

The momentum operator for the 1+1 free bosonic CFT under consideration is given by

$$P \equiv -\int dx\ \pi(x)\partial_x\phi(x) \tag{A.56}$$
$$= -i\int dk\ k\ \pi(-k)\phi(k) \tag{A.57}$$
$$= \int dk\ k\ a(k)^{\dagger}a(k), \tag{A.58}$$

whereas for the cMERA we define

$$P^{\Lambda} \equiv VPV^{\dagger} \tag{A.59}$$
$$= \int dk\ k\ a^{\Lambda}(k)^{\dagger}a^{\Lambda}(k). \tag{A.60}$$

We then have

$$
\begin{aligned}
P^{\Lambda} &= \int dk\ k\ \left(\sqrt{\frac{\alpha(k)}{2}}\phi(k) + \frac{i}{\sqrt{2\alpha(k)}}\pi(k)\right)^{\dagger} && \text{(A.61)}\\
&\times \left(\sqrt{\frac{\alpha(k)}{2}}\phi(k) + \frac{i}{\sqrt{2\alpha(k)}}\pi(k)\right) && \text{(A.62)}\\
&= \int dk\ k\ \left(\sqrt{\frac{\alpha(k)}{2}}\phi(-k) - \frac{i}{\sqrt{2\alpha(k)}}\pi(-k)\right) && \text{(A.63)}\\
&\times \left(\sqrt{\frac{\alpha(k)}{2}}\phi(k) + \frac{i}{\sqrt{2\alpha(k)}}\pi(k)\right) && \text{(A.64)}\\
&= -i\int dk\ k\ \pi(-k)\phi(k) && \text{(A.65)}\\
&= P. && \text{(A.66)}
\end{aligned}
$$

Given that $P^{\Lambda}|\Psi^{\Lambda}\rangle = 0$, we recover the known result [81] that the state $|\Psi^{\Lambda}\rangle$ is invariant under translations generated by $P$, $P|\Psi^{\Lambda}\rangle = 0$.

### A.1.11 Dilation operator $D^{\Lambda} = L + K$

From the CFT dilation operator

$$
\begin{aligned}
D &\equiv -\int dx\ x : \pi(x)\partial_x\phi(x) : && \text{(A.67)}\\
&= \int dk\ : \pi(-k)\left(k\partial_k + 1\right)\phi(k) : && \text{(A.68)}\\
&= i\int dk\ a(k)^{\dagger} sgn(k)\left(k\partial_k + \frac{1}{2}\right)a(k) && \text{(A.69)}
\end{aligned}
$$

we can also define a cMERA dilation operator

$$
\begin{aligned}
D^{\Lambda} &\equiv VDV^{\dagger} && \text{(A.70)}\\
&= i\int dk\ a^{\Lambda}(k)^{\dagger} sgn(k)\left(k\partial_k + \frac{1}{2}\right)a^{\Lambda}(k). && \text{(A.71)}
\end{aligned}
$$

Then we have

$$D^{\Lambda} = i \int dk \quad \left( \sqrt{\frac{\alpha(k)}{2}} \phi(k) + \frac{i}{\sqrt{2\alpha(k)}} \pi(k) \right)^{\dagger} \tag{A.72}$$

$$\times \quad sgn(k) \left( k\partial_k + \frac{1}{2} \right) \left( \sqrt{\frac{\alpha(k)}{2}} \phi(k) + \frac{i}{\sqrt{2\alpha(k)}} \pi(k) \right)$$

$$= \quad i \int dk \quad \left( \sqrt{\frac{\alpha(k)}{2}} \phi(-k) - \frac{i}{\sqrt{2\alpha(k)}} \pi(-k) \right) \tag{A.73}$$

$$\times \quad sgn(k) \left( k\partial_k + \frac{1}{2} \right) \left( \sqrt{\frac{\alpha(k)}{2}} \phi(k) + \frac{i}{\sqrt{2\alpha(k)}} \pi(k) \right)$$

$$= \quad \int dk \ \pi(-k) \left( k\partial_k + \frac{1}{2} \right) \phi(k) \tag{A.74}$$

$$+ \quad \int dk \ \frac{k\partial_k \alpha(k)}{2\alpha(k)} \pi(-k)\phi(k) \tag{A.75}$$

$$= \quad \int dk \ \pi(-k) \left( k\partial_k + \frac{1}{2} \right) \phi(k) \tag{A.76}$$

$$+ \quad \int dk \ g(k)\pi(-k)\phi(k) \tag{A.77}$$

$$= \quad L + K. \tag{A.78}$$

Note that we neglect constant terms in the calculation.

## A.2 Quasi-local entangler $K$

In this section we consider a concrete example of function $g(k)$ that produces an entangler $K$ that is quasi-local in real space, in that it is the integral of a smeared density with Gaussian tails $\approx e^{-\frac{1}{4}\sigma\Lambda^2(x-y)^2}$. We show that the corresponding cMERA fields $\phi^{\Lambda}(x)$ and $\pi^{\Lambda}(x)$ are also quasi-local. This time, they correspond to smeared fields with exponential tails $\approx e^{-\sqrt{\sigma}\Lambda|y-x|}$.

The authors thank Mr. Adrian Franco Rubio, *private communication*, for determining the exact value of $\sigma$ in the expressions bellow.

### A.2.1 Example of $g(k)$ and $\alpha(k)$ leading to a quasi-local entangler $K$

A specific example of quasi-local entangler $K$ is obtained with the choice

$$g(k) = \frac{1}{2}\exp\left(-\frac{1}{\sigma}\left(\frac{k}{\Lambda}\right)^2\right), \tag{A.79}$$

which is equivalent to that proposed in Ref. [81], except for the presence of a factor $\sigma \approx 1.78107$, namely the exponential of Euler's constant $\gamma \approx 0.57722$. Notice that $g(k)$ tends to $1/2$ and $0$ for small and large $|k|$, as in Eq. A.43. The corresponding $\alpha(k)$ satisfying the fixed point differential equation A.40 is

$$\alpha(k) = \Lambda\exp\left(\frac{1}{2}\mathrm{Ei}\Big(-\frac{1}{\sigma}(\frac{k}{\Lambda})^2\Big)\right), \tag{A.80}$$

where Ei is the special function known as exponential integral,

$$\mathrm{Ei}(y) \equiv -\int_{-y}^{\infty}\frac{e^{-t}}{t}dt, \tag{A.81}$$

which accepts the following convergent series

$$\mathrm{Ei}(y) = \gamma + \ln|y| + \sum_{k=1}^{\infty}\frac{y^k}{k\ k!}. \tag{A.82}$$

Therefore for $|k| \ll \Lambda$ we have

$$\alpha(k) \approx \Lambda\exp\frac{1}{2}\left(\gamma + \log\left(\frac{k^2}{\sigma\Lambda^2}\right)\right) = |k|\sqrt{\frac{e^\gamma}{\sigma}}. \tag{A.83}$$

We conclude that $\sigma \equiv e^\gamma$, which was missing in the Gaussian $g(k)$ of the proposal of Ref. [81], is required in $g(k)$ in order for $\alpha(k)$ to grow as $\alpha(k) = |k| + O(k^2)$ in the limit of small $|k|$.

In this case, the entangler reads

$$K = \frac{1}{2}\int dk\ e^{-\frac{k^2}{\sigma\Lambda^2}} : \pi(-k)\phi(k) : \tag{A.84}$$

$$= \sqrt{\frac{\sigma\Lambda^2}{8}}\iint dxdy\ e^{-\frac{1}{4}\sigma\Lambda^2(x-y)^2} : \pi(x)\phi(y) : \tag{A.85}$$

### A.2.2 Quasi-local scaling operators

Next we show that the absolute value of the (generalized) functions $\mu_\phi(x)$ and $\mu_\pi(x)$ for the smeared fields $\phi^\Lambda(x)$ and $\pi^\Lambda(x)$,

$$\phi^\Lambda(x) = V\phi(x)V^\dagger = \int dy\ \mu_\phi(x-y)\phi(y), \tag{A.86}$$

$$\pi^\Lambda(x) = V\pi(x)V^\dagger = \int dy\ \mu_\pi(x-y)\pi(y), \tag{A.87}$$

can be upper bounded by $O(\exp(-|\Lambda x|)$ for $|\Lambda x| \gg 1$, so that we can think of $\phi^\Lambda(x)$ and $\pi^\Lambda(x)$ as quasi-local fields with a characteristic length scale upper bounded by $1/\Lambda$.

The Fourier transforms of $\sqrt{\frac{\alpha(k)}{|k|}}$ and $\sqrt{\frac{|k|}{\alpha(k)}}$, see Eqs. A.51-A.52 are distributions and, as such, cannot be reliably obtained through a numerical Fourier transform. [That the profile functions $\mu_\phi(x)$ and $\mu_\pi(x)$ are actually distributions should not come as a surprise. In the original CFT, with sharp field operators $\phi(x)$ and $\pi(x)$, they are already distribitions, namely delta functions $\delta(x)$]. In order to analyse these distributions, we decompose them as sum of two pieces

$$\mu_\phi(x) = \mu_\phi^{(1)}(x) + \mu_\phi^{(2)}(x), \tag{A.88}$$

$$\mu_\pi(x) = \mu_\pi^{(1)}(x) + \mu_\pi^{(2)}(x), \tag{A.89}$$

where the first term is conveniently chosen such that (i) it is a distribution with an analytic Fourier transform and (ii) the remaining term is sufficiently regular that it can be reliably obtained by a numerical Fourier transform.

Since $\sqrt{\frac{\alpha(k)}{|k|}} \sim |k/\Lambda|^{-\frac{1}{2}}$ as $|k| \to \infty$, we choose $\mu_\phi^{(1)}(k) \equiv (1 + k^2/\Lambda^2)^{-\frac{1}{4}}$, which has the same asymptotic behavior for large $|k|$ (to leading order in $|k|$). This function has an analytical distributional Fourier transform,

$$\mu_\phi^{(1)}(x) \equiv \mathcal{F}\left((1+k^2/\Lambda^2)^{-\frac{1}{4}}\right)(x) = \frac{2^{3/4}K_{\frac{1}{4}}(|\Lambda x|)}{\Gamma\left(\frac{1}{4}\right)|\Lambda x|^{1/4}}, \tag{A.90}$$

where $K_n$ is the modified Bessel function of the second kind, and $\Gamma$ is the Euler gamma function. It can be shown that it has asymptotic behavior

$$\mu_\phi^{(1)}(x) \sim \begin{cases} |\Lambda x|^{-1/2}, & |\Lambda x| \ll 1; \\ \frac{2^{1/4}\sqrt{\pi}e^{-|\Lambda x|}}{\Gamma\left(\frac{1}{4}\right)|\Lambda x|^{3/4}}, & |\Lambda x| \gg 1. \end{cases} \tag{A.91}$$

Arguing similarly about $\sqrt{\frac{|k|}{\alpha(k)}}$, we choose $\mu_\pi^{(1)}(k) \equiv (1+k^2/\Lambda^2)^{\frac{1}{4}}$, which has analytical distributional Fourier transform,

$$\mu_\pi^{(1)}(x) \equiv \mathcal{F}\left((1+k^2/\Lambda^2)^{\frac{1}{4}}\right)(x) = \frac{2^{5/4}K_{\frac{3}{4}}(|\Lambda x|)}{\Gamma\left(-\frac{1}{4}\right)|\Lambda x|^{3/4}}. \tag{A.92}$$

Its asymptotic behavior is

$$\mu_\pi^{(1)}(x) \sim \begin{cases} -\frac{1}{2}|\Lambda x|^{-3/2}, & |\Lambda x| \ll 1; \\ \frac{2^{3/4}\sqrt{\pi}e^{-|\Lambda x|}}{\Gamma\left(-\frac{1}{4}\right)|\Lambda x|^{5/4}}, & |\Lambda x| \gg 1. \end{cases} \tag{A.93}$$

$\mu_\pi^{(1)}(x)$ should be understood as a distribution. Its action on a test function $f(x)$ is defined as the Hadamard finite-part integral [54]:

$$\begin{aligned} &\langle \mu_\pi^{(1)}, f\rangle \\ &\equiv \lim_{\epsilon\to 0^+}\left(\int_{\mathbb{R}\setminus(-\epsilon,\epsilon)} \mu_\pi^{(1)}(x)f(x)dx + 2\Lambda^{-\frac{3}{2}}\epsilon^{-\frac{1}{2}}f(0)\right). \end{aligned} \tag{A.94}$$

It is clear that $\mu_\phi^{(1)}(x)$ and $\mu_\pi^{(1)}(x)$ both decay exponentially for large $|x|$. Since $\mu_\phi^{(2)}(x)$ and $\mu_\pi^{(2)}(x)$ are non-singular, the singular behaviors of $\mu_\phi(x)$ and $\mu_\pi(x)$ for $|\Lambda x| \ll 1$ are the same as $\mu_\phi^{(1)}(x)$ and $\mu_\pi^{(1)}(x)$.

After the subtraction, we can readily apply a numerical Fourier transform to $\mu_\phi^{(2)}(k) \equiv \sqrt{\frac{\alpha(k)}{|k|}} - (1+k^2/\Lambda^2)^{-\frac{1}{4}}$ and $\mu_\pi^{(2)}(k) \equiv \sqrt{\frac{|k|}{\alpha(k)}} - (1+k^2/\Lambda^2)^{\frac{1}{4}}$. By summing the analytical part and numerical part, we can see that $\mu_\phi(x)$ and $\mu_\pi(x)$ decay roughly esxponentially for large $x$, and $\mu_\pi(x)$ also oscillates, as shown in Fig. A.1.

In fact, it can be proven that

$$\mu_\phi(x), \mu_\pi(x) = \exp\left\{-\Lambda x\sqrt{\sigma\log(\Lambda x)} + o(\Lambda x\sqrt{\log(\Lambda x)})\right\}, \tag{A.95}$$

as $x \to \infty$. The rigorous proof is rather lengthy, so here we only outline it for the asymptotic behavior of $\mu_\phi(x)$. That $\mu_\phi(x)$ is the Fourier transform of $\sqrt{\frac{\alpha(k)}{|k|}}$ is equivalent to the following integral equation,

$$(x\partial_x + \frac{1}{2})\mu_\phi(x) + \frac{1}{\sqrt{2\pi}}\int g(x-y)\mu_\phi(y)dy = 0, \tag{A.96}$$

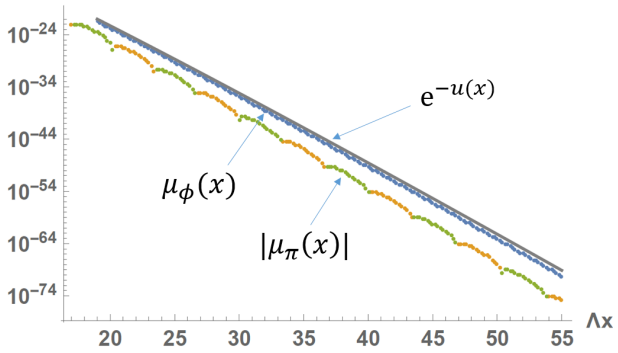


Figure A.1: Generalized functions $\mu_\phi(x)$ and $\mu_\pi(x)$ for large $\Lambda x \gg 1$, together with function $const. \times e^{-u(x)}$ for $u(x) = \Lambda x\sqrt{\sigma \log(\Lambda x)}$. Both $\mu_\phi(x)$ (blue) and $|\mu_\pi(x)|$ (in yellow when $\mu_\pi(x) > 0$ and green when $\mu_\pi(x) < 0$) where obtained numerically by adding the contributions (see Eqs. A.88-A.89) of an analytical Fourier transform and a numerical Fourier transform. The results were obtained using arbitrary precision arithmetic.

where $g(x) = \sqrt{\frac{\sigma\Lambda^2}{8}} e^{-\frac{1}{4}\sigma\Lambda^2 x^2}$ is the Fourier transform of $g(k)$. (This follows from requiring that $-i[D^\Lambda, \phi^\Lambda(x)] = (x\partial_x + 0)\phi^\Lambda(x)$ at $x = 0$). We define a new variable $u(x)$ such that,

$$\mu_\phi(x) = e^{-u(x)}. \tag{A.97}$$

We seek the solution to this integral equation among functions satisfying a few conditions:

$$\begin{aligned} &u'(x) \to \infty, \quad \log(u'(x)) = o(\log(\Lambda x)), \text{ as } x \to \infty; \\ &|u'(x) - u'(y)| = o(\sqrt{\log(\Lambda x)}) + o(\Lambda|x-y|), \\ &\qquad\qquad\qquad\qquad \text{as } x, y \to \infty. \end{aligned} \tag{A.98}$$

Then the convolution term in Eq. A.96 can be approximated as

$$\begin{aligned} &\int g(x-y)\mu_\phi(y)dy \\ &\quad = \sqrt{\frac{\pi}{2}}\mu_\phi(x) e^{\frac{1}{\sigma\Lambda^2}\left(u'(x)+o(\sqrt{\log\Lambda x})\right)^2 (1+o(1))}. \end{aligned} \tag{A.99}$$

One can show that there exists solution to Eq. A.96 satisfying conditions Eq. A.98, and it reads

$$u(x) = \Lambda x\sqrt{\sigma \log \Lambda x} + o(\Lambda x\sqrt{\log \Lambda x}). \tag{A.100}$$

Then we prove Eq. A.95 for $\mu_\phi(x)$. The proof for $\mu_\pi(x)$ is obtained similarly, starting from $-i[D^\Lambda, \pi^\Lambda(x)] = (x\partial_x + 1)\pi^\Lambda(z)$ at $x = 0$.

## A.3 Radial and N-S quantizations

In Chapter 2 we have analysed the spacetime symmetries of the cMERA state $|\Psi^\Lambda\rangle$ for the ground state $|\Psi\rangle$ of a 1+1 dimensional CFT where space corresponds to the real line $x \in \mathbb{R}$. We have done so in terms of a subset of generators of global conformal transformations on the real line (namely the Hamiltonian $H$, the momentum operator $P$, the dilation and boost generators $D$ and $B$, which can be completed with the generators of special conformal transformations $K_1$ and $K_2$).

The spacetime symmetries of a 1+1 CFT are usually analysed using instead radial quantization, where space corresponds to the circle. The Virasoro generators $L_n$ and $\bar{L}_n$ can then be mapped onto generators $L'_n$ and $\bar{L}'_n$ on the real line, producing the so-called N-S quantization (North pole - South pole quantization), as described e.g. in S. Rychkov's notes *EPFL Lectures on Conformal Field Theory in D >= 3 Dimensions*, arXiv:1601.05000, for the global conformal group in higher dimensions. The goal of this Section , which contains no original research, is to briefly review the connection between radial quantization and N-S quantization, following a detailed explanation kindly offered to the authors by John Cardy, and to clarify their relation to the generators $H, P, B, D$ used in the main text.

### A.3.1 Complex coordinates and stress-energy tensor

We can parameterize the Euclidean plane by the complex coordinate $z \equiv z^0 + iz^1$, and use $z$ and $\bar{z}$ as new coordinates,

$$\begin{aligned} z &= z^0 + iz^1 & z^0 &= \tfrac{1}{2}(z + \bar{z}) \\ \bar{z} &= z^0 - iz^1 & z^1 &= \tfrac{1}{2i}(z - \bar{z}) \\ \partial_z &= \tfrac{1}{2}(\partial_0 - i\partial_1) & \partial_0 &= \partial_z + \partial_{\bar{z}} \\ \partial_{\bar{z}} &= \tfrac{1}{2}(\partial_0 + i\partial_1) & \partial_1 &= i(\partial_z - \partial_{\bar{z}}) \end{aligned} \tag{A.101}$$

The stress-energy tensor $T_{\mu\nu}(z^0, z^1)$ of a CFT is symmetric ($T_{10} = T_{01}$) and traceless

$(T_{11} = -T_{00})$. In complex coordinates we obtain components

$$\begin{aligned} T_{zz} &= \frac{1}{4}\left(T_{00} - i(T_{10} + T_{01}) - T_{11}\right) && \text{(A.102)} \\ &= \frac{1}{2}\left(T_{00} - iT_{01}\right) && \text{(A.103)} \\ T_{\bar{z}\bar{z}} &= \left(T_{00} + i(T_{10} + T_{01}) - T_{11}\right) && \text{(A.104)} \\ &= \frac{1}{2}\left(T_{00} + iT_{01}\right) && \text{(A.105)} \end{aligned}$$

whereas $T_{z\bar{z}} = T_{\bar{z}z} = (T_{00}+T_{11})/4 = 0$. In addition, from the conservation law $g^{\alpha\mu}\partial_\alpha T_{\mu\nu} = 0$ it follows that $T_{zz}$ is a holomorphic function $(\partial_{\bar{z}} T_{zz} = 0)$ whereas $T_{\bar{z}\bar{z}}$ is antiholomorphic $(\partial_z T_{\bar{z}\bar{z}} = 0)$. Finally, the *renormalized* holomorphic and antiholomorphic components of the stress-energy tensor are given by

$$T(z) \equiv -2\pi T_{zz}(z), \qquad \bar{T}(\bar{z}) \equiv -2\pi T_{\bar{z}\bar{z}}(\bar{z}) \tag{A.106}$$

### A.3.2 Generators of conformal coordinate transformation

Holomorphic (antiholomorphic) conformal coordinate transformations $z \to f(z)$ (respectively $\bar{z} \to \bar{f}(\bar{z})$) preserve angles and are generated by infinitesimal transformations

$$z \to z + \sum_{n=-\infty}^{\infty} c_n z^{n+1} = (1 - \sum_{n=-\infty}^{\infty} c_n l_n) z \tag{A.107}$$

$$\bar{z} \to \bar{z} + \sum_{n=-\infty}^{\infty} \bar{c}_n \bar{z}^{n+1} = (1 - \sum_{n=-\infty}^{\infty} \bar{c}_n \bar{l}_n) \bar{z}, \tag{A.108}$$

where $c_n \in \mathbb{C}$ and the holomorphic and antiholomorphic generators $l_n$ and $\bar{l}_n$ are given by

$$l_n \equiv -z^{n+1}\partial_z, \qquad \bar{l}_n \equiv -\bar{z}^{n+1}\partial_{\bar{z}}, \tag{A.109}$$

which close the Witt algebra [44]

$$\begin{aligned} [l_m, l_n] &= (m-n) l_{m+n}, && \text{(A.110)} \\ [\bar{l}_m, \bar{l}_n] &= (m-n) \bar{l}_{m+n}, && \text{(A.111)} \\ [l_m, \bar{l}_n] &= 0. && \text{(A.112)} \end{aligned}$$

### A.3.3 Radial quantization

In radial quantization, the Virasoro generators are defined in terms of the (renormalized) holomorphic and antiholomorphic components $T(z)$ and $\bar{T}(\bar{z})$ of the stress-energy tensor as

$$L_n \equiv \frac{1}{2\pi i}\oint_{|z|=1} dz\; z^{n+1}T(z), \tag{A.113}$$

$$\bar{L}_n \equiv \frac{1}{2\pi i}\oint_{|\bar{z}|=1} d\bar{z}\; \bar{z}^{n+1}\bar{T}(\bar{z}), \tag{A.114}$$

where the integrals are over the unit circle $|z| = 1$ and $|\bar{z}| = 1$ respectively. They close the Virasoro algebra [44]

$$[L_m, L_n] = (m-n)L_{m+n} + \frac{c}{12}m(m^2-1)\delta_{m,-n}, \tag{A.115}$$

$$\left[\bar{L}_m, \bar{L}_n\right] = (m-n)\bar{L}_{m+n} + \frac{c}{12}m(m^2-1)\delta_{m,-n}, \tag{A.116}$$

$$\left[L_m, \bar{L}_n\right] = 0. \tag{A.117}$$

### A.3.4 From the circle to the real line

We would like to obtain an expression for the generators of the conformal group when the CFT is quantized on the real line. The usual strategy is to map the generators $L_n$ and $\bar{L}_n$ from the unit circle to the real line. For this purpose, consider the conformal map

$$z \to \xi(z) = x(z) + i\tau(z), \qquad z = \frac{1-i\xi}{1+i\xi}, \tag{A.118}$$

which indeed maps the unit circle $|z| = 1$ to the real line $\xi = x \in \mathbb{R}$, as illustrated in Fig. A.2. Specifically, the point $z = 1$ is mapped to the origin of the real line $x = 0$, whereas $\lim_{\theta\to\pi^{\pm}} e^{i\theta}$ are mapped to to $x = \pm\infty$. Notice also that the origin $z = 0$ is mapped to $\xi = -i$, which we will refer to as South pole $S$, while $z = \infty$ is mapped to $\xi = i$, which we will refer to as North pole $N$.

Notice that

$$\frac{dz}{d\xi} = \frac{-2i}{(1+i\xi)^2}, \qquad \text{or} \qquad \partial_z = \frac{i\,(1+i\xi)^2}{2}\partial_\xi \tag{A.119}$$

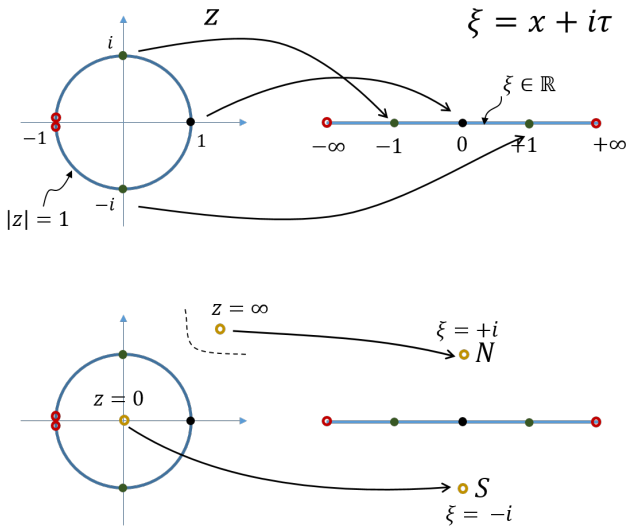


Figure A.2: Under the conformal map $z \to \xi \equiv x + i\tau$, where $z = (1 - i\xi)/(1 + i\xi)$, the unit circle $|z| = 1$ is mapped into the real line $\xi = x$, where $x \in \mathbb{R}$.

and therefore under $z \to \xi$ the generator $l_n$ is mapped into the generator $q_n$

$$q_n \equiv \left(\frac{1 - i\xi}{1 + i\xi}\right)^{n+1} \frac{(1 + i\xi)^2}{2i} \partial_\xi \tag{A.120}$$

$$= -\frac{i}{4}(1 - i\xi)^{n+1}(1 + i\xi)^{-n+1}(\partial_x - i\partial_\tau) \tag{A.121}$$

where we used $\partial_\xi = \frac{1}{2}(\partial_x - i\partial_\tau)$. Specializing the holomorphic generator $q_n$ to the real line $\xi = x$, and switching from Euclidean time $\tau$ to Lorentzian time $t$, where $\tau = it$, so that $\partial_\xi = \frac{1}{2}(\partial_x - \partial_t)$, we finally obtain the right moving generator

$$q_n = -\frac{i}{4}(1 - ix)^{n+1}(1 + ix)^{-n+1}(\partial_x - \partial_t). \tag{A.122}$$

Similarly, from $\bar{z} = (1 + i\bar{\xi})/(1 - i\bar{\xi})$, we can build antiholomorphic generators, which after switching to Lorentzian time turn into the left moving generators

$$\bar{q}_n = \frac{i}{4}(1 + ix)^{n+1}(1 - ix)^{-n+1}\left(\partial_x + \partial_t\right). \tag{A.123}$$

For later reference, we write explicitly the generators of global conformal transforma-

tion, namely

$$q_0 = -\frac{i}{4}\left(1+x^2\right)(\partial_x - \partial_t), \tag{A.124}$$

$$q_{\pm 1} = -\frac{i}{4}(1 \mp ix)^2(\partial_x - \partial_t), \tag{A.125}$$

$$\bar{q}_0 = \frac{i}{4}\left(1+x^2\right)(\partial_x + \partial_t), \tag{A.126}$$

$$\bar{q}_{\pm 1} = \frac{i}{4}(1 \pm ix)^2(\partial_x + \partial_t). \tag{A.127}$$

On the other hand, under the Mobius transformation $z \to \xi$, the stress-energy tensor changes simply as [44]

$$T(z)dz = \frac{T(\xi)d\xi}{dz/d\xi} = \frac{i(1+i\xi)^2}{2}T(\xi)d\xi. \tag{A.128}$$

Accordingly, the generators of conformal transformations become

$$Q_n = \frac{-1}{4\pi}\int dx\ \left(\frac{1-ix}{1+ix}\right)^{n+1}(1+ix)^2T(x) \tag{A.129}$$

$$= \frac{-1}{4\pi}\int dx\ (1-ix)^{n+1}(1+ix)^{-n+1}T(x). \tag{A.130}$$

where $\int dx \equiv \int_{\mathbb{R}} d\xi$. Similar derivations for the antiholomorphic component $\bar{T}(z)$ of the stress-energy lead to

$$\bar{Q}_n = \frac{-1}{4\pi}\int dx\ (1+ix)^{n+1}(1-ix)^{-n+1}\bar{T}(x) \tag{A.131}$$

In particular, for $n = 0, \pm 1$ we have the generators of the global conformal transformations,

$$Q_0 = \frac{-1}{4\pi}\int dx\ (1+x^2)T(x), \tag{A.132}$$

$$Q_{\pm 1} = \frac{-1}{4\pi}\int dx\ (1 \mp ix)^2T(x), \tag{A.133}$$

$$\bar{Q}_0 = \frac{-1}{4\pi}\int_{\mathbb{R}} dx\ (1+x^2)\bar{T}(x), \tag{A.134}$$

$$\bar{Q}_{\pm 1} = \frac{-1}{4\pi}\int dx\ (1 \pm ix)^2\bar{T}(x). \tag{A.135}$$

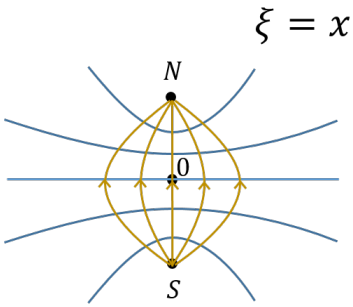


Figure A.3: In N-S quantization, the time translation is generated by $(1+x^2)\partial_\tau$.

### A.3.5 Global conformal transformations directly on the real line

Let us now consider conformal transformations acting on Minkowski space $\xi = x - t$. We specialize to their action on the $x$ axis, that is for $t = 0$. For simplicity, we restrict our attention to global conformal transformations,

$$\begin{array}{ll} (x,0) \to (x, t_0) & \text{time translations} \\ (x,0) \to (x + x_0, 0) & \text{space translations} \\ (x,0) \to \gamma(x, -vx) & \text{boosts} \\ (x,0) \to (\lambda x, 0) & \text{dilations} \\ (x,0) \to (x, ax^2) & \text{special conformal 1} \\ (x,0) \to (\frac{x}{1-bx}, 0) & \text{special conformal 2} \end{array} \tag{A.136}$$

where $t_0, x_0, \gamma, v, a, b$ are real parameters. They are generated, both as a coordinate transformation and as a Hilbert space transformation, by

$$\begin{array}{rll} i\partial_t, & H \equiv \int dx\ h(x) & \text{Hamiltonian} \\ -i\partial_x, & P \equiv \int dx\ p(x) & \text{momentum generator} \\ ix\partial_t, & B \equiv \int dx\ x\ h(x) & \text{boost generator} \\ -ix\partial_x, & D \equiv \int dx\ x\ p(x) & \text{dilation generator} \\ ix^2\partial_t, & K_1 \equiv \int dx\ x^2\ h(x) & \text{SC generator 1} \\ -ix^2\partial_x, & K_2 \equiv \int dx\ x^2\ p(x) & \text{SC generator 1} \end{array} \tag{A.137}$$

where we have expressed the generators in terms of the Hamiltonian and momentum densities $h(x)$ and $p(x)$,

$$h(z) = \frac{-1}{2\pi}\left(T(z) + \bar{T}(\bar{z})\right), \tag{A.138}$$

$$p(z) = \frac{-1}{2\pi}\left(T(z) - \bar{T}(\bar{z})\right). \tag{A.139}$$

These generators fulfil the expected commutation relations, including

$$[H, P] = 0, \qquad [B, D] = 0, \tag{A.140}$$
$$[B, H] = iP, \quad [B, P] = iH, \tag{A.141}$$
$$[D, H] = iH, \quad [D, P] = iP. \tag{A.142}$$
$$\tag{A.143}$$

The above two sets of global conformal generators on the real line can, of course, be written in terms of each other. Explicitly, we find

$$q_0 + \bar{q}_0 = \frac{1+x^2}{2} i\partial_t \tag{A.144}$$
$$q_0 - \bar{q}_0 = -\frac{1+x^2}{2} i\partial_x \tag{A.145}$$
$$(q_1 + q_{-1}) + (\bar{q}_1 + \bar{q}_{-1}) = (1-x^2) i\partial_t \tag{A.146}$$
$$(q_1 + q_{-1}) - (\bar{q}_1 + \bar{q}_{-1}) = -(1-x^2) i\partial_x \tag{A.147}$$
$$(q_1 - q_{-1}) + (\bar{q}_1 - \bar{q}_{-1}) = -2x\partial_x \tag{A.148}$$
$$(q_1 - q_{-1}) - (\bar{q}_1 - \bar{q}_{-1}) = 2x\partial_t \tag{A.149}$$

and, correspondingly,

$$Q_0 + \bar{Q}_0 = \frac{H + K_1}{2} \tag{A.150}$$
$$Q_0 - \bar{Q}_0 = \frac{P + K_2}{2} \tag{A.151}$$
$$(Q_1 + Q_{-1}) + \left(\bar{Q}_1 + \bar{Q}_{-1}\right) = H - K_1 \tag{A.152}$$
$$(Q_1 + Q_{-1}) - \left(\bar{Q}_1 + \bar{Q}_{-1}\right) = P - K_2 \tag{A.153}$$
$$(Q_1 - Q_{-1}) + \left(\bar{Q}_1 - \bar{Q}_{-1}\right) = -2iD \tag{A.154}$$
$$(Q_1 - Q_{-1}) - \left(\bar{Q}_1 - \bar{Q}_{-1}\right) = -2iB. \tag{A.155}$$

The ground state $|\Psi\rangle$ of CFT Hamiltonian $H$ on the line is the only state in the Hilbert space invariant under the global conformal group and thus annihilated by all these generators. More generally, $|\Psi\rangle$ is annihilated by

$$Q_n|\Psi\rangle = \bar{Q}_n|\Psi\rangle = 0, \qquad \forall n \geq -1. \tag{A.156}$$

Notice in particular that $|\Psi\rangle$ is also the ground state of

$$Q_0 + \bar{Q}_0 = \int dx \; \frac{1+x^2}{2} h(x) = \frac{1}{2}(H + K_1) \tag{A.157}$$

While the Hamiltonian $H = \int dx\ h(x)$ has a continuous spectrum, $Q_0 + \bar{Q}_0$ has the same discrete spectrum as $L_0 + \bar{L}_0$ on the circle, which is given in terms of the scaling dimensions $\Delta_\alpha \equiv h_\alpha + \bar{h}_\alpha$ of the local scaling operators $\phi_\alpha(x)$ of the theory [similarly, while the spectrum of $P$ is continuous, the spectrum of $Q_0 - \bar{Q}_0 = \frac{1}{2}(P + K_2)$ is discrete and given by the conformal spins $s_\alpha \equiv h_\alpha - \bar{h}_\alpha$].

## A.4 1+1 free boson CFT on the real line

In this section we specialize to the 1+1 dimensional free boson CFT on the real line discussed in Chapter 2. We collect from [44] a number of well-known fact that are used in the main text.

### A.4.1 Stress-energy tensor

Consider the action

$$S \equiv \int dx\ dt\ \frac{1}{2}\left((\partial_t\phi)^2 - (\partial_x\phi)^2\right) \tag{A.158}$$

which leads to a stress-energy tensor

$$T(x) = -2\pi\ :\partial\phi(x)\partial\phi(x): \tag{A.159}$$

$$\bar{T}(x) = -2\pi\ :\bar{\partial}\phi(x)\bar{\partial}\phi(x): \tag{A.160}$$

where $\partial\phi$ is a holomorphic (or right moving) field and $\bar{\partial}\phi$ is an antiholomorphic (or left moving) field,

$$\partial\phi(x) \equiv \frac{1}{2}\left(\partial_x\phi(x) - i\partial_\tau\phi(x)\right) \tag{A.161}$$

$$= \frac{1}{2}\left(\partial_x\phi(x) - \pi(x)\right), \tag{A.162}$$

$$\bar{\partial}\phi(x) \equiv \frac{1}{2}\left(\partial_x\phi(x) + i\partial_\tau\phi(x)\right) \tag{A.163}$$

$$= \frac{1}{2}\left(\partial_x\phi(x) + \pi(x)\right), \tag{A.164}$$

and where we have identified $\partial_t\phi(x)$ with $\pi(x)$. Therefore the normal-ordered energy and momentum densities are given by

$$h(x) \equiv\ :\frac{1}{2}\left[\pi(x)^2 + (\partial_x\phi(x))^2\right]:\ , \tag{A.165}$$

$$p(x) \equiv -:\pi(x)\partial_x\phi(x):\ . \tag{A.166}$$

### A.4.2 Generators of global conformal transformations

Introducing now the annihilation operators $a(k)$ that diagonalize the Hamiltonian $H = \int dx\ h(x) = \int dk\ |k|\ a(k)^\dagger a(k)$, namely

$$a(k) \equiv \sqrt{\frac{|k|}{2}}\phi(k) + i\sqrt{\frac{1}{2|k|}}\pi(k), \tag{A.167}$$

where $\phi(k) \equiv \frac{1}{\sqrt{2\pi}}\int dx\ e^{-ikx}\phi(x)$ and $\pi(k) \equiv \frac{1}{\sqrt{2\pi}}\int dx\ e^{-ikx}\pi(x)$ and $[a(k), a(q)^\dagger] = \delta(k-q)$, we can write the global conformal generators as

$$H = \int dk\ |k|\ a(k)^\dagger a(k), \tag{A.168}$$

$$P = \int dk\ k\ a(k)^\dagger a(k), \tag{A.169}$$

$$B = i\int dk\ a(k)^\dagger \left(k\partial_k + \frac{1}{2}\right) a(k), \tag{A.170}$$

$$D = i\int dk\ a(k)^\dagger sgn(k) \left(k\partial_k + \frac{1}{2}\right) a(k), \tag{A.171}$$

$$K_1 = -\int dk\ a(k)^\dagger sgn(k) \left(k\partial_k^2 + \partial_k - \frac{1}{4k}\right) a(k), \tag{A.172}$$

$$K_2 = -\int dk\ a(k)^\dagger \left(k\partial_k^2 + \partial_k - \frac{1}{4k}\right) a(k). \tag{A.173}$$

### A.4.3 Primary operators and OPE's

The primaries in this theory are $\mathbb{1}$, $\partial\phi$, $\bar\partial\phi$ and the so-called vertex operator $:e^{i\alpha\phi}:$, with conformal dimensions $(h, \bar h)$ being $(0,0)$, $(1,0)$, $(0,1)$ and $(\frac{\alpha^2}{8\pi}, \frac{\alpha^2}{8\pi})$ respectively.

From the free boson action $S$ above, we can compute the correlator

$$\langle\phi(x)\phi(y)\rangle = -\frac{1}{4\pi}\log((x-y)^2) + const., \tag{A.174}$$

by Gaussian integration. It follows that,

$$\langle\partial\phi(x)\partial\phi(y)\rangle = -\frac{1}{4\pi}\frac{1}{(x-y)^2}, \tag{A.175}$$

from which we can read the operator product expansion (OPE) of $\partial\phi$ with itself,

$$\partial\phi(x)\partial\phi(y) \sim -\frac{\mathbb{1}}{4\pi}\frac{1}{(x-y)^2}, \tag{A.176}$$

where $\sim$ indicates that we neglect regular terms. The stress tensor is precisely the ignored constant regular term,

$$\begin{aligned} T(x) &\equiv -2\pi : \partial\phi(x)\partial\phi(x) : & \text{(A.177)} \\ &\equiv -2\pi \lim_{y\to x} \left(\partial\phi(x)\partial\phi(y) - \langle\partial\phi(x)\partial\phi(y)\rangle\right). & \text{(A.178)} \end{aligned}$$

We can then apply Wick's theorem to obtain other OPEs. For example,

$$\begin{aligned} T(x)\partial\phi(y) &= -2\pi : \partial\phi(x)\partial\phi(x) : \partial\phi(y) & \text{(A.179)} \\ &\sim \frac{\partial\phi(y)}{(x-y)^2} + \frac{\partial^2\phi(y)}{(x-y)} & \text{(A.180)} \end{aligned}$$

and

$$\begin{aligned} T(x)T(y) &= 4\pi^2 : \partial\phi(x)\partial\phi(x) :: \partial\phi(y)\partial\phi(y) : & \text{(A.181)} \\ &\sim \frac{1/2}{(x-y)^4} + \frac{2T(y)}{(x-y)^2} + \frac{\partial T(y)}{(x-y)}. & \text{(A.182)} \end{aligned}$$

All these expressions hold also for the cMERA smeared operators $\partial\phi^\Lambda(x) = V\partial\phi(x)V^\dagger$, $T^\Lambda(x) = VT(x)V^\dagger$, etc. They can be obtained either by applying the symplectic map $V$ on the CFT expressions or, equivalently, by defining normal ordering with respect to the cMERA annihilation operators $a^\Lambda(k)$ and applying Wick's theorem directly on the smeared operators.

## A.5 Reuse and Permissions License

Chapter 2 and Appendix A of this thesis consist mostly of material published in Reference [1], whose copyright is held by the American Physical Society. In the following is the Reuse and Permissions License from the American Physical Society.

# American Physical Society
# Reuse and Permissions License

19-Jul-2020

This license agreement between the American Physical Society ("APS") and Qi Hu ("You") consists of your license details and the terms and conditions provided by the American Physical Society and SciPris.

## Licensed Content Information

| | |
|---|---|
| **License Number:** | **RNP/20/JUL/028484** |
| **License date:** | 19-Jul-2020 |
| **DOI:** | 10.1103/PhysRevLett.119.010603 |
| **Title:** | Spacetime Symmetries and Conformal Data in the Continuous Multiscale Entanglement Renormalization Ansatz |
| **Author:** | Q. Hu and G. Vidal |
| **Publication:** | Physical Review Letters |
| **Publisher:** | American Physical Society |
| **Cost:** | USD $ 0.00 |

## Request Details

**Does your reuse require significant modifications**: No

| | |
|---|---|
| **Specify intended distribution locations:** | Worldwide |
| **Reuse Category:** | Reuse in a thesis/dissertation |
| **Requestor Type:** | Student |
| **Items for Reuse:** | Whole Article |
| **Format for Reuse:** | Electronic |

## Information about New Publication:

| | |
|---|---|
| **University/Publisher:** | University of Waterloo |
| **Title of dissertation/thesis:** | Continuous Tensor Networks, Conformal Field Theory and Holography |
| **Author(s):** | Qi Hu |
| **Expected completion date:** | Jul. 2020 |

## License Requestor Information

| | |
|---|---|
| **Name:** | Qi Hu |
| **Affiliation:** | Individual |
| **Email Id:** | huuq10@gmail.com |
| **Country:** | Canada |

# American Physical Society
# Reuse and Permissions License

**TERMS AND CONDITIONS**

The American Physical Society (APS) is pleased to grant the Requestor of this license a non-exclusive, non-transferable permission, limited to Electronic format, provided all criteria outlined below are followed.

1. You must also obtain permission from at least one of the lead authors for each separate work, if you haven't done so already. The author's name and affiliation can be found on the first page of the published Article.

2. For electronic format permissions, Requestor agrees to provide a hyperlink from the reprinted APS material using the source material's DOI on the web page where the work appears. The hyperlink should use the standard DOI resolution URL, http://dx.doi.org/{DOI}. The hyperlink may be embedded in the copyright credit line.

3. For print format permissions, Requestor agrees to print the required copyright credit line on the first page where the material appears: "Reprinted (abstract/excerpt/figure) with permission from [(FULL REFERENCE CITATION) as follows: Author's Names, APS Journal Title, Volume Number, Page Number and Year of Publication.] Copyright (YEAR) by the American Physical Society."

4. Permission granted in this license is for a one-time use and does not include permission for any future editions, updates, databases, formats or other matters. Permission must be sought for any additional use.

5. Use of the material does not and must not imply any endorsement by APS.

6. APS does not imply, purport or intend to grant permission to reuse materials to which it does not hold copyright. It is the requestor's sole responsibility to ensure the licensed material is original to APS and does not contain the copyright of another entity, and that the copyright notice of the figure, photograph, cover or table does not indicate it was reprinted by APS with permission from another source.

7. The permission granted herein is personal to the Requestor for the use specified and is not transferable or assignable without express written permission of APS. This license may not be amended except in writing by APS.

8. You may not alter, edit or modify the material in any manner.

9. You may translate the materials only when translation rights have been granted.

10. APS is not responsible for any errors or omissions due to translation.

11. You may not use the material for promotional, sales, advertising or marketing purposes.

12. The foregoing license shall not take effect unless and until APS or its agent, Aptara, receives payment in full in accordance with Aptara Billing and Payment Terms and Conditions, which are incorporated herein by reference.

13. Should the terms of this license be violated at any time, APS or Aptara may revoke the license with no refund to you and seek relief to the fullest extent of the laws of the USA. Official written notice will be made using the contact information provided with the permission request. Failure to receive such notice will not nullify revocation of the permission.

14. APS reserves all rights not specifically granted herein.

15. This document, including the Aptara Billing and Payment Terms and Conditions, shall be the entire agreement between the parties relating to the subject matter hereof.

# Appendix B

# Appendices for Chapter 3

## B.1 Quasilocal smearing function

In this section we examine the constraints of the smearing function $\mu(\boldsymbol{x}, \boldsymbol{y})$ and illustrate a concrete example which fulfills the constraints. We will have four constraints. (i) The smearing function $\mu(\boldsymbol{x}, \boldsymbol{y})$ is translation and rotation invariant, which means that it only depends on $|\boldsymbol{x} - \boldsymbol{y}|$. (ii) To (quasi)preserve the local structure of the continuous partition function, we require the smearing function $\mu(x)$ to be quasilocal, in the sense that it is upper bounded by an exponentially decaying function at long distances. (iii) The smeared fields should be normalized such that they have the same behaviors as in the original field theory at long distances. This demands that $\int d\boldsymbol{x}\ \mu(|\boldsymbol{x}|) = 1$, or equivalently $\mu(k = 0) = 1$. (iv) We demand that there are only finite fluctuations at short distances, that is,

$$\left| \lim_{\boldsymbol{x} \to 0} \langle \phi(\boldsymbol{x}) \phi(\boldsymbol{0}) \rangle_\Lambda \right| < \infty, \tag{B.1}$$

where $\langle \phi(\boldsymbol{x}) \phi(\boldsymbol{0}) \rangle_\Lambda$ represents the correlation function for the smeared action $S^\Lambda[\phi]$ determined by the smearing function $\mu(x)$. Assuming $\langle \phi(\boldsymbol{k}) \phi(-\boldsymbol{k}) \rangle_\Lambda$ tends to a constant $\frac{1}{\Lambda^2}$, which results in a contact term in the correlation function $\langle \phi(\boldsymbol{x}) \phi(\boldsymbol{0}) \rangle_\Lambda$ in real space, constraint (iv) becomes

$$\left| \int d\boldsymbol{k} \left( \frac{1}{k^2 + m^2} \frac{1}{\mu(k)^2} - \frac{1}{\Lambda^2} \right) \right| < \infty. \tag{B.2}$$

Here the integral should be understood as the Hadamard finite-part integral if divergence occurs in the neighborhood of $k = 0$. In that case, the condition can also be written as

$$\left| \int_{k>\Lambda} d\boldsymbol{k} \, \left( \frac{1}{k^2 + m^2} \frac{1}{\mu(k)^2} - \frac{1}{\Lambda^2} \right) \right| < \infty. \tag{B.3}$$

An example of $\mu(x)$ that fulfills the four constraints is given by the 2D Fourier transform of the following:

$$\mu(k) = \frac{\Lambda}{k} \mathrm{Exp} \left( \frac{1}{2} \mathrm{Expi} \left( -\frac{k^2}{\sigma \Lambda^2} \right) \right). \tag{B.4}$$

Here $\sigma = e^{\gamma} \approx 1.78$, where $\gamma$ is Euler's constant. Next we show that constraints (i), (ii) and (iii) are satisfied. In the following section we will show that constraint (iv) is also fulfilled.

Constraint (i) is fulfilled because $\mu(k)$ only depends on $|\boldsymbol{k}|$. Constraint (iii) can be verified by plugging in the expansion

$$\mathrm{Expi}(x) = \gamma + \log x + O(x^2), \qquad \text{as } x \to 0, \tag{B.5}$$

in Eq. B.4, which yields

$$\mu(k) = 1 - \frac{k^2}{2\sigma\Lambda^2} + O(k^4), \qquad \text{as } k \to 0, \tag{B.6}$$

and in particular $\mu(k = 0) = 1$.

Constraint (ii) will follow from the analytical study of the asymptotic behavior of $\mu(x)$ for large $x$, which can be inferred from its 2D Fourier transform $\mu(k)$. We use the same strategy as in the appendix of [**?**]. Notice that $\mu(k)$ satisfies the differential equation

$$k \partial_k \mu(k) = g(k) \mu(k), \tag{B.7}$$

where $g(k) = -1 + e^{-\frac{k^2}{\sigma\Lambda^2}}$. Applying a 2D Fourier transform, we get the equation in real space,

$$(-\boldsymbol{x} \cdot \nabla - 1) \mu(\boldsymbol{x}) = \frac{\sigma\Lambda^2}{4\pi} \int d\boldsymbol{y} \; e^{-\frac{1}{4}\sigma\Lambda^2 y^2} \mu(\boldsymbol{x} - \boldsymbol{y}). \tag{B.8}$$

We define a new variable $u(\boldsymbol{x})$:

$$\mu(\boldsymbol{x}) = e^{-u(\boldsymbol{x})}. \tag{B.9}$$

Then the differential equation becomes

$$\boldsymbol{x} \cdot \nabla u(\boldsymbol{x}) - 1 = \frac{\sigma\Lambda^2}{4\pi} \int d\boldsymbol{y} \; e^{-\frac{1}{4}\sigma\Lambda^2 y^2 - u(\boldsymbol{x}-\boldsymbol{y}) + u(\boldsymbol{x})}. \tag{B.10}$$

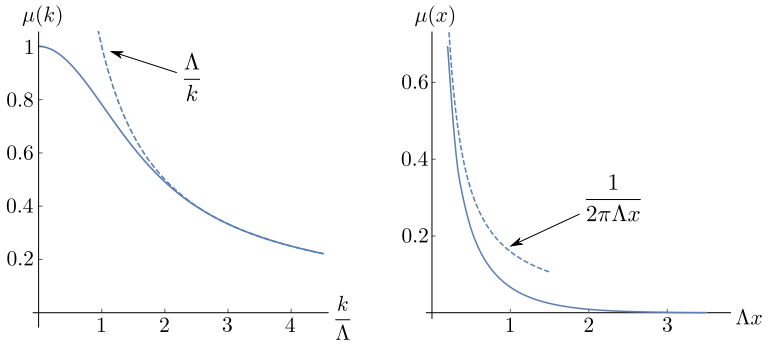


Figure B.1: (a) The smearing function $\mu(k)$ in momentum space. The dashed line is $\frac{\Lambda}{k}$, which represents the asymptotic behavior of $\mu(k)$ for large $k$. (b) The smearing function $\mu(x)$ in real space. The dashed line is $\frac{1}{2\pi\Lambda x}$, which represents the asymptotic behavior of $\mu(x)$ for small $x$.

We then expand $u(\boldsymbol{x}-\boldsymbol{y})$ around $\boldsymbol{x}$,

$$u(\boldsymbol{x}-\boldsymbol{y}) \approx u(\boldsymbol{x}) - \boldsymbol{y}\cdot\nabla u(\boldsymbol{x}). \tag{B.11}$$

In consequence, the right hand side of the differential equation is approximated by a Gaussian integral,

$$\begin{aligned} &\frac{\sigma\Lambda^2}{4\pi}\int d\boldsymbol{y}\; e^{-\frac{1}{4}\sigma\Lambda^2 y^2 - u(\boldsymbol{x}-\boldsymbol{y})+u(\boldsymbol{x})} \\ &\approx \frac{\sigma\Lambda^2}{4\pi}\int d\boldsymbol{y}\; e^{-\frac{1}{4}\sigma\Lambda^2 y^2 + \boldsymbol{y}\cdot\nabla u(\boldsymbol{x})} \\ &= e^{(\nabla u(\boldsymbol{x}))^2/(\sigma\Lambda^2)}. \end{aligned} \tag{B.12}$$

Since $\mu(\boldsymbol{x})$ is rotation invariant, it is only a function of $x$, and hence so is $u(\boldsymbol{x})$. Then we have

$$xu'(x) - 1 = e^{u'(x)^2/(\sigma\Lambda^2)}. \tag{B.13}$$

The approximate solution can be found in the large $x$ limit:

$$u'(x) = \Lambda\sqrt{\sigma\ \log\Lambda x}\ (1+o(1)),\ \text{as } x\to\infty. \tag{B.14}$$

Performing the integration we get

$$u(x) = \Lambda x\sqrt{\sigma\ \log\Lambda x}\ (1+o(1)),\ \text{as } x\to\infty. \tag{B.15}$$

Finally we obtain the asymptotic behavior of $\mu(x)$ for large $x$,

$$\mu(x) = e^{-\Lambda x\sqrt{\sigma\ \log\Lambda x}\ (1+o(1))},\ \text{as } x \to \infty. \tag{B.16}$$

It is then clear that $\mu(x)$ can be upper bounded by an exponentially decaying function in the limit of large $x$. Therefore our proposed smearing function fulfills constraint (ii).

Additionally, the asymptotic behavior of $\mu(x)$ for small $x$ can also be obtained from its Fourier transform. To do so, we divide $\mu(k)$ into two pieces $\mu^{(1)}(k) + \mu^{(2)}(k)$:

$$\mu^{(1)}(k) \equiv \frac{\Lambda}{k}, \tag{B.17}$$

$$\mu^{(2)}(k) \equiv \frac{\Lambda}{k}\mathrm{Exp}\Big(\frac{1}{2}\mathrm{Expi}(-\frac{k^2}{\sigma\Lambda^2})\Big) - \frac{\Lambda}{k}. \tag{B.18}$$

The 2D Fourier transform of $\mu^{(1)}(k)$ is $\frac{1}{2\pi\Lambda x}$, which is computed analytically, and the 2D Fourier transform of $\mu^{(2)}(k)$ can be shown to be finite around $x = 0$. Therefore, the asymptotic behavior of $\mu(x)$ at $x = 0$ is

$$\mu(x) = \frac{1}{2\pi\Lambda x} + O(1),\ \text{as } x \to 0. \tag{B.19}$$

## B.2 Correlation function

In this section we study the behavior of the correlation function $\langle\phi(\boldsymbol{x})\phi(\boldsymbol{0})\rangle_\Lambda$ for the smeared free boson action $S^\Lambda[\phi]$. For concreteness, the analysis of the short and long distance behavior of the correlator will focus on the massless case. At short distances, it can be shown to be finite, thus fulfilling constraint (iv) from the previous section. At long distances, it approaches the correlation function $\langle\phi(\boldsymbol{x})\phi(\boldsymbol{0})\rangle$ from the CFT.

For the 2D free boson theory in Euclidean spacetime, the action is given by

$$\begin{aligned} S[\phi] &= \frac{1}{2}\int d\boldsymbol{x}\left(-\phi(\boldsymbol{x})\Delta\phi(\boldsymbol{x}) + m^2\phi(\boldsymbol{x})^2\right) \\ &= \frac{1}{2}\int \frac{d\boldsymbol{k}}{(2\pi)^2}\ (k^2+m^2)\phi(\boldsymbol{k})\phi(-\boldsymbol{k}). \end{aligned} \tag{B.20}$$

To compute the correlation function $\langle\phi(\boldsymbol{k})\phi(-\boldsymbol{k})\rangle$, we introduce a source term in the action:

$$\begin{aligned} S[\phi,\lambda] &= \frac{1}{2}\int d\boldsymbol{x}\ \Big( -\phi(\boldsymbol{x})\Delta\phi(\boldsymbol{x}) + m^2\phi(\boldsymbol{x})^2\Big) \\ &\quad + \int d\boldsymbol{x}\ \lambda(x)\phi(\boldsymbol{x}) \\ &= \frac{1}{2}\int \frac{d\boldsymbol{k}}{(2\pi)^2}\ (k^2+m^2)\phi(\boldsymbol{k})\phi(-\boldsymbol{k}) \\ &\quad + \int \frac{d\boldsymbol{k}}{(2\pi)^2}\ \lambda(\boldsymbol{k})\phi(-\boldsymbol{k}). \end{aligned} \tag{B.21}$$

The partition function is given by the path integral:

$$\begin{aligned} Z(\lambda) &\equiv \int [d\phi] e^{-S[\phi,\lambda]} \\ &= Z(0) e^{\frac{1}{2}\int \frac{d\boldsymbol{k}}{(2\pi)^2}(k^2+m^2)^{-1}\lambda(\boldsymbol{k})\lambda(-\boldsymbol{k})}. \end{aligned} \tag{B.22}$$

The correlation function can then be computed as follows:

$$\begin{aligned} &\langle\phi(\boldsymbol{k})\phi(-\boldsymbol{k})\rangle \\ &= \frac{\int [d\phi] e^{-S[\phi]}\phi(\boldsymbol{k})\phi(-\boldsymbol{k})}{\int [d\phi] e^{-S[\phi]}} \\ &= Z(0)^{-1}\frac{\partial}{\partial\lambda(\boldsymbol{k})}\frac{\partial}{\partial\lambda(-\boldsymbol{k})}\int [d\phi] e^{-S[\phi,\lambda]}\Big|_{\lambda(\boldsymbol{k})=0} \\ &= Z(0)^{-1}\frac{\partial}{\partial\lambda(\boldsymbol{k})}\frac{\partial}{\partial\lambda(-\boldsymbol{k})} Z(\lambda)\Big|_{\lambda(\boldsymbol{k})=0} \\ &= \frac{1}{k^2+m^2}. \end{aligned} \tag{B.23}$$

In the massless case $m=0$, $\langle\phi(\boldsymbol{k})\phi(-k)\rangle = \frac{1}{k^2}$. Its 2D Fourier transform produces the real-space correlator,

$$\begin{aligned} \langle\phi(\boldsymbol{x})\phi(\boldsymbol{0})\rangle &= \int \frac{d\boldsymbol{k}}{(2\pi)^2}\langle\phi(\boldsymbol{k})\phi(-\boldsymbol{k})\rangle e^{i\boldsymbol{k}\cdot\boldsymbol{x}} \\ &= -\frac{1}{2\pi}\log(x) + \text{const.} \end{aligned} \tag{B.24}$$

Similarly we obtain the correlation function for the smeared action:

$$\begin{aligned}\langle\phi(\boldsymbol{k})\phi(-\boldsymbol{k})\rangle_\Lambda &= \frac{\int[d\phi]e^{-S[\phi^\Lambda]}\phi(\boldsymbol{k})\phi(-\boldsymbol{k})}{\int[d\phi]e^{-S[\phi^\Lambda]}} \\ &= \frac{1}{(k^2+m^2)\mu(k)^2}.\end{aligned} \tag{B.25}$$

In the massless case, $\langle\phi(\boldsymbol{k})\phi(-\boldsymbol{k})\rangle_\Lambda = \frac{1}{k^2\mu(k)^2}$. Note that $\frac{1}{k^2\mu(k)^2} \sim \frac{1}{k^2}$ as $k \to 0$, and $\frac{1}{k^2\mu(k)^2} \sim \frac{1}{\Lambda^2}$ as $k \to \infty$. To compute the numerical value of the Fourier transform, we subtract the divergent part $\frac{1}{k^2}+\frac{1}{\Lambda^2}$, which has analytical Fourier transform $-\frac{1}{2\pi}\log(\sigma\Lambda x)+\frac{1}{\Lambda^2}\delta(\boldsymbol{x})$ (where we have made a concrete choice of the arbitrary additive constant in Eq. B.24). We then perform the numerical Fourier transform to the rest and add it to the analytical part. The final result is shown in Fig. B.2. As we can see, at short distances the correlation function $\langle\phi(\boldsymbol{x})\phi(\boldsymbol{0})\rangle_\Lambda$ is finite apart from a contact term, and at long distances, $\langle\phi(\boldsymbol{x})\phi(\boldsymbol{0})\rangle_\Lambda$ asymptotically approaches the correlation function in the boson CFT. One can easily verify Eq. B.3, which also proves that the correlation function is finite at short distances. For example, in the massless case $m=0$, $\left|\int_{k>\Lambda} d\boldsymbol{k}\left(\frac{1}{k^2\mu(k)^2}-\frac{1}{\Lambda^2}\right)\right| \approx 1.855$.

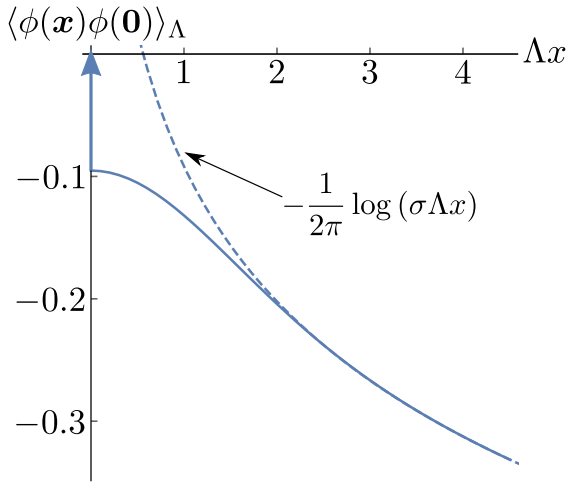


Figure B.2: Correlation function $\langle\phi(\boldsymbol{x})\phi(\boldsymbol{0})\rangle_\Lambda$. The arrow represents a delta function $\frac{1}{\Lambda^2}\delta(\boldsymbol{x})$. The dashed line is $-\frac{1}{2\pi}\log(\sigma\Lambda x)$, which represents the asymptotic behavior of the correlation function for large $x$, and matches the CFT correlation formula Eq. B.24.

## B.3 RG flow generated by $\mathfrak{L} + \mathfrak{K}_s$

In this section, we investigate how the action $S^\Lambda[\phi]$ and the smeared field $\phi^\Lambda(\boldsymbol{x})$ evolve along the RG flow generated by $\mathfrak{L} + \mathfrak{K}_s$. Recall the definition of $\mathfrak{L}$:

$$\mathfrak{L}\phi(\boldsymbol{x}) = (-\boldsymbol{x} \cdot \nabla_{\boldsymbol{x}} - \Delta_\phi)\phi(\boldsymbol{x}). \tag{B.26}$$

For the 2D free boson theory, $\phi(\boldsymbol{x})$ has classical scaling dimension $\Delta_\phi = 0$. Therefore, the above equation becomes

$$\mathfrak{L}\phi(\boldsymbol{x}) = -\boldsymbol{x} \cdot \nabla_{\boldsymbol{x}}\phi(\boldsymbol{x}). \tag{B.27}$$

In momentum space it reads

$$\mathfrak{L}\phi(\boldsymbol{k}) = (\boldsymbol{k} \cdot \nabla_{\boldsymbol{k}} + 2)\phi(\boldsymbol{k}). \tag{B.28}$$

The action of $\mathfrak{K}_s$ in real space is given by

$$\mathfrak{K}_s\phi(\boldsymbol{x}) = \int d\boldsymbol{y}\ g(s, |\boldsymbol{x} - \boldsymbol{y}|)\phi(\boldsymbol{y}). \tag{B.29}$$

In momentum space, it reads

$$\mathfrak{K}_s\phi(\boldsymbol{k}) = g(s, k)\phi(\boldsymbol{k}). \tag{B.30}$$

In flat spacetime, the path integration measure $[d\phi]$ can be decomposed as a product of measures for individual momentum modes, that is, $[d\phi] = \prod_{\boldsymbol{k}} d\phi(\boldsymbol{k})$. Eq. B.30 implies that $\mathfrak{K}$ acts diagonally in momentum space, and therefore only changes the integration measure by a constant factor. We further assume that $\mathfrak{L}$ also leaves the integration measure invariant up to a constant factor. Omitting both of these constant factors, we can generate an RG flow by directly applying $\mathfrak{L} + \mathfrak{K}_s$ to the action $S^\Lambda[\phi]$. In order to alleviate notation, we

only consider $\mathfrak{K}_s$ for $s=0$, and define $\mathfrak{K}\equiv\mathfrak{K}_0$, $g(k)\equiv g(0,k)$.

$$
\begin{aligned}
&(\mathfrak{L}+\mathfrak{K})S^{\Lambda}[\phi]\\
&=\frac{1}{2}\int\frac{d\boldsymbol{k}}{(2\pi)^2}(k^2+m^2)\mu(k)^2\Big[(\mathfrak{L}+\mathfrak{K})\phi(\boldsymbol{k})\phi(-\boldsymbol{k})\\
&\quad+\phi(\boldsymbol{k})(\mathfrak{L}+\mathfrak{K})\phi(-\boldsymbol{k})\Big]\\
&=\frac{1}{2}\int\frac{d\boldsymbol{k}}{(2\pi)^2}\Big[(k^2+m^2)\mu(k)^2\\
&\quad\Big(\boldsymbol{k}\cdot\nabla_{\boldsymbol{k}}+4+2g(k)\Big)\Big(\phi(\boldsymbol{k})\phi(-\boldsymbol{k})\Big)\Big]\\
&=\frac{1}{2}\int\frac{d\boldsymbol{k}}{(2\pi)^2}\Big[\Big(-\boldsymbol{k}\cdot\nabla_{\boldsymbol{k}}+2+2g(k)\Big)\\
&\quad\Big((k^2+m^2)\mu(k)^2\Big)\phi(\boldsymbol{k})\phi(-\boldsymbol{k})\Big]\\
&=\frac{1}{2}\int\frac{d\boldsymbol{k}}{(2\pi)^2}\Big[k^2\Big(-\boldsymbol{k}\cdot\nabla_{\boldsymbol{k}}+2g(k)\Big)\Big(\mu(k)^2\Big)\\
&\quad+m^2\Big(-\boldsymbol{k}\cdot\nabla_{\boldsymbol{k}}+2+2g(k)\Big)\Big(\mu(k)^2\Big)\Big]\phi(\boldsymbol{k})\phi(-\boldsymbol{k})\\
&=\int\frac{d\boldsymbol{k}}{(2\pi)^2}\Big\{k^2\mu(k)\Big[\big(-k\partial_k+g(k)\big)\mu(k)\Big]\\
&\quad+m^2\mu(k)\Big[\big(-k\partial_k+1+g(k)\big)\mu(k)\Big]\Big\}\phi(\boldsymbol{k})\phi(-\boldsymbol{k}).
\end{aligned}
\tag{B.31}
$$

Similarly, we can obtain the change of the smeared field $\phi^{\Lambda}(\boldsymbol{x})$ under the action of $\mathfrak{L}+\mathfrak{K}$. For simplicity, we only consider $\phi^{\Lambda}(\boldsymbol{x})$ for $\boldsymbol{x}=\boldsymbol{0}$.

$$
\begin{aligned}
&(\mathfrak{L}+\mathfrak{K}_s)\phi^{\Lambda}(\boldsymbol{0})\\
&=\int\frac{d\boldsymbol{k}}{(2\pi)^2}\mu(k)(\mathfrak{L}+\mathfrak{K}_s)\phi(\boldsymbol{k})\\
&=\int\frac{d\boldsymbol{k}}{(2\pi)^2}\mu(k)\Big(\boldsymbol{k}\cdot\nabla_{\boldsymbol{k}}+2+g(k)\Big)\phi(\boldsymbol{k})\\
&=\int\frac{d\boldsymbol{k}}{(2\pi)^2}\Big[\Big(-\boldsymbol{k}\cdot\nabla_{\boldsymbol{k}}+g(k)\Big)\mu(k)\Big]\phi(\boldsymbol{k})\\
&=\int\frac{d\boldsymbol{k}}{(2\pi)^2}\Big[\Big(-k\partial_k+g(k)\Big)\mu(k)\Big]\phi(\boldsymbol{k}).
\end{aligned}
\tag{B.32}
$$

In the massless case, the action $S^\Lambda$ is invariant if and only if

$$g(k) = \frac{k\partial_k \mu(k)}{\mu(k)}. \tag{B.33}$$

Let $\mathfrak{K}_\star$ denote the fixed-point disentangler given by the above condition and $S^\Lambda_\star$ the massless action. Then we have

$$(\mathfrak{L} + \mathfrak{K}_\star) S^\Lambda_\star = 0. \tag{B.34}$$

Note that Eq. B.32 implies that the smeared field $\phi^\Lambda(\mathbf{0})$ is also invariant under the action of $\mathfrak{L} + \mathfrak{K}_\star$.

For a massive theory, $\mathfrak{L} + \mathfrak{K}_\star$ generates an RG flow, given by

$$(\mathfrak{L} + \mathfrak{K}_\star) S^\Lambda[\phi] = \int \frac{d\boldsymbol{k}}{(2\pi)^2} m^2 \mu(k)^2 \phi(\boldsymbol{k})\phi(-\boldsymbol{k}), \tag{B.35}$$

or equivalently,

$$\begin{aligned} &S^\Lambda_s[\phi] \equiv e^{s(\mathfrak{L}+\mathfrak{K}_\star)} S^\Lambda[\phi] \\ &= \frac{1}{2}\int d\boldsymbol{x}\Big( - \phi^\Lambda(\boldsymbol{x})\Delta\phi^\Lambda(\boldsymbol{x}) + m^2 e^{2s}\phi^\Lambda(\boldsymbol{x})^2\Big). \end{aligned} \tag{B.36}$$

We can also compute the correlation function along the RG flow:

$$\begin{aligned} \langle \phi(\boldsymbol{k})\phi(-\boldsymbol{k})\rangle_{\Lambda,s} &\equiv \frac{\int [d\phi] e^{-S^\Lambda_s[\phi]} \phi(\boldsymbol{k})\phi(-\boldsymbol{k})}{\int [d\phi] e^{-S^\Lambda_s[\phi]}} \\ &= \frac{1}{(k^2 + m^2 e^{2s})\mu(k)^2}. \end{aligned} \tag{B.37}$$

As Fig. B.3(a) shows, the correlation function $\langle \phi(\boldsymbol{k})\phi(-\boldsymbol{k})\rangle_{\Lambda,s}$ approaches a constant $\frac{1}{m^2 e^{2s}}$ for small $k$, and a constant $\frac{1}{\Lambda^2}$ for large $k$. Therefore, the theory behaves trivially at long distances and short distances. The IR regulator $\mathfrak{K}_{IR}(s)$ and UV regulator $\mathfrak{K}_{UV}(s)$ are approximately $me^s$ and $\Lambda$ respectively. The nontrivial information of the theory for a given value of $s$ is contained in the correlation function $\langle \phi(\boldsymbol{k})\phi(-\boldsymbol{k})\rangle_{\Lambda,s}$ for $\mathfrak{K}_{IR}(s) < k < \mathfrak{K}_{UV}(s)$. This window has a decreasing width along the RG flow. This is expected because the disentangler $\mathfrak{K}_\star$ sequentially removes correlations at different scales. As a comparison, we compute the correlation function for the theory $e^{sL} S^\Lambda[\phi]$. The evolution of the smeared theory generated by $\mathfrak{L}$ is given by

$$\begin{aligned} &e^{s\mathfrak{L}} S^\Lambda[\phi] \\ &= \int \frac{d\boldsymbol{k}}{(2\pi)^2} (k^2 + m^2)\mu(k)^2 e^{2s}\phi(\boldsymbol{k}e^s) e^{2s}\phi(-\boldsymbol{k}e^s) \\ &= \int \frac{d\boldsymbol{k}}{(2\pi)^2} (k^2 + m^2 e^{2s})\mu(ke^{-s})^2 \phi(\boldsymbol{k})\phi(-\boldsymbol{k}). \end{aligned} \tag{B.38}$$

Then we can easily compute the correlation function

$$\begin{aligned}\langle\phi(\boldsymbol{k})\phi(-\boldsymbol{k})\rangle^{(L)}_{\Lambda,s} &\equiv \frac{\int[d\phi]e^{-e^{s\mathfrak{L}}S^{\Lambda}[\phi]}\phi(\boldsymbol{k})\phi(-\boldsymbol{k})}{\int[d\phi]e^{-e^{s\mathfrak{L}}S^{\Lambda}[\phi]}} \\ &= \frac{1}{(k^2+m^2e^{2s})\mu(ke^{-s})^2}.\end{aligned} \tag{B.39}$$

As Fig. B.3(b) shows, the width of the window containing the nontrivial information of the theory does not change. This is because $\mathfrak{L}$ only rescales the spacetime and fields, but it does not remove any correlations.

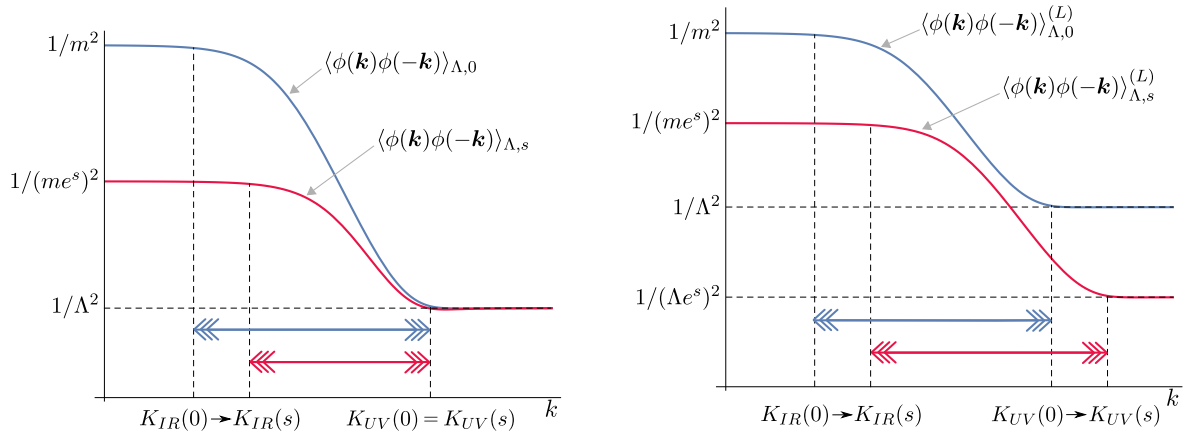


Figure B.3: (a) Evolution of $\langle\phi(\boldsymbol{k})\phi(-\boldsymbol{k})\rangle_{\Lambda,s}$ as a function of $s$, generated by $\mathfrak{L}+\mathfrak{K}_\star$. The plot is in log-log scale. The correlation is close to a constant outside the window $\mathfrak{K}_{IR}(s)<k<\mathfrak{K}_{UV}(s)$, where $\mathfrak{K}_{IR}\sim me^s$, and $\mathfrak{K}_{UV}\sim\Lambda$. The width of the window keeps decreasing along the RG flow generated by $\mathfrak{L}+\mathfrak{K}_\star$. (b) The evolution of $\langle\phi(\boldsymbol{k})\phi(-\boldsymbol{k})\rangle^{(L)}_{\Lambda,s}$ as a function of $s$, generated by $\mathfrak{L}$. The plot is in log-log scale. The correlation is close to a constant outside the window $\mathfrak{K}_{IR}(s)<k<\mathfrak{K}_{UV}(s)$, where $\mathfrak{K}_{IR}\sim me^s$, and $\mathfrak{K}_{UV}\sim\Lambda e^s$. The width of the window remains invariant along the RG flow generated by $\mathfrak{L}$.

## B.4 2D free boson CFT

In this section, we give a brief introduction to the free boson CFT in 2 dimensions. The action is

$$S[\phi] = \frac{1}{2}\int dx_1 dx_2 \Big( (\partial_{x_1}\phi)^2 + (\partial_{x_2}\phi)^2 \Big). \tag{B.40}$$

It is convenient to parametrize the Euclidean plane by complex coordinates:

$$z = x_1 + i x_2, \qquad \bar{z} = x_1 - i x_2. \tag{B.41}$$

The primaries in this theory are $\mathbb{1}$, $\partial\phi \equiv \partial_{x_1}\phi - i\partial_{x_2}\phi$, $\bar{\partial}\phi \equiv \partial_{x_1}\phi + i\partial_{x_2}\phi$ and the vertex operators $\mathcal{V}_\alpha \equiv\!: e^{i\alpha\phi} :$. Their conformal dimensions are $(0,0)$, $(1,0)$, $(0,1)$ and $(\frac{\alpha^2}{8\pi}, \frac{\alpha^2}{8\pi})$, respectively.

The correlation of $\partial\phi$ with itself is

$$\langle \partial\phi(z)\partial\phi(w)\rangle = -\frac{1}{4\pi}\frac{1}{(z-w)^2}, \tag{B.42}$$

from which we can derive the OPE

$$\partial\phi(z)\partial\phi(w) \sim -\frac{\mathbb{1}}{4\pi}\frac{1}{(z-w)^2}. \tag{B.43}$$

The holomorphic component of the stress tensor $T$ is the regular part of the product of $\partial\phi$ with itself:

$$\begin{aligned} T(z) &= -2\pi :\partial\phi(z)\partial\phi(z): \\ &= -2\pi \lim_{w\to z}\Big( \partial\phi(z)\partial\phi(w) - \langle\partial\phi(z)\partial\phi(w)\rangle \Big). \end{aligned} \tag{B.44}$$

Here, the normal ordering $:A(z)B(z):$ of two fields $A(z)$ and $B(w)$ is defined as usual by subtracting all the singular terms of $A(z)B(w)$ in the limit $w \to z$. The OPE of $T(z)$ with $\partial\phi$ can be calculated from Wick's theorem:

$$\begin{aligned} T(z)\partial\phi(w) &= -2\pi :\partial\phi(z)\partial\phi(z): \partial\phi(w) \\ &\sim \frac{\partial\phi(z)}{(z-w)^2} \\ &\sim \frac{\partial\phi(w)}{(z-w)^2} + \frac{\partial^2\phi(w)}{(z-w)}. \end{aligned} \tag{B.45}$$

Furthermore, we can calculate the OPE of $T(z)$ with itself:

$$\begin{aligned} T(z)T(w) &= 4\pi^2 : \partial\phi(z)\partial\phi(z) :: \partial\phi(w)\partial\phi(w) : \\ &\sim \frac{1/2}{(z-w)^4} + \frac{2T(w)}{(z-w)^2} + \frac{\partial T(w)}{(z-w)}. \end{aligned} \tag{B.46}$$

We can read off the central charge $c = 1$ from this expression, since the OPE of $T(z)$ with itself for a general CFT is

$$T(z)T(w) \sim \frac{c/2}{(z-w)^4} + \frac{2T(w)}{(z-w)^2} + \frac{\partial T(w)}{(z-w)}. \tag{B.47}$$

## B.5 Correspondence between sharp and smeared scaling operators

The massless free boson theory $S[\phi]$ is invariant not only under Euclidean symmetries (translations and rotations), but also under change of scale generated by $\mathfrak{L}$, and more generally under the conformal group. It has been shown that Euclidean symmetry is preserved in the quasilocal action $S^\Lambda$. However, scale invariance is explicitly broken by the introduction of a UV cutoff, namely the smearing length $\frac{1}{\Lambda}$. Nevertheless, we can define scale invariance with respect to $\mathfrak{L} + \mathfrak{K}_\star$. More generally, the smeared theory realizes the whole conformal group although in a quasilocal way, as we explain next.

Since the smearing is diagonal in momentum space, $\phi^\Lambda(\boldsymbol{k}) = \mu(k)\phi(\boldsymbol{k})$, it changes the integration measure only by a constant factor. Therefore the partition function $Z^\Lambda$ is proportional to the partition function $Z$ of the original CFT.

$$Z^\Lambda = \int [d\phi] e^{-S[\phi^\Lambda]} \propto \int [d\phi^\Lambda] e^{-S[\phi^\Lambda]} = Z. \tag{B.48}$$

In consequence, we can construct a one-to-one correspondence between smeared fields in the smeared theory and sharp fields in the original CFT. For example, we associate each linear field $\mathcal{O}(\boldsymbol{x})$ (linear in terms of $\phi(\boldsymbol{x})$) in the CFT with a smeared field $\mathcal{O}^\Lambda(\boldsymbol{x})$ in the smeared theory by the following relation:

$$\mathcal{O}^\Lambda(\boldsymbol{x}) \equiv \int d\boldsymbol{y}\ \mu(|\boldsymbol{x}-\boldsymbol{y}|)\mathcal{O}(\boldsymbol{y}) \tag{B.49}$$

In particular Eq. B.49 maps the linear local scaling operators $\mathcal{O}_\alpha(\boldsymbol{x})$ in the free boson CFT to the linear quasilocal scaling operators $\mathcal{O}^\Lambda_\alpha(\boldsymbol{x})$ in the smeared theory.

Local scaling operators are the eigenvectors of $\mathfrak{L}$ and $\mathfrak{R}$:

$$\begin{aligned} \mathfrak{L}\ \mathcal{O}_\alpha(\mathbf{0}) &= -\Delta_\alpha \mathcal{O}_\alpha(\mathbf{0}), \\ \mathfrak{R}\ \mathcal{O}_\alpha(\mathbf{0}) &= s_\alpha \mathcal{O}_\alpha(\mathbf{0}), \end{aligned} \tag{B.50}$$

while quasilocal scaling operators are the eigenvectors of $\mathfrak{L} + \mathfrak{K}_\star$ and $\mathfrak{R}$:

$$\begin{aligned} (\mathfrak{L} + \mathfrak{K}_\star)\ \mathcal{O}^\Lambda_\alpha(\mathbf{0}) &= -\Delta_\alpha \mathcal{O}^\Lambda_\alpha(\mathbf{0}), \\ \mathfrak{R}\ \mathcal{O}^\Lambda_\alpha(\mathbf{0}) &= s_\alpha \mathcal{O}^\Lambda_\alpha(\mathbf{0}). \end{aligned} \tag{B.51}$$

The rotation $\mathfrak{R}$ is unchanged because the smearing function $\mu(x)$ is rotation invariant. Now we associate each linear local scaling operator $\mathcal{O}_\alpha(\mathbf{0})$ with a linear smeared operator $\mathcal{O}^\Lambda_\alpha(\mathbf{0}) \equiv \int d\boldsymbol{x}\ \mu(x)\mathcal{O}_\alpha(\boldsymbol{x})$, and show that the equations Eq. B.50 imply the equations Eq. B.51.

Since $\mu(x)$ is rotation invariant, obviously $\mathcal{O}^\Lambda_\alpha(\mathbf{0})$ is an eigenvector of $\mathfrak{R}$ with the same conformal spin $s_\alpha$. Applying $(\mathfrak{L} + \mathfrak{K}_\star)$ to $\mathcal{O}^\Lambda_\alpha(\mathbf{0})$ we get

$$\begin{aligned} &(\mathfrak{L} + \mathfrak{K}_\star)\ \mathcal{O}^\Lambda_\alpha(\mathbf{0}) \\ &= \int d\boldsymbol{x}\ \mu(x)(\mathfrak{L} + \mathfrak{K}_\star)\mathcal{O}_\alpha(\boldsymbol{x}) \\ &= \int d\boldsymbol{x}\ \mu(x)\Big((-\boldsymbol{x}\cdot\nabla_{\boldsymbol{x}} - \Delta_\alpha)\mathcal{O}_\alpha(\boldsymbol{x}) + \int g(|\boldsymbol{x}-\boldsymbol{y}|)O_\alpha(\boldsymbol{y})\Big) \\ &= \int d\boldsymbol{k}\ \mu(k)(\boldsymbol{k}\cdot\nabla_{\boldsymbol{k}} + 2 - \Delta_\alpha + g(k))\mathcal{O}_\alpha(\boldsymbol{k}) \\ &= \int d\boldsymbol{k}\ (-\boldsymbol{k}\cdot\nabla_{\boldsymbol{k}} - \Delta_\alpha + g(k))\mu(k)\mathcal{O}_\alpha(\boldsymbol{k}) \\ &= \int d\boldsymbol{k}\ (-k\partial_k + g(k) - \Delta_\alpha)\mu(k)\mathcal{O}_\alpha(\boldsymbol{k}) \\ &= -\int d\boldsymbol{k}\ \Delta_\alpha \mu(k)\mathcal{O}_\alpha(\boldsymbol{k}) \\ &= -\Delta_\alpha \mathcal{O}^\Lambda_\alpha(\mathbf{0}). \end{aligned} \tag{B.52}$$

Therefore, $\mathcal{O}^\Lambda_\alpha(\mathbf{0})$ is a smeared scaling operator with the same scaling dimension $\Delta_\alpha$. Thus, for linear operators, we have proved that the smearing process Eq. B.49 maps local scaling operators in the CFT to the quasilocal scaling operators in the smeared theory. Since the local scaling operators are known for the CFT, we can just use the smearing to find their counterparts in cTNR. For example, the right-moving field $\partial\phi(\boldsymbol{x}) \equiv (\partial_{x_1} - i\partial_{x_2})\phi(\boldsymbol{x})$ is a primary with scaling dimension $\Delta_{\partial\phi} = 1$ and conformal spin $s_{\partial\phi} = 1$. Therefore, $\partial\phi^\Lambda(\boldsymbol{x})$

has the same scaling dimension and conformal spin in the smeared theory. In addition, we can similarly find the quadratic scaling operators such as the holomorphic component of the stress tensor, $T^\Lambda(\boldsymbol{x}) = -2\pi : \partial\phi^\Lambda(\boldsymbol{x})\partial\phi^\Lambda(\boldsymbol{x}) :$ with $\Delta_{T^\Lambda} = s_{T^\Lambda} = 2$. Using Wick's theorem, we can then consider any higher powers of the field, and even vertex operators $V_\nu^\Lambda(\boldsymbol{x}) \equiv :e^{i\nu\phi^\Lambda}:$. Furthermore, the operator product expansion (OPE) of the boson CFT is preserved in the smeared theory. For instance, the OPE of the stress tensor $T^\Lambda$ and the primary $\partial\phi^\Lambda(\boldsymbol{x})$ is the same as in CFT:

$$T^\Lambda(z)\partial\phi^\Lambda(w) \sim \frac{\partial\phi^\Lambda(w)}{(z-w)^2} + \frac{\partial^2\phi^\Lambda(w)}{z-w}, \tag{B.53}$$

where $z$ and $w$ are complex coordinates introduced in the previous section. Finally, the OPE of $T^\Lambda$ with itself gives the value of the central charge $c = 1$:

$$T^\Lambda(z)T^\Lambda(w) \sim \frac{1/2}{(z-w)^4} + \frac{2T^\Lambda(w)}{(z-w)^2} + \frac{\partial T^\Lambda(w)}{z-w}. \tag{B.54}$$

Importantly, the quasilocal stress tensor $T^\Lambda(z)$ generates conformal transformations in the smeared theory through the Ward identities as the local stress tensor $T(z)$ does in the CFT. Since $T^\Lambda(z)$ is quasilocal, the conformal symmetries of the smeared theory is realized in a quasilocal fashion.

# Appendix C

# Appendices for Chapter 4

## C.1 Review of 2D CFT

In this section we have a brief review of CFT on a 2-dimensional plane. The conformal symmetry are enhanced in 2 dimensions such that there exists an infinite variety of conformal transformations. It is convenient to use complex coordinates to parametrize the spacetime:

$$z = z^0 + iz^1, \quad \bar{z} = z^0 - iz^1. \tag{C.1}$$

Here $z^0$ and $z^1$ represents the Euclidean time and the space respectively. Conformal transformations can then be expressed as holomorphic mappings:

$$z \to w(z). \tag{C.2}$$

An infinitesimal holomorphic mapping may be expanded as a Laurent expansion:

$$z' = z + \epsilon(z), \tag{C.3}$$

$$\epsilon(z) = \sum_{n=-\infty}^{\infty} c_n z^{n+1}. \tag{C.4}$$

Under such an infinitesimal transformation, the change of a classical field $\phi(z, \bar{z})$ with zero spin and scaling dimension is given by

$$\delta\phi = -\epsilon(z)\partial_z\phi - \bar{\epsilon}(\bar{z})\partial_{\bar{z}}\phi \tag{C.5}$$

$$= \sum_n \left[c_n l_n \phi(z, \bar{z}) + \bar{c}_n \bar{l}_n \phi(z, \bar{z})\right], \tag{C.6}$$

where we have introduced the generators

$$l_n = -z^{n+1}\partial_z, \quad \bar{l}_n = -\bar{z}^{n+1}\partial_{\bar{z}}. \tag{C.7}$$

The corresponding conformal algebra is the direct sum of two Witt algebras:

$$\begin{aligned} [l_n, l_m] =& (n-m)l_{m+n}, \\ [\bar{l}_n, \bar{l}_m] =& (n-m)\bar{l}_{m+n}, \\ [l_n, \bar{l}_m] =& 0. \end{aligned} \tag{C.8}$$

In the commonly used radial quantization, where time slices are circles centered at $z = 0$, the conformal symmetry is generated by two copies of Virasoro algebras, which are the quantum versions of Witt algebras. The Virasoro generators are given by the integrals of the stress tensor around $z = 0$:

$$\begin{aligned} L_n =& \frac{1}{2\pi i}\oint dz\ z^{n+1}T(z), \\ \bar{L}_n =& \frac{1}{2\pi i}\oint d\bar{z}\ \bar{z}^{n+1}\bar{T}(\bar{z}). \end{aligned} \tag{C.9}$$

They satisfy the commutation relations:

$$\begin{aligned} [L_n, L_m] &= (n-m)L_{n+m} + \frac{c}{12}n(n^2-1)\delta_{m+n,0}, \\ [\bar{L}_n, \bar{L}_m] &= (n-m)\bar{L}_{n+m} + \frac{c}{12}n(n^2-1)\delta_{m+n,0}, \\ [L_n, \bar{L}_m] &= 0. \end{aligned} \tag{C.10}$$

The change of a generic field $\Phi(z, \bar{z})$ is given by the Ward identity:

$$\begin{aligned} \delta\Phi =& -\frac{1}{2\pi i}\oint_z dw\ \epsilon(w)T(w)\Phi \\ &+ \frac{1}{2\pi i}\oint_{\bar{z}} d\bar{w}\ \bar{\epsilon}(\bar{w})\bar{T}(\bar{w})\Phi \\ =& \sum_n -\left\{c_n[L_n, \Phi] + \bar{c}_n[\bar{L}_n, \Phi]\right\} \end{aligned} \tag{C.11}$$

## C.2 Virasoro algebra in 2D BCFT

Now we consider a CFT on the upper half-plane $z^0 > 0$, where some conformal boundary conditions are imposed on the boundary (the real axis). Conformal transformations keep

the boundary invariant if and only if $\epsilon(z) = \bar{\epsilon}(\bar{z})$. Therefore the holomorphic and anti-holomorphic transformations are coupled together, such that the conformal symmetry has been reduced to a single copy of Virasoro algebra. In order to apply the CFT machinery developed in the whole complex plane, we analytically continue the theory to the lower half-plane by defining

$$T(z) = \begin{cases} T(z) & \text{for } \mathrm{Im}(z) > 0, \\ \bar{T}(\bar{z}) & \text{for } \mathrm{Im}(z) < 0. \end{cases} \tag{C.12}$$

In radial quantization, the Virasoro generators are given by

$$\begin{aligned} L_n =& \frac{1}{2\pi i} \oint dz \; z^{n+1} \tilde{T}(z), \\ =& \frac{1}{2\pi i} \int_{\mathcal{C}} \left[ dz \; z^{n+1} T(z) - d\bar{z} \; \bar{z}^{n+1} \bar{T}(\bar{z}) \right], \end{aligned} \tag{C.13}$$

where the integration contour $\mathcal{C}$ is a semicircle in the upper half-plane going counterclockwise around the origin. The ward identity for the field $\Phi(z, \bar{z})$ can be rewritten as

$$\begin{aligned} \delta\Phi =& -\frac{1}{2\pi i} \oint_z dw \; \epsilon(w) \tilde{T}(w) \Phi \\ & -\frac{1}{2\pi i} \oint_{\bar{z}} dw \; \epsilon(w) \tilde{T}(w) \Phi \\ =& -\frac{1}{2\pi i} \oint_{|w|>|z|} dw \; \epsilon(w) \tilde{T}(w) \Phi \\ & +\frac{1}{2\pi i} \oint_{|w|<|z|} dw \; \epsilon(w) \tilde{T}(w) \Phi \\ =& \sum_n -c_n [L_n, \Phi]. \end{aligned} \tag{C.14}$$

In the following we derive the expressions of $L_n$ in $w$ and $u$ coordinates. For a conformal transformation $z \to w(z)$, the stress tensor transforms as follows:

$$\begin{aligned} T(z) &= \left( \frac{dz}{dw} \right)^{-2} \left( T'(w) - \frac{c}{12} \{z; w\} \right), \\ \bar{T}(\bar{z}) &= \left( \frac{d\bar{z}}{d\bar{w}} \right)^{-2} \left( \bar{T}'(\bar{w}) - \frac{c}{12} \{\bar{z}; \bar{w}\} \right), \end{aligned} \tag{C.15}$$

where we have introduced the Schwarzian derivative:

$$\{z; w\} = \frac{d^3 z / dw^3}{dz/dw} - \frac{3}{2} \left( \frac{d^2 z / dw^2}{dz/dw} \right)^2. \tag{C.16}$$

Recall that

$$z = i \exp\left(-\frac{i\pi w}{2l}\right), \tag{C.17}$$

and then we obtain the relations

$$\begin{aligned} T(z)dz =& \frac{2il}{\pi z}\left(T'(w) - \frac{c}{12}\cdot\frac{\pi^2}{8l^2}\right)dw, \\ \bar{T}(\bar{z})d\bar{z} =& -\frac{2il}{\pi\bar{z}}\left(\bar{T}'(\bar{w}) - \frac{c}{12}\cdot\frac{\pi^2}{8l^2}\right)d\bar{w}. \end{aligned} \tag{C.18}$$

Now in $w$ coordinates $L_n$ reads

$$\begin{aligned} L_n =& -\frac{l}{\pi^2}\int_{-l}^{l} dw \left[z^n\left(T(w) - \frac{c}{12}\cdot\frac{\pi^2}{8l^2}\right)\right. \\ & \left. +\bar{z}^n\left(\bar{T}(w) - \frac{c}{12}\cdot\frac{\pi^2}{8l^2}\right)\right] \\ =& -\frac{l}{\pi^2}\int_{-l}^{l} dw \left[z^n T(w) + \bar{z}^n\bar{T}(w)\right. \\ & \left. -\frac{c}{12}\cdot\frac{\pi^2}{8l^2}\cdot(z^n + \bar{z}^n)\right] \\ =& -\frac{l}{\pi^2}\int_{-l}^{l} dw \left[e^{-\frac{in\pi}{2l}(w-l)}T(w)\right. \\ & \left. +e^{\frac{in\pi}{2l}(w-l)}\bar{T}(w)\right] + \frac{c}{24}\delta_{n,0}. \end{aligned} \tag{C.19}$$

Similarly for the conformal transformation

$$w = \log\left(\frac{R+u}{R-u}\right), \tag{C.20}$$

we have relations

$$\begin{aligned} T(w)dw =& \left(\frac{R^2-u^2}{2R}T'(u) - \frac{c}{12}\cdot\frac{R}{R^2-u^2}\right)du, \\ \bar{T}(\bar{w})d\bar{w} =& \left(\frac{R^2-\bar{u}^2}{2R}\bar{T}'(\bar{u}) - \frac{c}{12}\cdot\frac{R}{R^2-\bar{u}^2}\right)d\bar{u}, \end{aligned} \tag{C.21}$$

Then $L_n$ in the $u$ coordinates reads

$$\begin{aligned}
L_n =& -\frac{l}{\pi^2}\int_{-R}^{R} du \left\{ \frac{R^2-u^2}{2R}\left[ e^{-\frac{in\pi}{2l}(w-l)}T(u) \right.\right. \\
& \left.\left. + e^{\frac{in\pi}{2l}(w-l)}\bar{T}(u)\right] - \frac{c}{12}\cdot\frac{R}{R^2-u^2}(z^n+\bar{z}^n)\right\} \\
& + \frac{c}{24}\delta_{n,0} \\
=& -\frac{l}{\pi^2}\int_{-R}^{R} du \frac{R^2-u^2}{2R}\left[ e^{-\frac{in\pi}{2l}(w-l)}T(u) \right. \\
& \left. + e^{\frac{in\pi}{2l}(w-l)}\bar{T}(u)\right] + \frac{l}{\pi^2}\int_{-l}^{l} dw\ \frac{c}{24}\cdot(z^n+\bar{z}^n) \\
& + \frac{c}{24}\delta_{n,0} \\
=& \frac{c}{24}\left(1+\frac{4\ell^2}{\pi^2}\right)\delta_{n,0} - \frac{\ell}{\pi^2}\int_{-R+\epsilon}^{R-\epsilon} du \frac{R^2-u^2}{2R} \\
& \left\{ \exp\left[ -\frac{in\pi}{2\ell}\left(\log\left(\frac{R+u}{R-u}\right)-\ell\right)\right] T(u) \right. \\
& \left. + \exp\left[ \frac{in\pi}{2\ell}\left(\log\left(\frac{R+u}{R-u}\right)-\ell\right)\right] \bar{T}(u)\right\}.
\end{aligned} \tag{C.22}$$

## C.3 Free fermion formalism for the Ising Model

Via a Jordan-Wigner transformation we can change to complex fermion variables:

$$a_j = \left(\prod_{k<j} Z_k\right)\frac{X_j + iY_j}{2} \tag{C.23}$$

in which the Hamiltonian takes the form:

$$H = -\sum_j \left[(a_{j+1}+a_{j+1}^\dagger)(a_j - a_j^\dagger) - 2a_j^\dagger a_j\right] \tag{C.24}$$

Now we define the fermion operators in Fourier space, and rewrite the Hamiltonian (up to additive constants):

$$a_p = \frac{1}{\sqrt{2\pi}} \sum_j a_j e^{ipj} \qquad \{a_p, a_q^\dagger\} = \delta(p-q) \tag{C.25}$$

$$\begin{aligned} H = \int_{-\pi}^{\pi} dp \Big[ & (1-\cos p) \left( a_p^\dagger a_p + a_{-p}^\dagger a_p \right) \\ & + i \sin p \left( a_{-p} a_p + a_{-p}^\dagger a_p^\dagger \right) \Big] \end{aligned} \tag{C.26}$$

The Hamiltonian can then be diagonalized in momentum space by means of the Bogoliubov transformation

$$a_p = \cos\theta(p)\ b_p - i \sin\theta(p)\ b_{-p}^\dagger \tag{C.27}$$

$$a_{-p} = \cos\theta(p)\ b_{-p} + i \sin\theta(p)\ b_p^\dagger \tag{C.28}$$

with $\theta(p) = \frac{\pi - p}{4}, p \in [0, \pi]$. Again up to an additive constant, we have

$$H = 2 \int_{-\pi}^{\pi} dp\ \left| \sin\left(\frac{p}{2}\right) \right|\ b_p^\dagger b_p \tag{C.29}$$

The ground state correlation functions are therefore

$$\langle b_p b_q \rangle = 0, \tag{C.30}$$

$$\langle b_p b_q^\dagger \rangle = \delta(p-q). \tag{C.31}$$

Hence

$$\langle a_p a_q \rangle = \frac{i}{2} \cos\left(\frac{p}{2}\right) \mathrm{sign}(p) \delta(p+q), \tag{C.32}$$

$$\langle a_p a_q^\dagger \rangle = \frac{1}{2} \left( 1 + \left| \sin\left(\frac{p}{2}\right) \right| \right) \delta(p-q), \tag{C.33}$$

which implies, back to position space

$$\langle a_n a_m \rangle = \frac{1}{\pi} \frac{2(n-m)}{4(n-m)^2 - 1} \tag{C.34}$$

$$\langle a_n a_m^\dagger \rangle = \frac{1}{2} \delta_{nm} - \frac{1}{\pi} \frac{1}{4(n-m)^2 - 1} \tag{C.35}$$

Thanks to the free fermion formalism, we can obtain the spectrum of the density matrix $\rho$ for $N$ sites by diagonalizing a $2N \times 2N$ correlation matrix, which is a significant improvement with respect to the exponential growth of the dimensionality of $\rho$. The procedure is as follows: let $c_1, \ldots, c_{2N}$ be the $2N$ creation-annihilation operators on the sites of the interval whose reduced density matrix we want to compute. We then build the (Hermitian, positive definite) correlation matrix:

$$\Gamma_{ij} = \langle c_i^\dagger c_j \rangle. \tag{C.36}$$

We can diagonalize it via a unitary matrix $U$ preserving the anti-commutation relations:

$$c_i \longrightarrow \tilde{c}_i = U_{ij} c_j. \tag{C.37}$$

This way we have found a set of $N$ uncorrelated fermionic degrees of freedom $\{\tilde{a}_i, \tilde{a}_i^\dagger\}_{i=1}^N$ (related to the original ones by a nonlocal transformation), and the density matrix factorizes as the tensor product of density matrices associated to each of them:

$$\rho = \bigotimes_{i=1}^{N} \rho_i. \tag{C.38}$$

The entanglement spectrum can be obtained from the eigenvalues of $\Gamma$, which naturally come in pairs $(\lambda_i, 1 - \lambda_i)$.

## C.4 Ising model conformal data

The underlying CFT for the Ising model is a minimal model with two nonidentity primary fields: the spin density $\sigma$, and the energy density $\varepsilon$, whose conformal dimensions are

$$h_\sigma = \bar{h}_\sigma = \frac{1}{16}, \quad h_\varepsilon = \bar{h}_\varepsilon = \frac{1}{2}. \tag{C.39}$$

As explained in the main text, the Hilbert space of the CFT on a manifold with boundaries depends on the boundary conditions. The Ising CFT admits three conformal boundary conditions that correspond in the statistical model to fixing the boundary spins to be up or down, or leaving them free. In our case of study, we observe results compatible with the presence of free boundary conditions on both boundaries (the circumferences of the disks we removed). The Hilbert space consists then of the conformal towers of the identity and energy density operators. Figure 4.7) represents the 18 lowest energy states.

# Appendix D

# Appendices for Chapter 5

## D.1 Asymptotic Behavior of $\bar{T}_{\tau,x}$

In this appendix, we examine the asymptotic behavior of $\bar{t}_{i+r,i}$ as $|\tau| \to \infty$ and $x \to \infty$ in $D = 1+1$ and $D = 2+1$. In $1+1$ dimensions, the Fourier transform of Eq. (5.39) gives

$$\bar{t}_{i+r,i}(z) = \frac{m^2 e^{2z}}{(e^{2z}-1)^2} \cdot e^{-k_s^2 \tau} \cdot \frac{e^{\frac{x^2}{4\tau}}}{4\sqrt{\pi}} \Big[ -\theta(\tau) \frac{i}{\sqrt{\tau}} \Big( erf(\frac{x - 2ik_s\tau}{2\sqrt{\tau}}) - erf(\frac{x + 2ik_s\tau}{2\sqrt{\tau}}) \Big) + \theta(-\tau) \frac{1}{\sqrt{-\tau}} \Big( 2 - erf(\frac{ix - 2k_s\tau}{2\sqrt{-\tau}}) + erf(\frac{ix + 2k_s\tau}{2\sqrt{-\tau}}) \Big) \Big], \tag{D.1}$$

where $erf(x)$ is the error function. The asymptotic form is given by Eq. (5.40) and Eq. (5.41).

In $2+1$ dimensions, the Fourier transformation of Eq. (5.39) becomes

$$\bar{t}_{i+r,i}(z) = \int_{-\pi}^{\pi} \int_{0}^{\infty} \bar{T}_{\tau,\boldsymbol{k}}(z) e^{-ikxcos\theta} \cdot k \cdot \frac{dkd\theta}{(2\pi)^2}. \tag{D.2}$$

For large $|\tau|$, Eq. (5.39) shows that $\bar{T}_{\tau,k}(z)$ falls very fast as $|k|$ goes away from $k_s$. Since

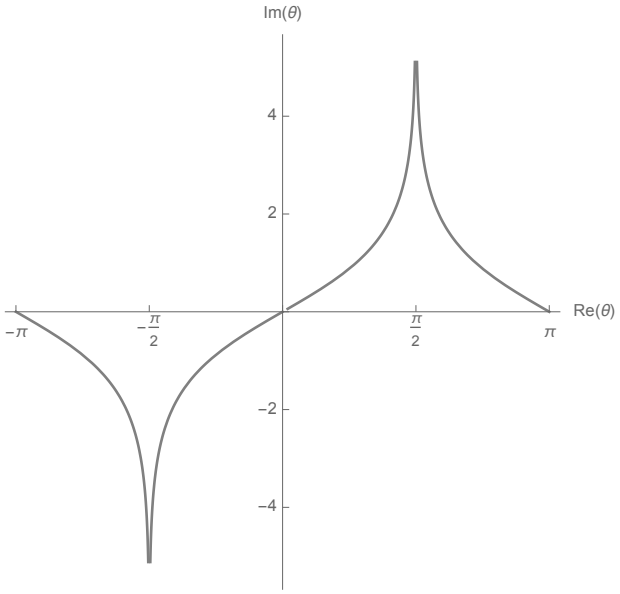


Figure D.1: integral contour of $\theta$ where $\mathrm{Re}(\cos\theta) = \pm 1$

the integration over $k$ is concentrated near $k_s$, we obtain

$$\begin{aligned}\int_0^\infty \bar{T}_{\tau,\boldsymbol{k}}(z)e^{-ikxcos\theta}\cdot k\cdot\frac{dk}{2\pi} &= -\frac{m^2e^{2z}}{(e^{2z}-1)^2}\int_0^{k_s} e^{(k^2-k_s^2)\tau}e^{-ikxcos\theta}\cdot k\cdot\frac{dk}{2\pi} \\ &\approx -\frac{m^2e^{2z}}{(e^{2z}-1)^2}\int_{-\infty}^{k_s} k_s\cdot e^{2k_s(k-k_s)\tau}e^{-ik_sxcos\theta}\frac{dk}{2\pi} \\ &= -\frac{m^2e^{2z}}{(e^{2z}-1)^2}\cdot\frac{1}{4\pi\tau}\cdot e^{-ik_sxcos\theta},\end{aligned} \tag{D.3}$$

and

$$\begin{aligned}\bar{t}_{i+r,i} &\approx -\frac{m^2e^{2z}}{(e^{2z}-1)^2}\cdot\frac{1}{8\pi^2\tau}\int_{-\pi}^{\pi} e^{-ik_sxcos\theta}d\theta \\ &= -\frac{m^2e^{2z}}{(e^{2z}-1)^2}\cdot\frac{1}{8\pi^2\tau}\cdot J_0(k_sx).\end{aligned} \tag{D.4}$$

On the other hand, for large $|x|$, we first perform the radial integration in momentum to obtain

$$\int_0^\infty \bar{T}_{\tau,\boldsymbol{k}}(z)e^{-ikxcos\theta}\cdot k\cdot\frac{dk}{2\pi} \approx \frac{m^2e^{2z}}{(e^{2z}-1)^2}\cdot\frac{k_se^{-ik_sxcos\theta}}{2i\pi xcos\theta}. \tag{D.5}$$

To evaluate the remaining angle integration,

$$\bar{t}_{i+r,i} \approx \frac{m^2 e^{2z}}{(e^{2z}-1)^2} \cdot \frac{k_s}{4i\pi^2} \int_{-\pi}^{\pi} \frac{e^{-ik_s x cos\theta}}{x cos\theta} d\theta \tag{D.6}$$

we use the method of steepest descent for large $|x|$, where the integral contour is deformed as in Fig. D.1. The main contributions are from $\theta = \pm\pi$ and $\theta = 0$. Expansions around these points give Eq. (5.43).